Role of Surface Carboxylates Deposition on the Deactivation of Fischer-Tropsch Synthesis Catalysts

Gonugunta, P.

DOI
10.4233/uuid:09ad251c-fc03-4252-9c25-e205f0b5a5a1

Publication date
2021

Document Version
Final published version

Citation (APA)
Gonugunta, P. (2021). *Role of Surface Carboxylates Deposition on the Deactivation of Fischer-Tropsch Synthesis Catalysts*. https://doi.org/10.4233/uuid:09ad251c-fc03-4252-9c25-e205f0b5a5a1

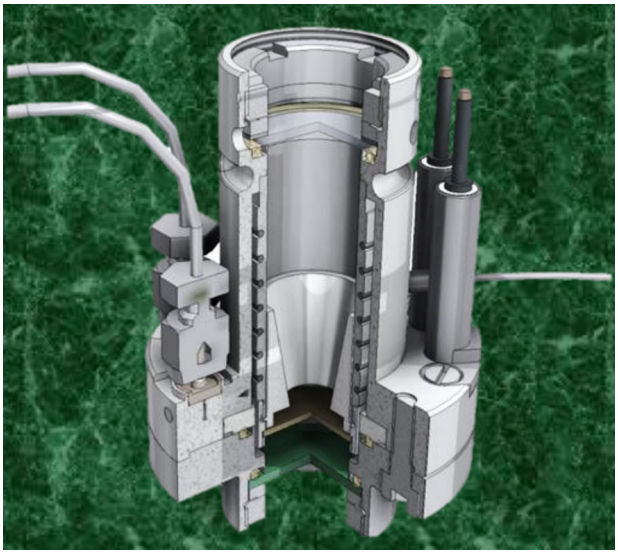

Role of Surface Carboxylates Deposition on the Deactivation of Fischer-Tropsch Synthesis Catalysts

Prasad Gonugunta

The research described in this thesis was performed at the section Fundamental Aspects of Materials and Energy of the department of Radiation Science and Technology, Faculty of Applied Sciences, Delft University of Technology, Mekelweg 15, 2629 JB Delft, The Netherlands.

Role of Surface Carboxylates Deposition on the Deactivation of Fischer-Tropsch Synthesis Catalysts

Proefschrift

ter verkrijging van de graad van doctor
aan de Technische Universiteit Delft,
op gezag van de rector magnificus, prof. dr. ir. T.H.J.J van der Hagen,
voorzitter van het College voor Promoties,
in het openbaar te verdedigen op
vrijdag 12 februari 2021 om 10:00 uur

door

Prasad GONUGUNTA

Master of Applied Science in Biological Engineering, University of Guelph, Canada

geboren te Ilavara, Andhra Pradesh, India

This dissertation has been approved by the promotors.

Composition of the doctoral committee:

Rector Magnificus	Voorzitter
Prof. dr. E.H. Brück	Delft University of Technology, promotor
Dr. A.I. Dugulan	Delft University of Technology, copromotor
Independent Members:	
Prof. dr.ir. A. Urakawa	Delft University of Technology
Dr. M.A. van der Veen	Delft University of Technology
Prof. dr.ir. E.J.M. Hensen	Eindhoven University of Technology
Prof. dr.ir. W. de Jong	Delft University of Technology
Other Member:	
Dr. G.L. Bezemer	Shell Global Solutions International B.V., advisor

The research described in this thesis was financially supported by Shell Global Solutions International B.V.

This thesis is part of NanoNextNL, a micro and nanotechnology innovation consortium of the Government of the Netherlands and 130 partners from academia and industry.

More information on www.nanonextnl.nl

ISBN: 978-94-6421-233-4
Printed by: Ipskamp Printing B.V.
An electronic copy of theis dissertation is available at https://repository.tudelft.nl/

Dedicated to my parents

పూజ్యశ్రీ అమ్మనాన్నలకు అంకితం

Contents

Chapter 1

General introduction

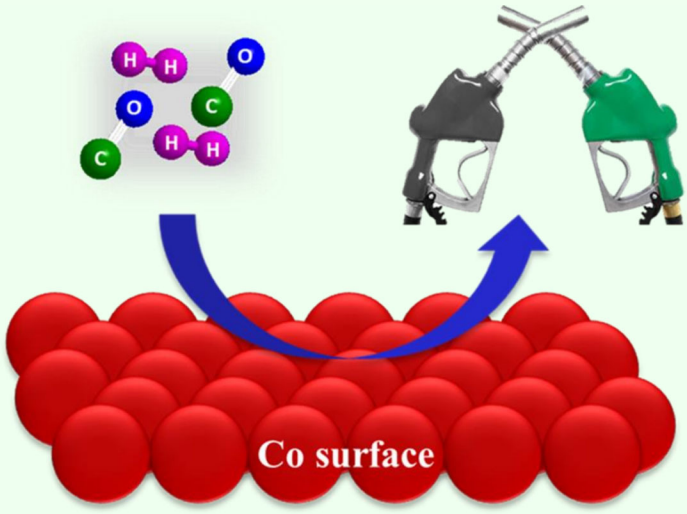

Fischer-Tropsch synthesis (FTS) is a catalytic reaction, which involves the production of long chain hydrocarbons (wax) from synthesis gas obtained from natural gas, biomass and coal via gasification and steam reforming. Cobalt metal is considered as a favourable catalyst in FTS processes due to its high activity, high selectivity to linear paraffins and low water-gas shift activity. However, cobalt-based FTS catalysts are relatively expensive and deactivate in time. Therefore, the development of catalysts with a long lifetime is required to make the process economically efficient. This requires a fundamental understanding of the various catalyst deactivation mechanisms. Sintering of active phase and deposition of carbon and oxygenated compounds are believed to be the main causes for deactivation. However, the exact role of the carboxylates in the catalyst deactivation is not yet fully understood. Therefore, it is aimed to investigate this deactivation mechanism by evaluating the deposition of high molecular weight carboxylates on the catalyst surface at industrial conditions by employing operando spectroscopy techniques, for the prospective development of better industrial catalysts.

1.1. Fischer-Tropsch synthesis

Fischer-Tropsch synthesis (FTS) is the well-established catalytic chemical process to produce ultra clean liquid transportation fuels and various other chemicals from synthesis gas which is a mixture of CO and H_2 [1–4]. This process was invented by two German researchers Franz Fischer and Hans Tropsch at Kaiser-Wilhelm institute for coal research in 1923 [5–7]. The synthesis gas for FTS process is obtained from alternative energy sources such as natural gas, biomass and coal via gasification and steam reforming [8–10]. The schematic representation of FTS process is shown in Figure 1.1. The ideal FTS process of producing hydrocarbons of various molecular weights is according to Equation 1 [2,11]:

1

$$n\,CO + (2n+1)\,H_2 \rightarrow C_nH_{2n+2} + n\,H_2O \quad (1)$$

where 'n' is a positive integer. When n=1, the reaction represents the formation of methane, which is an undesirable byproduct. Apart from the major hydrogenation reaction, there are other side reactions taking place in this process, of which the unwanted water-gas-shift (WGS) reaction is the most predominant as shown in Equation 2 [2,12,13]. Also, small quantities of undesired oxygenated compounds (alcohols, carboxylic acids, ketones etc.) are produced in FTS [14–16]. Based on the source of the synthesis gas, the process is often referred to as gas-to-liquids (GTL), coal-to-liquids (CTL) and biomass to liquids (BTL) [17].

$$CO + H_2O \rightarrow H_2 + CO_2 \quad (2)$$

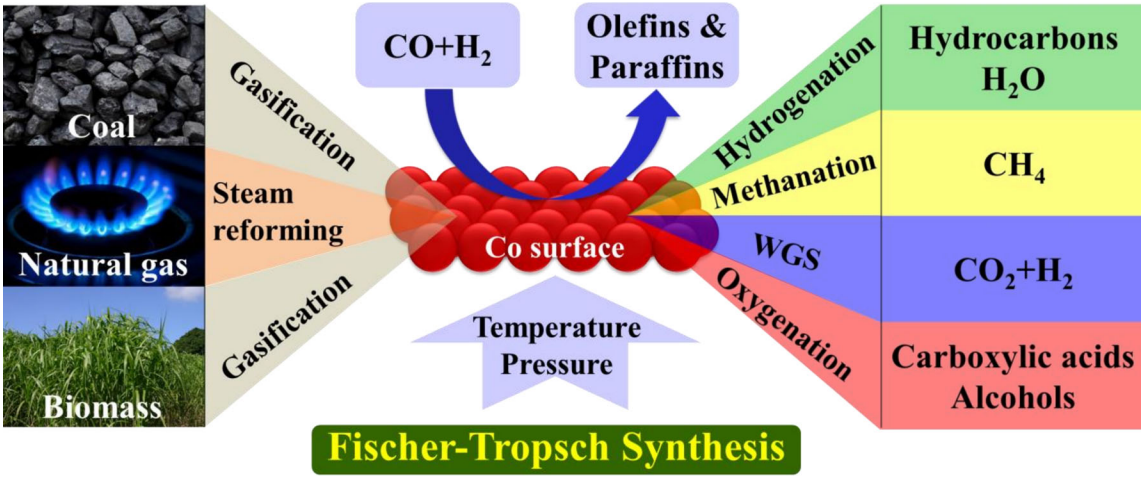

Figure 1.1: Schematic illustration of Fischer-Tropsch synthesis.

FTS process rapidly gained academic and industrial importance and eventually is used to generate nearly 2% of the total world's fuel [18]. The products obtained in this process became major alternative transportation fuels due to their high quality and compatibility with existing petroleum infrastructure and vehicles [19]. Besides the environmental concerns, ample reserves of natural gas in many areas of the world ignited the global interest in the FTS process and new plants based on the FTS technology are commissioned periodically [2]. The BTL process gained more importance in recent years, where biomass is used as a resource of the synthesis gas. In future biomass will play a major and valuable role in the production of

fuels due to its abundant availability, renewable, carbon neutral and cost effective [20,21]. However, a cleaning process of the synthesis gas produced from biomass is necessary to remove impurities [20]. In future, all companies will use only biomass as the source of synthesis gas to produce more environmentally friendly fuels.

Several companies are working on the FTS process such as Shell, Sasol, ExxonMobil, Rentech, Syntroleum, Johnson Matthey, BASF etc. Shell's Pearl GTL plant in Qatar is one of the largest industrial applications of the FTS process producing 140,000 barrels of high quality liquid products per day, as shown in Figure 1.2 and it is one of the largest, challenging and the most complicated energy projects ever successfully commissioned in the world [22]. Another Shell GTL plant in Bintulu, Malaysia producing 14,700 barrels per day is shown in Figure 1.3 [24].

Figure 1.2: Shell's Pearl GTL plant in Qatar [22].

Figure 1.3: Shell's GTL plant in Bintulu, Malaysia [23].

1.2. Reaction kinetics and product selectivity

FTS process has been recognized as a very complex polymerization reaction with a large number of species involved. The general proposed mechanism of FTS consists of chain initiation, chain propagation and chain termination steps. Various reaction mechanisms, like carbide [24,25], enolic [25] and CO insertion [26–28] have been proposed to explain the FTS reaction.

The FTS reaction products form a multi-component mixture with considerable variation in carbon number and type of the products [11]. However, the major products are linear paraffins and α-olefins. The distribution of products obtained in FTS can be understood by the frequently used Anderson-Schultz-Flory (ASF) kinetic model given by Equation 3 [29–31]:

$$W_n = n(1-\alpha)^2\alpha^{(n-1)} \quad (3)$$

where W_n is the mass fraction of the carbon atoms with a chain containing n carbon atoms. The chain growth probability factor (α) is given by Equation 4, where R_p and R_t represent the rate of chain propagation and the rate of chain termination, respectively:

$$\alpha = \frac{R_p}{R_P + R_t} \quad (4)$$

The value of α depends upon process conditions and type of the catalyst [11,32–34] and generally, the range of α value for FTS catalysts is 0.7-0.95 [35]. Significant deviations from the ASF distribution are reported in the literature [31]. These deviations are predominantly caused by secondary reactions of readsorbed α–olefins on the active sites of the catalyst surface and reinsertion of primary hydrocarbon products into the chain growth process [36,37]. A graphical representation of the ASF distribution of FTS products is illustrated in Figure 1.4.

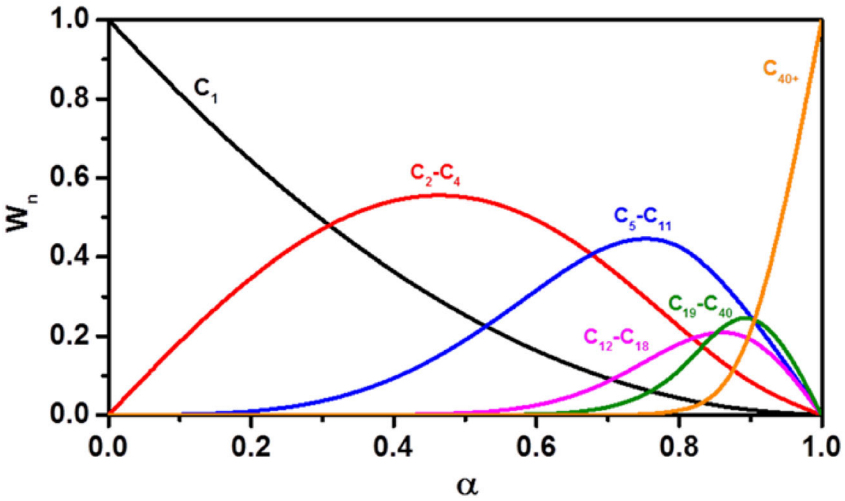

Figure 1.4: ASF distribution of FTS products as a function of chain growth probability (α).

1.3. Co-based catalysts for Fischer-Tropsch synthesis

Several transition metals can be used as catalysts for FTS process, of which Fe, Co, Ni and Ru are commonly accepted as the best catalytic materials [38]. Among all these metals, Ru is the most active one for FTS producing long chain hydrocarbons without the requirement of any promoters. However, its limited availability and relatively high price make industrial applications unfeasible [4]. Ni is a very active catalyst in FTS, but it shows a high selectivity towards the undesired product CH_4. Therefore, only Fe and Co are deemed as the best catalyst materials for FTS process in industrial scale applications [1]. The advantage of Fe is its availability and significantly lower price, but it is much less active compared to Co and shows a low selectivity to paraffins, favouring the production of olefins. The advantage of Co catalyst is its low unwanted WGS activity, leading to less formation of CO_2. Therefore, Co is the preferred catalyst particularly in GTL process to produce long chain paraffins at industrial scale [2,38]. For example, Shell's Pearl GTL plant in Qatar and the GTL plant in Bintulu, Malaysia are operating using Co-based FTS catalysts [22,23].

1.4. Deactivation of Co-based FTS catalysts

Co-based catalysts have been used in large scale industries, however, they have major drawbacks like their high cost and deactivation in time [39–45]. Therefore, it is very important to increase the lifetime of the catalysts to make the process economically more efficient. This requires a fundamental understanding of the various catalyst deactivation mechanisms. Already, the deactivation mechanisms of Co-based FTS catalysts have been studied by many research groups, but there is no consistent picture [40,46–48]. The general proposed mechanisms of deactivation are poisoning of active phase, re-oxidation of Co, sintering of the active phase and deposition of carbonaceous and oxygenated compounds on the catalyst surface [40,41]. Here, the main catalyst deactivation mechanisms of FTS catalysts are discussed briefly.

1.4.1. Poisoning

Poisoning is a strong chemisorption of reactants or impurities on catalytic sites, thereby blocking the sites for catalytic reaction. FTS catalysts are very sensitive to poisoning by sulphur, nitrogen compounds and alkali or alkali earth metals in the feed gas. Sulphur poisons the metal since it adsorbs strongly on active sites. A sulphur atom adsorbed on a cobalt catalyst poisons more than two cobalt atoms [40]. This poisoning effect can be prevented by purifying the synthesis gas, particularly in the process using coal and biomass as feedstock [20]. For example, zinc oxide or lead oxide beds can be used to remove effectively trace amount of sulphur and other impurities [49–51].

1.4.2. Oxidation

Water is the major by-product of the FTS reaction and it may react with active cobalt sites to form inactive cobalt oxides. Although bulk oxidation of Co metal is not favourable in FTS conditions, thermodynamic calculations have shown that nanosized Co particles can be oxidized in steam hydrogen environments at FTS conditions [52]. This may be due to the

contribution of the surface energy of nanosized Co particles to the overall oxidation process. The effect of water addition in FTS on oxidation of Co catalyst has been studied by many researchers [53–57]. Bezemer et al. [54] found that oxidation is not a deactivation mechanism during commercial operation, even for the smallest Co crystallites, when they studied the Co supported on carbon nanofiber using *in-situ* Mössbauer emission spectroscopy. Also, van de Loosdrecht et al. [58] studied the deactivation of an industrial Co/Al_2O_3 catalyst by pseudo in-situ X-ray diffraction (XRD), magnetic measurements and X-ray absorption near-edge structure (XANES) spectroscopy. From these studies, it was concluded that Co oxidation can be ruled out as a major deactivation mechanism.

1.4.3. Sintering

Another common catalyst deactivation mechanism in Co-based FTS is sintering of small metallic particles, which leads to a reduction of the active surface area either through Ostwald ripening or/and coalescence. The high temperature operation and presence of water vapour during the FTS reaction accelerate the sintering [59]. A study by Storsæter et al. [55] suggested that the presence of water during FTS promotes deactivation of Co-based catalysts by sintering mechanism. From transmission electron microscopy (TEM) experiments on Co/SiO_2 catalyst, Kistamurty et al. [60] proposed that Ostwald ripening is the dominant sintering mechanism and could contribute to catalyst deactivation. Duff et al. [61] explained sintering of Co particles via Ostwald ripening using density functional theory of the adsorption and migration energies of different cobalt moieties. The sintering mechanism of Co-based FTS catalysts has been studied extensively to improve the catalyst activity by preventing sintering or regeneration of sintered phase. Saib et al. [41,62–64] studied the sintering mechanism of Co particles supported on a flat SiO_2 support and they reported an oxidative regeneration method to restore the activity of the spent sintered catalyst.

1.4.4. Carbon deposition

Carbon is a major element present on the surface of the FTS catalysts due to the dissociation of CO and conversion into FTS products via hydrogenation. During FTS reaction, the catalyst surface consists of a wide range of carbon containing molecules. These molecules might interact with the catalyst in different ways via side reactions like the Boudouard reaction and enhance carbon deposition on the catalyst [65]. The carbon may also be transformed to more stable species over time that may influence FTS activity by blocking active sites [43]. The potential carbon compounds that could be present on the catalyst surface are wax, graphite, atomic carbon, carbide etc. and the reactivity of these species towards oxygen, hydrogen and carbon monoxide would differ. The formation of different types of carbon compounds on the catalyst surface and their role on deactivation of Co-based FTS catalysts have also been studied earlier [41–43]. Pena et al. [66,67] identified different types of carbon species on a spent Co/Al_2O_3 FTS catalyst using conventional *ex-situ* characterisation techniques. They found that strongly adsorbed hydrocarbons and polymeric carbon contribute to catalyst deactivation. Moodley et al. [7] identified three different carbon species (atomic carbon, residual wax in the pores of the catalyst and polymeric carbon), when a spent $Co/Pt/Al_2O_3$ FTS catalyst was studied with temperature-programmed hydrogenation mass spectrometry

(TPH-MS) experiments. From their studies, it was concluded that only polymeric carbon contributes to the long-term deactivation.

1.4.5. Oxygenated compounds deposition

Along with olefins and paraffins, small amounts of oxygenated compounds (carboxylic acids, alcohols, ketones etc.) are formed in FTS [14]. These oxygenated compounds interact strongly with the support and the catalyst because of their high polarity [68]. In addition, the boiling points of oxygenated compounds are higher compared to olefins and paraffins. These oxygenated compounds deposited on the catalyst surface may block the active sites because it may be difficult for these oxygenated compounds to desorb from the catalyst surface. Pena et al. [66] identified branched fatty acids (C_7-C_{28}) and α-alkyl aldehydes (C_{12}-C_{32}), when the organic extract from a spent Co/Al_2O_3 catalyst was analysed using gas chromatograph and Mass spectrometer (GC-MS). Scalbert et al. [69] found on a Co/Al_2O_3 FTS catalyst increased amount of oxygenated and unsaturated compounds with reaction time using X-ray diffraction - Diffusive reflective infrared Fourier-transform (XRD-DRIFT) spectroscopy. They proposed that these strongly adsorbed species are responsible for catalyst deactivation by covering the active sites. Pinard et al. [70] analysed the carbon species present on a spent $Co/Ru/Al_2O_3$ FTS catalyst using temperature programmed hydrogenation–infrared (TPH-IR) technique. Atomic carbon, alcohols, carboxylic acids and polymeric carbon were found on the spent catalyst surface. TPH-IR of the spent catalyst indicated that complete removal of carboxylate species from the catalyst surface requires temperatures above 600 °C as shown in Figure 1.5. Only carboxylic acids and polymeric carbon were resistant to a rejuvenation treatment under hydrogen. From these studies, Pinard et al. [70] proposed that carboxylates on the catalyst surface deactivate the catalyst, but the exact role of the carboxylates on the catalyst surface is not fully understood yet.

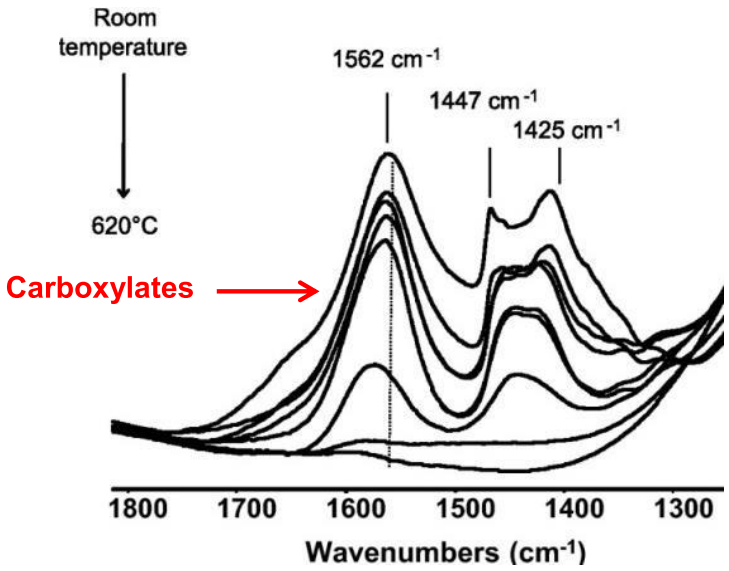

Figure 1.5: TPH-IR of the spent $Co/Ru/Al_2O_3$ FTS catalyst (adapted from [70] with permission*).

*Reprinted from L. Pinard, P. Bichon, A. Popov, J.L. Lemberton, C. Canaff, F. Maugé, P. Bazin, E.F. S.-Aguiar, P. Magnoux, Identification of the carbonaceous compounds present on a deactivated cobalt based Fischer–Trospch catalyst resistant to "rejuvenation treatment," Appl. Catal. A Gen. 406, 73–80, copyright (2011) with permission from Elsevier.

1.5. Effect of carboxylic acids and alcohols addition

It has been proposed that oxygenated compounds deposited on the catalyst surface probably block the Co active sites, decreasing the activity of the catalyst [69,70]. Gu et al. [71] found significant effects on the activity and selectivity of the Co/Al_2O_3 FTS catalyst in the presence of carboxylic acids in the feed gas. The activity decreased to half in the presence of acetic acid and stabilised afterwards. They proposed that the decrease in activity is due to the formation of inactive cobalt acetate species in the presence of acetic acid, which was confirmed by identifying the cobalt acetate species on the spent catalyst using FTIR and XRD spectroscopy. Also, a shift in the selectivity from paraffins to olefins in the presence of acids has been observed. This effect is attributed to the intermediate esters formed on the catalyst surface, which prevent secondary hydrogenation of olefins. Addition of butyric acid to the feed gas also showed a similar effect on the performance of the catalyst. Jalama et al. [72] investigated the effect of ethanol addition during FTS using Co/TiO_2 catalyst in a stirred basket reactor and found that the ethanol addition increased the olefin to paraffin ratio and significantly decreased the catalyst activity. These effects were reversible when ethanol was removed from the feed. They proposed that the increase in olefin to paraffin ratio is due to the transformation of ethanol to olefins on the catalyst surface.

1.6. Aim of the research

It has been proposed that deposition of high molecular weight carboxylates on the surface of the catalyst in FTS reaction deactivates the catalysts. However, the possible role of carboxylates and their effect of catalyst deactivation are not yet fully understood. Therefore, we aimed to investigate this hypothetical deactivation mechanism at industrial conditions by employing the operando spectroscopy techniques. Operando characterisation techniques open new ways to understand the phenomena occurring during the reaction. This understanding helps to develop better industrial catalysts. Operando diffusive reflective infrared Fourier transform (DRIFT) spectroscopy to monitor the surface species and reaction intermediates on the catalyst and ^{57}Co Mössbauer emission spectroscopy (MES) to study the state of the active sites of the catalyst are adopted for this study.

1.7. Outline of the thesis

The thesis is divided into six chapters. After this introduction, in **chapter 2**, the design and employment of operando DRIFT and MES spectroscopy setups for Co-based FTS catalysts studies are described in detail.

In **chapter 3**, the effect of pressure and temperature on the performance of Co/TiO_2 FTS catalysts is described. The formation of different types of carboxylates and hydrocarbons on the surface of the catalyst is monitored with variation in the operating conditions. We find high molecular weight carboxylates are dominant at high pressure and low temperature.

In **chapter 4**, the influence of synthesis method on the catalyst deactivation is studied. Two different Co-based catalyst samples synthesised with incipient wetness impregnation (IWI) and homogeneous deposition precipitation (HDP) methods are investigated with operando DRIFT and MES spectroscopy. We find that the surface carboxylate species are not involved in the catalyst deactivation, being most likely spectator species on the titania support.

In **chapter 5**, the influence of formic acid co-feeding on the catalyst during FTS and its interaction with the Co/TiO_2 catalyst are described. To understand the role of formic acid in FTS reaction mechanism, the catalyst performance is examined by varying the concentration of formic acid in the feed gas. We observe that when formic acid interacted alone with the Co/TiO2 catalyst, it decomposed into CO and H_2 on the catalyst surface and produced different hydrocarbons. However, formic acid influence on the catalyst performance is insignificant.

In **chapter 6**, the role of acetic acid in the deactivation of Co/TiO_2 FTS catalyst and its interaction with Co/TiO_2 catalyst are described. This is achieved by investigating the performance of the catalyst in acetic acid co-feeding. A decrease in the catalyst activity in the presence of acetic acid in the feed is investigated by monitoring the catalyst surface with operando DRIFT spectroscopy. The decrease in activity is most likely due to the formation of inactive cobalt acetate species. The deposition of excess amount of carboxylates on the Co/TiO_2 catalyst surface is observed during acetic co-feeding, are removed easily by decomposition or hydrogenation. The carboxylates formed during co-feeding are very mobile, easily removed and they are not involved in a deactivation mechanism.

Finally, in the summary section, notable findings and their significance for this project are summarised. Major challenges involved in this project and future perspectives on further development of efficient catalysts for economically and environmentally effective industrial applications are discussed.

References

[1] H. Schulz, Short history and present trends of Fischer–Tropsch synthesis, Appl. Catal. A Gen. 186 (1999) 3–12.

[2] A.Y. Khodakov, W. Chu, P. Fongarland, Advances in the development of novel cobalt Fischer-Tropsch catalysts for synthesis of long-chain hydrocarbons and clean fuels, Chem. Rev. 107 (2007) 1692–1744.

[3] B.H. Davis, M.L. Occelli, eds., Advances in Fischer-Tropsch Synthesis, Catalysts, and Catalysis, 1st Editio, CRC Press, Taylor & Francis Group, Boca Raton, 2009.

[4] M.E. Dry, The Fischer–Tropsch process: 1950–2000, Catal. Today. 71 (2002) 227–241.

[5] H. Fischer, F. Tropsch, The preparation of synthetic oil mixtures (synthol) from carbon monoxide and hydrogen, Brennstoff-Chem. 4 (1923) 276–285.

[6] H. Fischer, F. Tropsch, Synthesis of Petroleum at Atmospheric Pressure From Gasification Products of Coal, Brennstoff-Chem. 7 (1926) 97–104.

[7] H. Fischer, F. Tropsch, Process for the production of paraffin-hydrocarbons with more than one carbon atom, US1746464, 1930.

[8] K. Aasberg-Petersen, I. Dybkjær, C.V. Ovesen, N.C. Schjødt, J. Sehested, S.G. Thomsen, Natural gas to synthesis gas – Catalysts and catalytic processes, J. Nat. Gas Sci. Eng. 3 (2011) 423–459.

[9] D. Leckel, Diesel production in coal-based high-temperature Fischer–Tropsch plants using fixed bed dry bottom gasification technology, Fuel Process. Technol. 92 (2011) 959–969.

[10] R. Rauch, J. Hrbek, H. Hofbauer, Biomass gasification for synthesis gas production and applications of the syngas, Wiley Interdiscip. Rev. Energy Environ. 3 (2014) 343–362.

[11] G.P. Van der laan, A.A.C.M. Beenackers, Kinetics and Selectivity of the Fischer–Tropsch Synthesis: A Literature Review, Catal. Rev. 41 (1999) 255–318.

[12] Y.-Y. Chen, M. Dong, J. Wang, H. Jiao, On the Role of a Cobalt Promoter in a Water-Gas-Shift Reaction on Co-MoS_2, J. Phys. Chem. C. 114 (2010) 16669–16676.

[13] R. Hakkarainen, T. Salmi, R.L. Keiski, Water-gas shift reaction on a cobalt-molybdenum oxide catalyst, Appl. Catal. A Gen. 99 (1993) 195–215.

[14] Y. Pei, J. Liu, Y. Zhao, Y. Ding, T. Liu, W. Dong, H. Zhu, H. Su, L. Yan, J. Li, W. Li, High Alcohols Synthesis via Fischer–Tropsch Reaction at Cobalt Metal/Carbide Interface, ACS Catal. 5 (2015) 3620–3624.

[15] R.R. Anderson, C.M. White, Analysis of Fischer-Tropsch by-product waters by gas chromatography, J. High Resolut. Chromatogr. 17 (1994) 245–250.

[16] R.J.J. Nel, A. de Klerk, Fischer−Tropsch Aqueous Phase Refining by Catalytic Alcohol Dehydration, Ind. Eng. Chem. Res. 46 (2007) 3558–3565.

[17] R. Luque, A.R. de la Osa, J.M. Campelo, A.A. Romero, J.L. Valverde, P. Sanchez, Design and development of catalysts for Biomass-To-Liquid-Fischer–Tropsch (BTL-FT) processes for biofuels production, Energy Environ. Sci. 5 (2012) 5186–5202.

[18] V. Navarro, M.A. van Spronsen, J.W.M. Frenken, In-situ observation of self-assembled hydrocarbon Fischer–Tropsch products on a cobalt catalyst, Nat. Chem. 8 (2016) 929–934.

[19] T. Takeshita, K. Yamaji, Important roles of Fischer–Tropsch synfuels in the global energy future, Energy Policy. 36 (2008) 2773–2784.

[20] J. Hu, F. Yu, Y. Lu, Application of Fischer–Tropsch Synthesis in Biomass to Liquid Conversion, Catalysts. 2 (2012) 303–326.

[21] S.S. Ail, S. Dasappa, Biomass to liquid transportation fuel via Fischer Tropsch synthesis – Technology review and current scenario, Renew. Sustain. Energy Rev. 58 (2016) 267–286.

[22] Pear GTL - Overview, (n.d.). http://www.shell.com/about-us/major-projects/pearl-gtl/pearl-gtl-an-overview.html (accessed October 11, 2016).

[23] The Oil Drum, (2010). http://www.theoildrum.com/node/7118 (accessed August 23, 2017).

[24] F. Kapteijn, R.M. de Deugd, J.A. Moulijn, Fischer–Tropsch synthesis using monolithic catalysts, Catal. Today. 105 (2005) 350–356.

[25] R.M. de Deugd, Fischer-Tropsch Synthesis Revisited; Efficiency and Selectivity Benefits from Imposing Temporal and/or Spatial Structure in the Reactor, Delft University of Technology, 2004.

[26] R.A. van Santen, A.J. Markvoort, Chain Growth by CO Insertion in the Fischer-Tropsch Reaction, ChemCatChem. 5 (2013) 3384–3397.

[27] R.A. van Santen, A.J. Markvoort, I.A.W. Filot, M.M. Ghouri, E.J.M. Hensen, Mechanism and microkinetics of the Fischer–Tropsch reaction, Phys. Chem. Chem. Phys. 15 (2013) 17038–17063.

[28] R.A. van Santen, M. Ghouri, E.M.J. Hensen, Microkinetics of oxygenate formation in the Fischer–Tropsch reaction, Phys. Chem. Chem. Phys. 16 (2014) 10041–10058.

[29] P. Chaumette, C. Verdon, P. Boucot, Influence of the hydrocarbons distribution on the heat produced during Fischer-Tropsch synthesis, Top. Catal. 2 (1995) 301–311.

[30] R.B. Anderson, R.A. Friedel, H.H. Storch, Fischer-Tropsch Reaction Mechanism Involving Stepwise Growth of Carbon Chain, J. Chem. Phys. 19 (1951) 313–319.

[31] D. Förtsch, K. Pabst, E. Groß-Hardt, The product distribution in Fischer–Tropsch synthesis: An extension of the ASF model to describe common deviations, Chem. Eng. Sci. 138 (2015) 333–346.

[32] M. Matsuka, R.D. Braddock, T. Hanaoka, K. Shimura, T. Miyazawa, S. Hirata, Effect of Process-Condition-Dependent Chain Growth Probability and Methane Formation on Modeling of the Fischer–Tropsch Process, Energy & Fuels. 30 (2016) 7971–7981.

[33] B. Johnson, C.H. Bartholomew, D.W. Goodman, The role of surface structure and dispersion in CO hydrogenation on cobalt, J. Catal. 128 (1991) 231–247.

[34] Z. Yan, Z. Wang, D.B. Bukur, D.W. Goodman, Fischer–Tropsch synthesis on a model Co/SiO_2 catalyst, J. Catal. 268 (2009) 196–200.

[35] W. De Jong, J.R. Van Ommen, eds., Biomass as a Sustainable Energy Source for the Future, John Wiley & Sons, Inc, Hoboken, NJ, 2014.

[36] E.W. Kuipers, C. Scheper, J.H. Wilson, I.H. Vinkenburg, H. Oosterbeek, Non-ASF Product Distributions Due to Secondary Reactions during Fischer–Tropsch Synthesis, J. Catal. 158 (1996) 288–300.

[37] T. Bhatelia, C. Li, Y. Sun, P. Hazewinkel, N. Burke, V. Sage, Chain length dependent olefin re-adsorption model for Fischer–Tropsch synthesis over $Co\text{-}Al_2O_3$ catalyst, Fuel Process. Technol. 125 (2014) 277–289.

[38] H. Jahangiri, J. Bennett, P. Mahjoubi, K. Wilson, S. Gu, A review of advanced catalyst development for Fischer–Tropsch synthesis of hydrocarbons from biomass derived syn-gas, Catal. Sci. Technol. 4 (2014) 2210–2229.

[39] A.P. Steynberg, S.R. Deshmukh, H.J. Robota, Fischer-Tropsch catalyst deactivation in commercial microchannel reactor operation, Catal. Today. 299 (2018) 10–13.

[40] N.E. Tsakoumis, M. Rønning, Ø. Borg, E. Rytter, A. Holmen, Deactivation of cobalt based Fischer–Tropsch catalysts: A review, Catal. Today. 154 (2010) 162–182.

[41] A.M. Saib, D.J. Moodley, I.M. Ciobîcă, M.M. Hauman, B.H. Sigwebela, C.J. Weststrate, J.W. Niemantsverdriet, J. van de Loosdrecht, Fundamental understanding of deactivation and regeneration of cobalt Fischer–Tropsch synthesis catalysts, Catal. Today. 154 (2010) 271–282.

[42] E. Rytter, A. Holmen, Deactivation and Regeneration of Commercial Type Fischer-Tropsch Co-Catalysts A Mini-Review, Catalysts. 5 (2015) 478–499.

[43] D.J. Moodley, J. van de Loosdrecht, A.M. Saib, M.J. Overett, A.K. Datye, J.W. Niemantsverdriet, Carbon deposition as a deactivation mechanism of cobalt-based Fischer–Tropsch synthesis catalysts under realistic conditions, Appl. Catal. A Gen. 354 (2009) 102–110.

[44] G. Jacobs, P.M. Patterson, Y. Zhang, T. Das, J. Li, B.H. Davis, Fischer–Tropsch synthesis: deactivation of noble metal-promoted Co/Al_2O_3 catalysts, Appl. Catal. A Gen. 233 (2002) 215–226.

[45] T.O. Eschemann, K.P. de Jong, Deactivation Behavior of Co/TiO_2 Catalysts during Fischer–Tropsch Synthesis, ACS Catal. 5 (2015) 3181–3188.

[46] M. Sadeqzadeh, S. Chambrey, S. Piché, P. Fongarland, F. Luck, D. Curulla-Ferré, D. Schweich, J. Bousquet, A.Y. Khodakov, Deactivation of a Co/Al_2O_3 Fischer–Tropsch catalyst by water-induced sintering in slurry reactor: Modeling and experimental investigations, Catal. Today. 215 (2013) 52–59.

[47] J. Clarkson, P.R. Ellis, R. Humble, G.J. Kelly, M. McKenna, J. West, Deactivation of alumina supported cobalt FT catalysts during testing in a Continuous-stirred tank reactor (CSTR), Appl. Catal. A Gen. 550 (2018) 28–37.

[48] M.W.J. Crajé, A.M. van der Kraan, J. van de Loosdrecht, P.J. van Berge, The application of Mössbauer emission spectroscopy to industrial cobalt based Fischer–Tropsch catalysts, Catal. Today. 71 (2002) 369–379.

[49] I. Rosso, C. Galletti, M. Bizzi, G. Saracco, V. Specchia, Zinc Oxide Sorbents for the Removal of Hydrogen Sulfide from Syngas, Ind. Eng. Chem. Res. 42 (2003) 1688–1697.

[50] S.P. Hernández, M. Chiappero, N. Russo, D. Fino, A novel ZnO-based adsorbent for biogas purification in H2 production systems, Chem. Eng. J. 176–177 (2011) 272–279.

[51] M.J. Watson, Guard bed containing lead compounds upstream of a bed of copper-containing catalyst to prevent its contamination by chlorine and sulphur contaminants, EP1210175 B1, 2003.

[52] E. van Steen, M. Claeys, M.E. Dry, J. van de Loosdrecht, E.L. Viljoen, J.L. Visagie, Stability of Nanocrystals: Thermodynamic Analysis of Oxidation and Re-reduction of Cobalt in Water/Hydrogen Mixtures, J. Phys. Chem. B. 109 (2005) 3575–3577.

[53] T.K. Das, W.A. Conner, J. Li, G. Jacobs, M.E. Dry, B.H. Davis, Fischer−Tropsch Synthesis: Kinetics and Effect of Water for a Co/SiO_2 Catalyst, Energy & Fuels. 19 (2005) 1430–1439.

[54] G.L. Bezemer, T.J. Remans, A.P. Van Bavel, A.I. Dugulan, Direct evidence of water-assisted sintering of cobalt on carbon nanofiber catalysts during simulated Fischer-Tropsch conditions revealed with in-situ Mössbauer spectroscopy, J. Am. Chem. Soc. 132 (2010) 8540–8541.

[55] S. Storsæter, Ø. Borg, E.A. Blekkan, A. Holmen, Study of the effect of water on Fischer–Tropsch synthesis over supported cobalt catalysts, J. Catal. 231 (2005) 405–419.

[56] W. Ma, G. Jacobs, D.E. Sparks, R.L. Spicer, B.H. Davis, J.L.S. Klettlinger, C.H. Yen, Fischer–Tropsch synthesis: Kinetics and water effect study over 25%Co/Al_2O_3 catalysts, Catal. Today. 228 (2014) 158–166.

[57] P.J. van Berge, J. van de Loosdrecht, S. Barradas, A.M. van der Kraan, Oxidation of cobalt based Fischer–Tropsch catalysts as a deactivation mechanism, Catal. Today. 58 (2000) 321–334.

[58] J. van de Loosdrecht, B. Balzhinimaev, J.-A. Dalmon, J.W. Niemantsverdriet, S.V. Tsybulya, A.M. Saib, P.J. van Berge, J.L. Visagie, Cobalt Fischer-Tropsch synthesis: Deactivation by oxidation?, Catal. Today. 123 (2007) 293–302.

[59] C.H. Bartholomew, Mechanisms of catalyst deactivation, Appl. Catal. A Gen. 212 (2001) 17–60.

[60] D. Kistamurthy, A.M. Saib, D.J. Moodley, J.W. Niemantsverdriet, C.J. Weststrate, Ostwald ripening on a planar Co/SiO_2 catalyst exposed to model Fischer-Tropsch synthesis conditions, J. Catal. 328 (2015) 123–129.

[61] K.K.B. Duff, L. Spanu, N.D.M. Hine, Impact of Carbonyl Formation on Cobalt Ripening over Titania Surface, J. Phys. Chem. C. 121 (2017) 15880–15887.

[62] C.J. Weststrate, M.M. Hauman, D.J. Moodley, A.M. Saib, E. van Steen, J.W. Niemantsverdriet, Cobalt Fischer–Tropsch Catalyst Regeneration: The Crucial Role of the Kirkendall Effect for Cobalt Redispersion, Top. Catal. 54 (2011) 811–816.

[63] M.M. Hauman, A. Saib, D.J. Moodley, E. du Plessis, M. Claeys, E. van Steen, Re-dispersion of Cobalt on a Model Fischer-Tropsch Catalyst During Reduction-Oxidation-Reduction Cycles, ChemCatChem. 4 (2012) 1411–1419.

[64] P.C. Thüne, C.J. Weststrate, P. Moodley, A.M. Saib, J. van de Loosdrecht, J.T. Miller, J.W. Niemantsverdriet, Studying Fischer–Tropsch catalysts using transmission electron microscopy and model systems of nanoparticles on planar supports, Catal. Sci. Technol. 1 (2011) 689–697.

[65] M. Kogler, E.-M. Köck, B. Klötzer, T. Schachinger, W. Wallisch, R. Henn, C.W. Huck, C. Hejny, S. Penner, High-Temperature Carbon Deposition on Oxide Surfaces by CO Disproportionation, J. Phys. Chem. C. 120 (2016) 1795–1807.

[66] D. Peña, A. Griboval-Constant, C. Lancelot, M. Quijada, N. Visez, O. Stéphan, V. Lecocq, F. Diehl, A.Y. Khodakov, Molecular structure and localization of carbon species in alumina supported cobalt Fischer–Tropsch catalysts in a slurry reactor, Catal. Today. 228 (2014) 65–76.

[67] D. Peña, A. Griboval-Constant, V. Lecocq, F. Diehl, A.Y. Khodakov, Influence of operating conditions in a continuously stirred tank reactor on the formation of carbon species on alumina supported cobalt Fischer–Tropsch catalysts, Catal. Today. 215 (2013) 43–51.

[68] A. de Klerk, F. Edward, Catalysis in the Refining of Fischer-Tropsch Syncrude, Royal Society of Chemistry, Cambridge, 2010.

[69] J. Scalbert, I. Clémençon, P. Lecour, L. Braconnier, F. Diehl, C. Legens, Simultaneous investigation of the structure and surface of a Co/alumina catalyst during Fischer–Tropsch synthesis: discrimination of various phenomena with beneficial or disadvantageous impact on activity, Catal. Sci. Technol. 5 (2015) 4193–4201.

[70] L. Pinard, P. Bichon, A. Popov, J.L. Lemberton, C. Canaff, F. Maugé, P. Bazin, E.F. S.-Aguiar, P. Magnoux, Identification of the carbonaceous compounds present on a deactivated cobalt based Fischer–Trospch catalyst resistant to “rejuvenation treatment,” Appl. Catal. A Gen. 406 (2011) 73–80.

[71] B. Gu, A.Y. Khodakov, V. V. Ordomsky, Selectivity shift from paraffins to α-olefins in low temperature Fischer–Tropsch synthesis in the presence of carboxylic acids, Chem. Commun. 54 (2018) 2345–2348.

[72] K. Jalama, N.J. Coville, D. Hildebrandt, D. Glasser, L.L. Jewell, Fischer-Tropsch synthesis over Co/TiO_2: Effect of ethanol addition, Fuel. 86 (2007) 73–80.

1

Chapter 2

Employment of operando DRIFT and Mössbauer emission spectroscopy for the study of Fischer-Tropsch synthesis catalysts

Sophisticated and dedicated instruments are necessary to study the Fischer-Tropsch synthesis catalysts at industrial conditions. To investigate the chemical and physical properties and structure-activity relationships of the catalyst during the reaction, operando DRIFT and Mössbauer emission spectroscopy has been employed under industrial FTS conditions. The spectroscopy setups were tested and the operating conditions were optimised for Co-based FTS catalysts studies. With these dedicated and versatile operando DRIFT and Mössbauer emission spectroscopy setups, not only FTS reactions but also other industrially relevant reactions in the field of sustainable energy and materials can be investigated. In addition, a general introduction to infrared spectroscopy, ^{57}Co Mössbauer emission spectroscopy, Gas chromatography and Mass spectroscopy for the characterization of catalysts is given.

2.1. Importance of operando spectroscopy

Heterogeneous catalysis plays a valuable role in many industries in the production of fuels, fine chemicals and many consumer products [1]. Many large companies such as Shell develop catalysts by focusing on understanding the fundamental mechanisms that influence commercial performance. Understanding the structure-activity relationships at the molecular and atomic scale is very important in the improvement of existing catalytic processes as well as developing new catalytic processes. In operando spectroscopy, the spectroscopic characterization of a catalyst during reaction is combined with the simultaneous measurement of performance of the catalyst [2–9]. Operando spectroscopy techniques have brought significant advances in catalysis science by providing fundamental information about the structure-activity relationships of catalysts under realistic processing conditions, offering insight into the catalytically active species and catalyst deactivation mechanisms [2–14]. To study the chemical and physical properties of the Co-based Fischer-Tropsch catalysts, infrared and Mössbauer spectroscopic techniques were adopted. Employment of operando diffusive reflectance infrared Fourier transform (DRIFT) and Mössbauer spectroscopy techniques for FTS catalysts studies are described here in detail.

2.2. Operando DRIFT spectroscopy

2.2.1. Diffusive reflectance infrared Fourier transform spectroscopy

In infrared (IR) spectroscopy, infrared radiation is used to excite the vibrations of molecules. The molecules possess discrete levels of vibrational energy and transitions between the vibration levels occur via absorption of photons with frequency in the mid infrared range. The vibrational frequencies depend on the bond strength and mass of vibrating atoms. In DRIFT spectroscopy, IR rays are incident on the sample and reflected rays from the sample are collected. In spectra, the peak position depends on the absorption frequency of molecules. In catalysis research, infrared spectroscopy is used to identify the nature of chemical species on the surface of the catalysts [15–19]. Also, the infrared spectrum of adsorbed probe molecules is used to find adsorption sites on the catalyst. DRIFT spectra thus yield information about active sites, reaction intermediates and products. Using DRIFT, not only qualitative information but also quantitative information can be obtained, such as concentration of surface species and heats of adsorption [20,21]. The advantage of DRIFT technique is easy sample preparation; powder samples can be analysed and catalysts can be studied *in-situ* [22,23]. This technique also permits analysis not only at atmospheric pressure but also at high pressure, to study chemical reactions at industrial conditions. *In-situ* DRIFT spectroscopy can provide valuable information about the evolution of the catalyst with time during the FTS. The Thermo Nicolet Nexus 670 FT-IR Spectrometer and the DRIFT reaction cell used in these studies of FTS catalysts are shown in Figure 2.1.

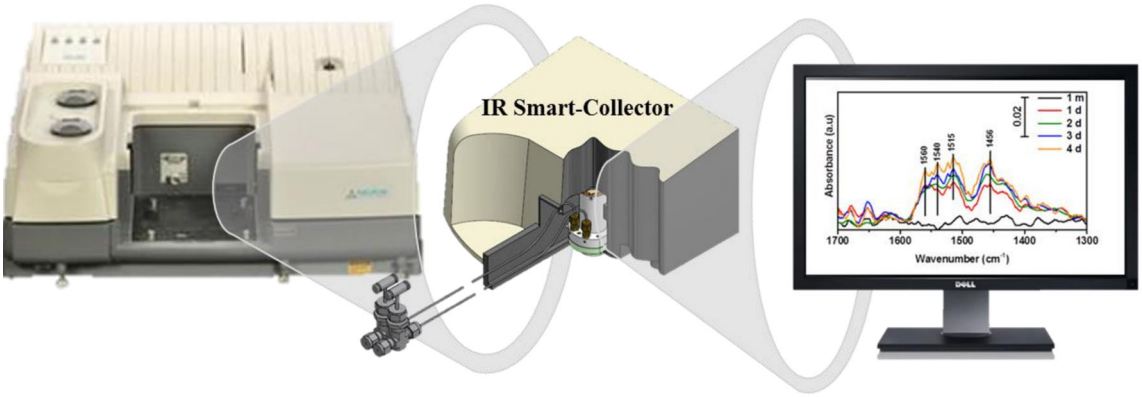

Figure 2.1: Thermo Nicolet Nexus 670 FT-IR Spectrometer.

2.2.2. Gas Chromatography/Mass Spectrometry (GC-MS)

Using GC-MS a complex mixture of chemicals can be separated, identified and quantified [24,25]. In gas chromatography, the sample is vaporised and injected into the inlet of chromatographic separation column and transported through the column by the flow of an inert carrier gas. The compounds in the sample are separated in the column due to differences in their partitioning behaviour between the stationary phase in the column and the mobile gas phase [26,27]. The separated compounds are identified by a thermal conductivity detector (TCD) and a flame ionization detector (FID). The permanent gases are analysed by TCD detector and organic compounds are analysed by FID detector. In Mass spectroscopy (MS), the individual compounds eluting from the GC column enter into an electron ionization detector (MS detector). There, the compounds are bombarded with a stream of electrons to break into fragments of the original molecules. The fragments are charged ions with a certain mass and the mass to charge ratio (M/Z) of each fragment is measured by MS. Most of the fragments have a charge of +1, thus the M/Z generally represents the molecular weight of the fragment. The compounds eluted from the GC column are identified and quantified based on the molecular weight of the fragmented compounds and the position of peaks in the MS spectra. The Thermo Scientific Trace Ultra GC-MS used in this study is shown in Figure 2.2.

Figure 2.2: Thermo Scientific Gas chromatograph and Mass spectrometer.

2.2.3. Design of operando DRIFT spectroscopy setup

Operando spectroscopy methodology has been demonstrated to be very effective and useful to understand reaction mechanisms and catalyst deactivation [3–9]. To obtain relevant information about the catalyst sample, catalytic and spectroscopic measurements have to be performed on the same catalyst and at the same time under optimal catalytic and spectroscopic conditions [10,13,14]. The catalyst material has to be placed in a reaction cell that allows measuring of spectroscopic data under realistic reaction conditions. The catalytic activity and selectivity are obtained from on-line gas chromatography (GC). The applicable design and construction of the *in-situ* cell is a crucial step in obtaining combined spectroscopic and catalytic data. In addition, the challenge in designing an *in-situ* reaction cell is obtaining optimal conditions for performing spectroscopic and catalytic measurements simultaneously. In general, high temperature and high pressure measurements always give less resolved spectroscopic data, which makes the analysis difficult [28–30]. For the construction of a high quality *in-situ* reaction cell, many parameters need to be considered such as catalyst temperature, catalyst form, volume of the reaction cell and safety specifications [28].

It has been proposed that high molecular weight oxygenated compounds deposited on the FTS catalyst surface deactivate the catalysts [31]. To study these adsorbed molecules on the surface of the FTS catalyst at industrial conditions, an *in-situ* DRIFT reaction cell has been developed for Fe and Co based FTS catalysts studies at Reactor Institute Delft (RID), Delft University of Technology (TU Delft) as shown in Figure 2.3a. The reaction cell was made from stainless steel to sustain high pressure and high temperature industrial operating conditions. The top portion of the reaction cell was fitted with a chemical vapour deposition (CVD) diamond window that is transparent for infrared rays for infrared measurements and the bottom of the reaction cell was fitted with a Beryllium (Be) window that is transparent for γ-rays for Mössbauer measurements. A porous graphite disc was fitted at the lower portion of the cell to place the catalyst material. A conical shaped aluminium (Al) mirror was placed above the catalyst chamber to focus infrared rays on the catalyst bed and reflect back to the detector. The temperature in the reaction cell is maintained by Thermocoax heating elements and a thermocouple. The reaction cell is insulated with a ceramic case to avoid heat dissipation. This reaction cell is suitable for operation at industrial FTS conditions (up to 400 ^{o}C and 3 MPa). This DRIFT cell is not a plug-flow reactor, having a large dead-volume (~7 cm^3) at the top of the catalyst bed (gas flows top to bottom through the sample). To monitor the reaction intermediates and surface products on the catalyst, the reaction cell is inserted in the smart collector of a Thermo Nicolet Nexus 670 FT-IR spectrometer as shown in Figure 2.3b. A schematic diagram of the path of infrared rays through the reaction cell for DRIFT measurements is shown in Figure 2.3c.

The inlet and outlet of the reaction cell are heat-traced to pre-heat the reactants and maintain the products in the gaseous phase. A hot-trap is maintained at 60 ^{o}C to catch heavy wax products. Thereafter the line is connected to a GC-MS to analyse the reaction effluents. Siltek®/Sulfinert® deactivated stainless steel tubing was used for outlet connections, because the Siltek®/Sulfinert® coating is the most inert substrate to transfer low concentrations of polar and non-polar compounds, particularly for traces of organosulphur compounds [32]. The

required flow rate of the gases into the reaction cell is maintained by Brooks mass flow controllers [33]. The pressure in the reaction cell is maintained by a GO back pressure regulator [34] and a Ceraphant pressure reader [35]. The scheme of the operando DRIFT spectroscopy setup is shown in Figure 2.4.

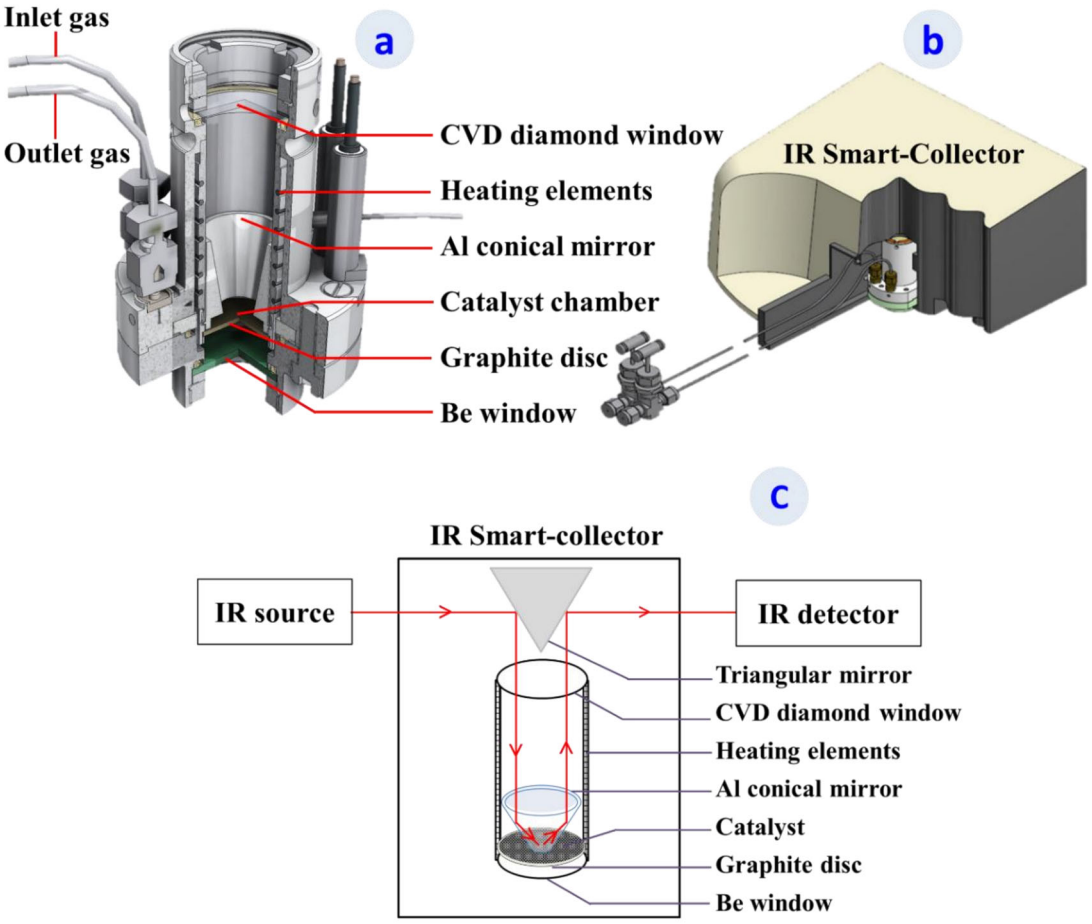

Figure 2.3: (a) High-pressure DRIFT spectroscopy cell, **(b)** Smart collector of Thermo Nicolet Nexus 670 FT-IR Spectrometer, **(c)** Schematic diagram of the path of infrared rays through the reaction cell.

2.2.4. Temperature controlled saturator for co-feeding experiments

To co-feed small concentrations 50-2000 parts per million by volume (ppmv) of alcohols, carboxylic acids and other liquid compounds into the reaction gas, a temperature-controlled saturator is placed in the CO or H_2 gas lines as shown in Figure 2.4. The temperature necessary to flow the required concentration of liquids is calculated using the Antoine vapor pressure temperature relationship [36–39]. The calculated values of vapor pressure are in agreement with experimental values of Coolidge [38]. The saturator is kept in a liquid bath and the liquid is circulated continuously to maintain an uniform temperature throughout the bath, when the required temperature of the saturator is less than room temperature. The temperature of the bath is controlled by a Cryocool immersion cooler. Temperature of the saturator is maintained by a heating tape wrapped around the saturator, when the required temperature of the saturator is higher than room temperature. The outlet gas from the saturator is diluted with Ar and H_2 to maintain the required concentration of carboxylic acids in the inlet gas flow.

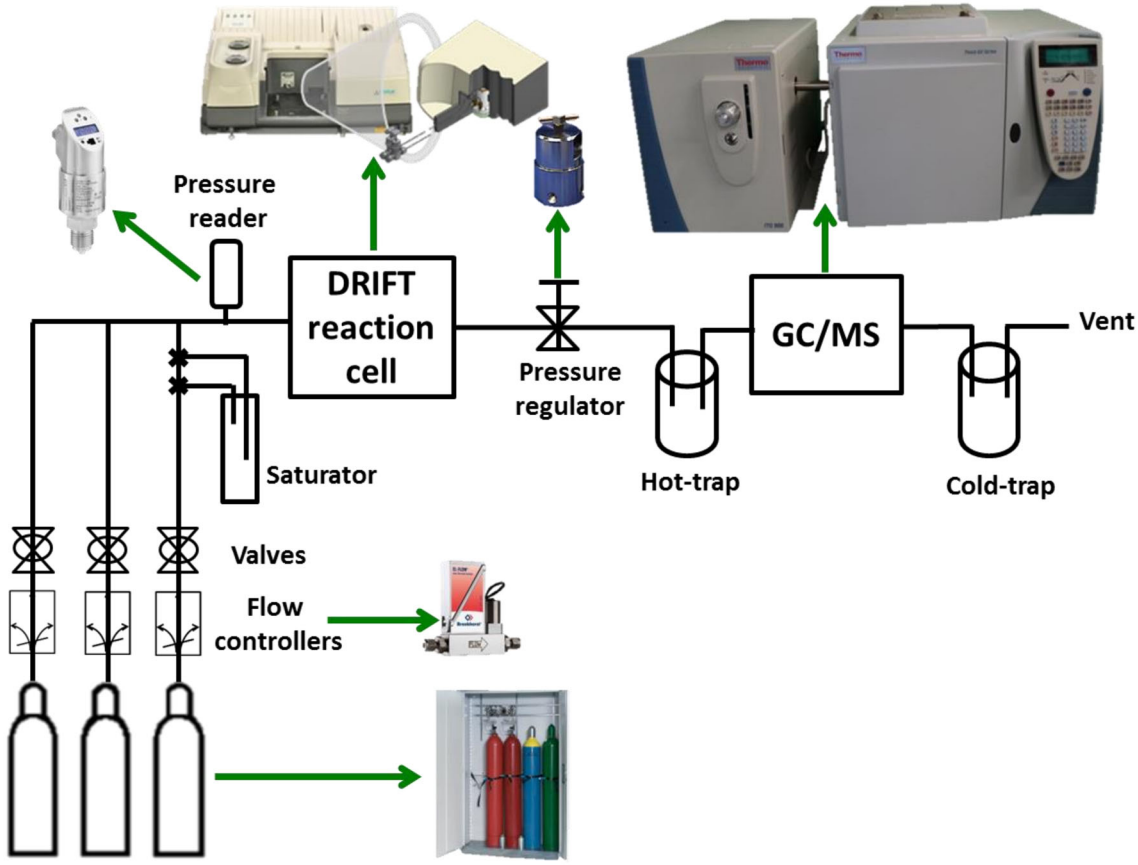

Figure 2.4: Scheme of the operando FTS reaction setup.

2.2.5. Catalysts preparation for DRIFT experiments

Co/TiO_2 catalysts were prepared by incipient wetness impregnation (IWI) and homogeneous deposition precipitation (HDP) methods. A Co/TiO_2 - IWI catalyst provided by Shell Global Solutions International B.V., Amsterdam was prepared by two step impregnation. First, the support material (Degussa P25 with surface area 50 $m^2.g^{-1}$ and pore volume 0.319 $mL.g^{-1}$) was dried and impregnated with 1 pore volume of an aqueous solution of $Co(NO_3)_2$ (17.25 wt% Co). In the second impregnation, the obtained material (pore volume 0.283 $mL.g^{-1}$) was impregnated with 0.95 pore volume of an aqueous solution of $Co(NO_3)_2$ (20.02 wt% Co). After each impregnation step, the obtained material was dried in an oven at 60 ^oC overnight under static air and calcined at 400 ^oC for 2 hours under N_2 flow. The final Co loading on TiO_2 support after two impregnations is 10 wt%.

Another Co(9.3 wt%)/TiO_2 - IWI catalyst provided by Utrecht University was also prepared by two step impregnation. The support material (Degussa P25) was dried and impregnated with an aqueous solution of $Co(NO_3)_2 \cdot 6H_2O$ (4 Molar) in two steps. After each impregnation, the obtained material was dried in an oven at 60 ^oC overnight under static air and calcined at 350 ^oC for 2 hours under N_2 flow.

For the preparation of Co(8.9 wt%)/TiO_2 catalyst by the HDP method (provided by Utrecht University), 24.75 g of $CoCO_3$ and 24.75 g of $(NH_4)_2CO_3$ were dissolved in 255.6 g of 25 wt%

of ammonia solution and the mixture was diluted with distilled water to make a total of 500 mL. 5 mL of this stock solution was mixed with 70 mL of 9 wt% ammonia solution to suspend 2 g of P25 TiO_2 powder in a round bottom flask that was stirred and heated at 100 ^oC for 3 hours using a reflux cooler. After cooling down to room temperature, the material was filtered off, washed with water and dried at 60 ^oC overnight. The obtained material was crushed, sieved and heat-treated in N_2 flow at 400 ^oC for 4 hours. The catalyst samples were ground into fine powder using a mortar and a pestle before loading into the reaction cell. The catalysts prepared for this work are similar to the catalysts studied by Eschemann et al. [40] in a study of the effect of the synthesis method on the catalytic performance.

Co(10 wt%)/TiO_2 - IWI catalyst sample studied in Chapters 3, 5 and 6 was provided by Shell Global Solutions International B.V., Amsterdam.

Co(9.3 wt%)/TiO_2 - IWI and Co(8.9 wt%)/TiO_2 - HDP catalyst samples studied in Chapter 4 were provided by Thomas Eschemann from Utrecht University.

2.2.6. Study of FTS catalysts by operando DRIFT spectroscopy setup

To perform FTS experiments, the catalyst sample is loaded into the reaction cell. The reaction products are analysed with an on-line Thermo Scientific Trace Ultra GC with split injection mode. Each injected sample is analysed with increasing the temperature of the GC oven from 50 ^oC to 250 ^oC. Permanent gases are analysed with a Carboxen 1010 column connected to a TCD detector and hydrocarbons are analysed with a Rtx-1 column connected to a FID detector. The carboxylic acids in the stream are analysed by manually injecting the sample with a syringe into a Stabilwax column connected to a mass spectrometer (MS) detector. Helium is used as a carrier gas for all chromatography columns because of its high thermal conductivity. Argon is used as an internal calibration gas. All chromatograms are analysed with Xcalibur software. The instrumental standard deviations of the GC are calculated from the measurements of known amount permanent gases and hydrocarbons. The standard deviations for Ar, H_2, CO, C_1-C_2, C_3-C_4 and C_5 measurements are 0.74%, 1.8%, 0.84%, 0.17%, 0.16%, 0.12% and 0.3% respectively.

Simultaneously, the DRIFT spectra of the catalyst during the reaction are measured with 128 scans at a resolution of 4 cm^{-1}. The DRIFT spectra of the data obtained are presented in the absorbance mode because the reaction intermediates and products are poorly adsorbed on the surface of the catalysts. Sirita et al. [41] reported on quantitative analysis of adsorbate concentration by DRIFT. It was observed that a baseline shift occurs due to the changes in the absorption and scattering properties of the catalyst with adsorbate deposition and the treatment of data in Kubelka-Munk units sometimes leads to the disappearance of peaks particularly when baseline shift occurs. They found that reporting the intensity in absorbance mode is more appropriate for poorly adsorbing species.

The percentage of CO conversion (X_{CO}) and reaction rate are calculated as:

$$X_{CO} = \frac{F_{in,CO} - F_{out,CO}}{F_{in,CO}} \times 100$$

$$-r_{CO} = \frac{F_{in,CO} - F_{out,CO}}{M_{Co}} \times 100$$

Where:

X_{CO}= Percentage of CO conversion

$-r_{CO}$= Rate of CO conversion (moles.s^{-1}.g_{Co}^{-1})

$F_{in,CO}$= Molar flow rate (moles.s^{-1}) of CO in the inlet gas

$F_{out,CO}$= Molar flow rate (moles.s^{-1}) of CO in the outlet gas

M_{Co}= Mass of the cobalt

$$\text{Selectivity of product } C_n(\%) = \left(\frac{\text{Moles of } C_n \text{product x Carbon number}}{\text{Moles of } CO_{in} - \text{Moles of } CO_{out}}\right) x100$$

$$\text{Olefinity} = \frac{\text{Moles of olefins}}{\text{Moles of paraffins}}$$

The mole fraction of a compound is calculated as follows:

$$y_{C_n} = \frac{nF_{C_n}}{\sum_{n=1}^{N} nF_{C_n}} \times 100$$

Where: F_{C_n}= Number of moles of a compound C_n

2.3. Operando Mössbauer emission spectroscopy

Mössbauer spectroscopy is a versatile and high-resolution spectroscopic technique suitable to investigate the materials that contain nuclei exhibiting the Mössbauer effect. It is based on the recoilless emission and absorption of γ-photons by an atomic nucleus which was discovered by Rudolph Mössbauer [42]. The Mössbauer spectroscopic technique has been developed rapidly as an effective tool in many scientific fields including solid-state physics, mineralogy, geochemistry, metallurgy and inorganic chemistry. With the Mössbauer spectroscopy technique, the spacing of nuclear energy levels with a high-energy resolution can be measured. With Mössbauer spectroscopy information about oxidation states, magnetic fields, lattice symmetry and lattice vibrations can be obtained. The main advantage of Mössbauer spectroscopy is that the technique can be applied for *in-situ* experiments because highly penetrating γ-radiation is used to study the materials [43]. Mössbauer spectroscopy has a wide range of applications in catalyst characterization. It is used for the determination of direct structural and chemical information of catalysts under realistic conditions and quantitative determination of the different phases. Using Mössbauer spectroscopy, phase, oxidation state, kinetics of bulk transformations, structure and particle size about the catalyst particles under realistic conditions can be identified and quantified [44]. The fundamentals of Mössbauer spectroscopy [45–47] and its applications in the studies of various catalysts [48–56] have been reviewed earlier by many researchers.

2.3.1. The Mössbauer effect

Nuclei of atoms experience different energy level transitions associated with the absorption or emission of γ -rays. When an isolated and stationary nucleus transits form a high-energy excited state to the low energy ground state, a γ-photon is emitted from the nucleus. The nucleus takes kinetic recoil energy because of the conservation of momentum and the energy of the emitted γ-ray is lower than the energy required for bringing of a nucleus from ground state to excited state. This is why the Mössbauer effect is not noticed for free atoms in liquid and gas phases [57]. When the source of γ-rays atoms and absorber atoms are fixed in a rigid lattice framework, the nucleus is not able to recoil freely but it vibrates the total framework of the atoms around it. Then the recoil momentum of the total lattice framework is the same as for a free nucleus, but is shared by the total lattice framework. This phenomenon of recoilless emission and absorption of γ-rays by atomic nuclei is called resonant absorption or Mössbauer effect [45,46,58,59].

Mössbauer effect can be observed only if both the emitting and the absorbing nuclei have an identical chemical environment [47]. However, the energy of the emitted γ-rays can be adjusted to make equal to the absorber nuclei energy levels using the Doppler effect. The Doppler effect is the apparent change in the frequency when the source and the observer are in relative motion. In this way, using Doppler effect, the energy of the γ-rays is adjusted by moving the source relative to the absorber. The Mössbauer spectra of the materials are measured by detecting the transmission of γ-rays through the absorber as a function of the source velocity ($\vec{v}$) [57,58].

$$E(\vec{v}) = E_O\left(1 + \frac{\vec{v}}{c}\right)$$

Where E_o is the energy of the stationary source and c the velocity of the light.

2.3.2. ^{57}Co Mössbauer emission spectroscopy

^{57}Co-Mössbauer emission spectroscopy (MES) is used to monitor the oxidation and sintering of Co particles as deactivation mechanisms of Co-based FTS catalysts [44,51]. Radioactive ^{57}Co is introduced into the catalyst and used as a source of γ-rays. The decay of ^{57}Co to ^{57}Fe happens by electron capture, with 9% decaying directly to the ground state with a spin of 1/2. The remaining 91% decay in two steps first to a state of spin of 3/2, next to the ground state of spin of 1/2, including the 14.4 KeV Mössbauer transition as shown in Figure 2.5. In MES a single line absorber ($K_4Fe(CN)_6 \cdot 3H_2O$) is used to investigate the sample containing ^{57}Co as a source of γ-rays. The schematic representation of the experimental setup of MES is shown in Figure 2.6.

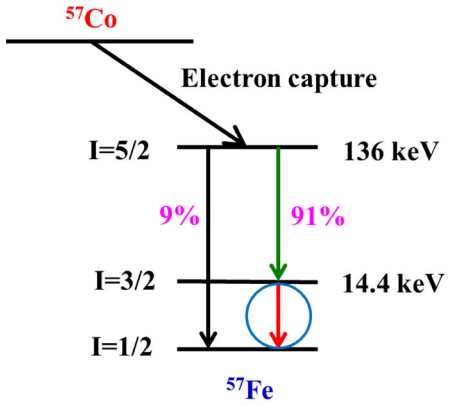

Figure 2.5: The decay scheme of ^{57}Co to stable ^{57}Fe.

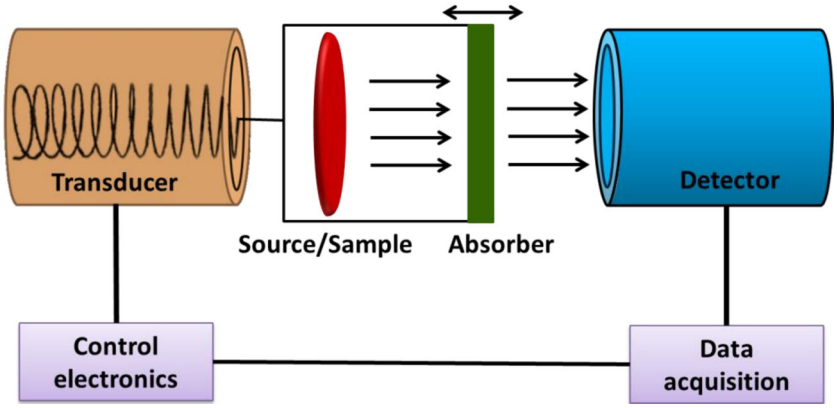

Figure 2.6: Scheme of the experimental setup for ^{57}Co Mössbauer emission studies.

The positions of the absorption peaks in Mössbauer spectra are very sensitive to the interaction of the nucleus with its surroundings. The interaction between nuclear charge distributions and external electric and magnetic fields affect the Mössbauer spectra. The main parameters in the Mössbauer spectra are isomer shift (IS), quadrupole splitting (QS) and magnetic splitting. The hyperfine interactions and splitting of nuclear energy levels of ^{57}Fe and Mössbauer spectra are shown in Figure 2.7. Isomer shift is due to a change in the interaction of the negatively charged electron cloud with the positively charged nucleus. This interaction results in a small shift of the nuclear energy-level of ground and excited states as shown in Figure 2.7a. Isomer shift provides information about the electron density at the nucleus and yields the information about the oxidation state. A quadrupole moment occurs when there is a non-spherical electric charge distribution around the nucleus. In the presence of an electric field gradient or non-uniform electric fields, the nuclear energy levels split. The spectrum consists of two peaks called quadrupole doublet as shown in Figure 2.7b. This quadrupole splitting provides information about the electron configuration in the material. This type of doublet spectrum is observed often for highly dispersed Fe (III) oxides. Magnetic splitting is caused by the interaction of the magnetic dipole moment of the nucleus with a magnetic field. The spectrum consists of six equidistant peaks called sextuplet as shown in Figure 2.7c. The separation between peaks is proportional to the strength of the magnetic field at the nucleus. Measurements of the magnetic splitting give information about the magnetic properties of the materials.

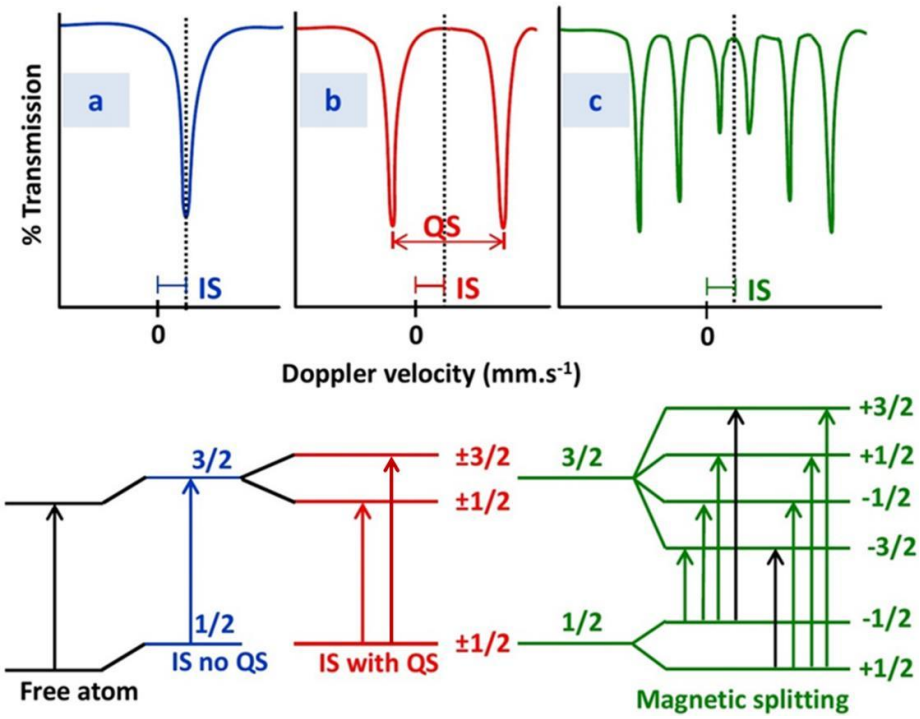

Figure 2.7: Effect of hyperfine interactions: **(a)** Isomer shift, **(b)** Quadrupole splitting and **(c)** Magnetic splitting, on the nuclear energy levels of ^{57}Fe and resulting spectra (redrawn after reference [46]).

The Mössbauer spectra obtained from the samples are deconvoluted into subspectra that consist of Lorentzian-shaped lines to derive hyperfine parameters (IS, QS and Magnetic splitting) to identify and quantify the phase, oxidation state, structure and kinetics of bulk transformations [60]. MES spectra of Co supported on carbon nanofiber (Co/CNF) catalyst after different treatments adapted from Bezemer et al. [51] are given in Figure 2.8 as an example. The recorded MES spectra with varying conditions were fitted using the MossWinn 3.0i program [61]. MES spectrum of the Co/CNF catalyst measured after reduction at 350 ^{o}C in H_2 shown in Figure 2.8A consists of a singlet originating from Co atoms in very small super paramagnetic (SPM) Co particles and a sextuplet originating from Co atoms in larger Co particles that are ordered magnetically. The contributions of SPM small particles and larger clusters are 42% and 58% respectively. This indicates that CoO is completely converted into small SPM Co particles and larger Co clusters in the reduction process. Figure 2.8B shows the MES spectrum of the catalyst at 2 MPa and at 220 °C with H_2O/H_2 = 30 ratio of feed gas composition after 4 days. The MES spectrum does not show any changes in the contributions of singlet and sextuplet, clearly indicating that the Co particles only acted as catalyst and do not react with water even at very high H_2O/H_2 ratio. However, when the H_2 flow was stopped the shape and position of the MES spectrum completely changed as seen in Figure 2.8C. The singlet of the SPM small cobalt particles and sextuplet of larger cobalt clusters disappeared and new peaks with oxidation states +2 and +3 corresponding to the formation of CoO and Co_2O_3 due to oxidation of both SPM small Co particles and larger Co particles by H_2O. This indicated that Co oxidation is possible by water, but only in the absence of H_2. Figure 2.8D shows the MES spectrum of the catalyst at 2 MPa and 200 ^{o}C with high humidity conditions after re-reduction

at 350 °C in H_2. The singlet corresponding to SPM small particles and the sextuplet corresponding to larger Co particles ordered magnetically appeared again and the peaks corresponding to Co^{2+} and Co^{3+} completely vanished. This attributes to the complete reduction of CoO and Co_2O_3 into Co. Interestingly, the SPM spectral contribution of small Co particles decreased to 23% from 42% and the contribution of magnetically ordered larger Co particles increased 58% from to 77%. This is due to the sintering of the small Co particles into larger particles.

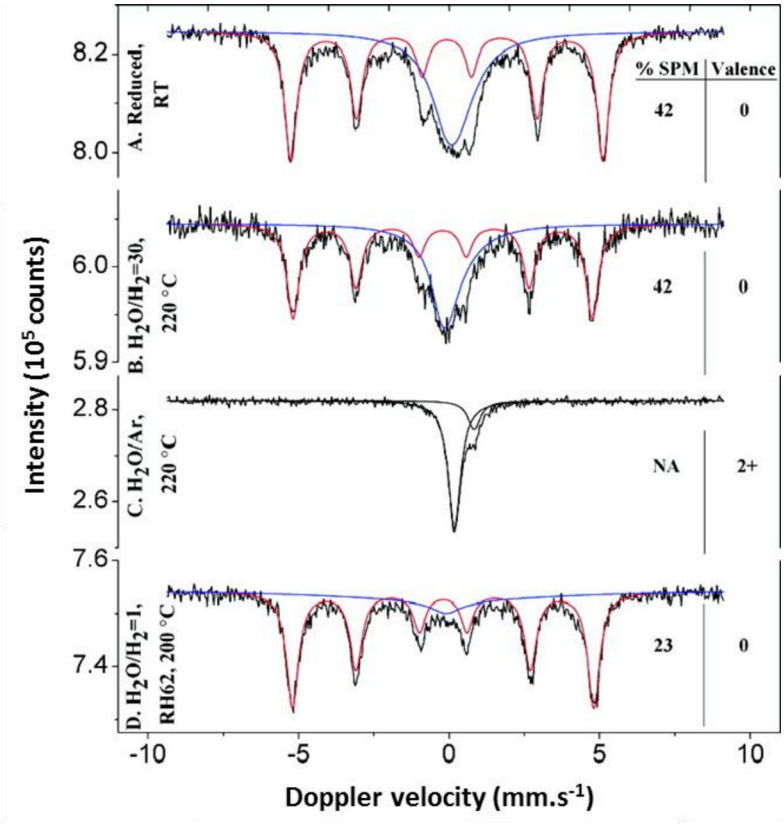

Figure 2.8: MES spectra of Co/CNF catalyst measured after reduction **(A)** and at conditions with varying H_2O/H_2 ratio (**B**, **C** and **D**). MES spectra are fitted with a superparamagnetic (blue line) and a magnetic ordered (red line) contributor (adapted from [51] with permission*).

2.3.3. High pressure Mössbauer emission reaction cell

To study the Co based FTS catalysts at industrial conditions, an *in-situ* high pressure MES reaction cell that can be operated at industrial conditions was developed at Reactor Institute Delft (RID), TU Delft. The design details of this high-pressure MES reaction cell, safety and Mössbauer spectroscopic aspects were explained in detail previously by Crajé et al [44]. The Mössbauer cell is not a plug-flow reactor, having a large dead-volume (~10 cm^3) at the top of the catalyst bed (gas flows top to bottom through the sample). The high-pressure MES reaction cell and its schematic representation are shown in Figures 2.9 and 2.10.

*Reprinted with permission from G.L. Bezemer, T.J. Remans, A.P. Van Bavel, A.I. Dugulan, Direct evidence of water-assisted sintering of cobalt on carbon nanofiber catalysts during simulated Fischer-Tropsch conditions revealed with in-situ Mössbauer spectroscopy, J. Am. Chem. Soc. 132, 8540–8541, copyright (2010) American Chemical Society.

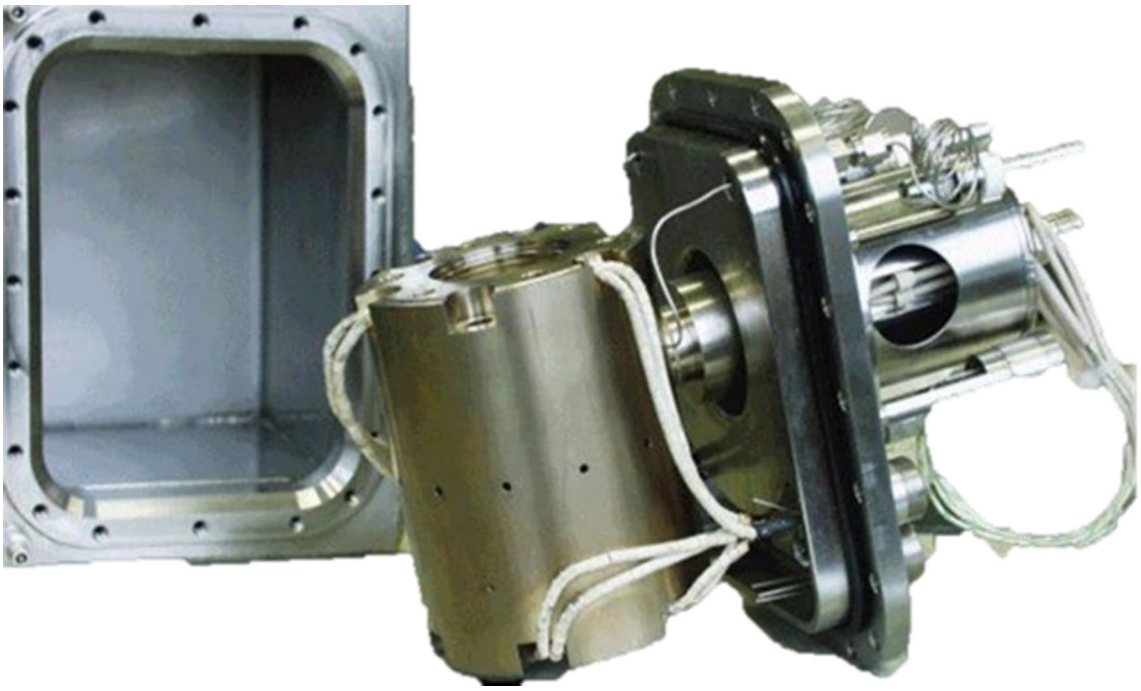

Figure 2.9: Photograph of the high-pressure MES cell (adapted from [44] with permission*).

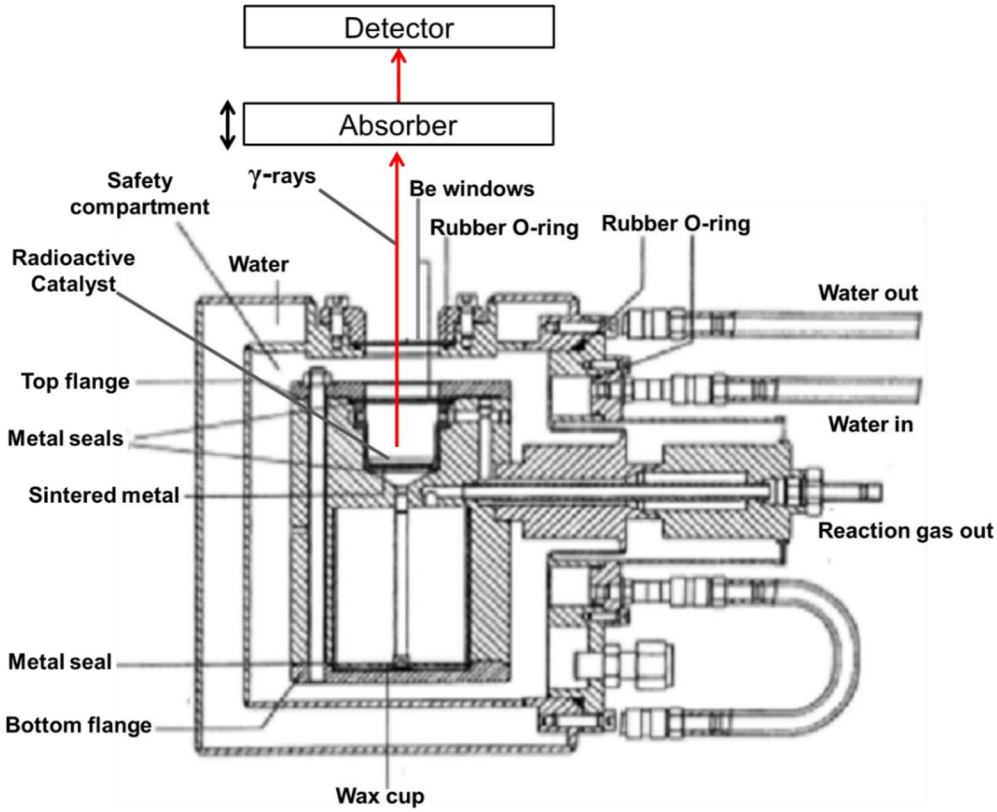

Figure 2.10: Schematic representation of the high-pressure MES cell (adapted from [44] with permission*).

*Reprinted from M.W.J. Crajé, A.M. van der Kraan, J. van de Loosdrecht, P.J. van Berge, The application of Mössbauer emission spectroscopy to industrial cobalt based Fischer–Tropsch catalysts, Catal. Today. 71, 369–379, copyright (2002) with permission from Elsevier.

The main process conditions considered in designing the MES cell are: temperatures up to 450 ^{o}C, pressures up to 2 MPa, 1 MPa steam injection, managing of wax production, long FTS runs up to 2 months, use of air, CO, Ar and H_2 flows through the catalyst bed and the construction of reaction cell with stainless steel. For 1 MPa steam injection, a commercially available system was installed and demineralised water is used to generate steam. The catalyst sample is placed on a sintered metal filter with pore diameter of 5 μm to flow gasses through the catalyst bed. This filter thus allows wax that was produced on the catalyst surface to drain into a collecting chamber.

2.3.4. Catalysts preparation for MES experiments

The two catalyst samples (IWI and HDP) together with an empty P25 TiO_2 support material were used in an additional ^{57}Co incipient wetness impregnation procedure, for the Mössbauer emission measurements. The amount of radioactive cobalt introduced into the sample via the additional impregnation was about 0.3-0.4 μg. All samples were dried in air at 120 °C for 6 h, after the additional impregnation step.

2.3.5. Study of FTS catalysts by operando Mössbauer emission spectroscopy setup

About 500 mg of catalyst particles containing ^{57}Co were used for the experiments, with 50 mg of non-radioactive catalyst particles also present in the high-pressure Mössbauer reactor. The FTS measurements were performed out at 200 °C and 2 MPa, H_2/CO feed ratio (FR) of 4. The products were analysed with thermal conductivity detectors on a Varian Micro-GC CP4900 (Dual channel) gas chromatograph, equipped with molecular sieve and Porapaq Q columns. The ^{57}Co-MES measurements were performed using a constant acceleration spectrometer with a single line absorber of $K_4Fe(CN)_6 \cdot 3H_2O$ enriched in ^{57}Fe. Positive and negative velocities are corresponding to the absorber when moving away from the source and moving towards the source respectively. The velocity scale was calibrated with the Mössbauer spectrum of $Na_2(Fe(CN)_5NO) \cdot 2H_2O$, obtained with a ^{57}Co:Rh source. The recorded Mössbauer spectra were fitted using the MossWinn 3.0i program [61]. The spectra of the superparamagnetic (SPM) species were fitted using the two-state magnetic relaxation model of Blume and Tjon [62], which assumes the presence of a fluctuating magnetic field that jumps between the values ±H, perpendicular to the principal axis of the electric field gradient.

2.4. Summary

Sophisticated and dedicated instruments are necessary to study the Fischer-Tropsch synthesis catalysts at relevant industrial conditions. To investigate the chemical and physical properties and structure-activity relationships of the catalyst during the reaction, operando DRIFT and Mössbauer emission spectroscopy setups have been employed that can be operated at FTS industrial conditions. Operando spectroscopy setups were tested and the operating conditions for Co-based FTS catalyst studies were optimised. With these dedicated operando DRIFT and Mössbauer emission spectroscopy setups, not only FTS reactions but also other industrially relevant reactions in the field of sustainable energy and materials can be investigated.

References

[1] S.M. George, Introduction: Heterogeneous Catalysis, Chem. Rev. 95 (1995) 475–476.

[2] A. Chakrabarti, M.E. Ford, D. Gregory, R. Hu, C.J. Keturakis, S. Lwin, Y. Tang, Z. Yang, M. Zhu, M.A. Bañares, I.E. Wachs, A decade+ of operando spectroscopy studies, Catal. Today. 283 (2017) 27–53.

[3] M.A. Bañares, Operando methodology: combination of in situ spectroscopy and simultaneous activity measurements under catalytic reaction conditions, Catal. Today. 100 (2005) 71–77.

[4] A.M. Beale, M.G. O'Brien, B.M. Weckhuysen, Techniques Coupling for Catalyst Characterisation, in: Charact. Solid Mater. Heterog. Catal., Wiley-VCH Verlag GmbH & Co. KGaA, Weinheim, Germany, 2012: pp. 1075–1117.

[5] A. Paredes-Nunez, D. Lorito, Y. Schuurman, N. Guilhaume, F.C. Meunier, Origins of the poisoning effect of chlorine on the CO hydrogenation activity of alumina-supported cobalt monitored by operando FT-IR spectroscopy, J. Catal. 329 (2015) 229–236.

[6] J. Scalbert, F.C. Meunier, C. Daniel, Y. Schuurman, An operando DRIFTS investigation into the resistance against CO_2 poisoning of a Rh/alumina catalyst during toluenehydrogenation, Phys. Chem. Chem. Phys. 14 (2012) 2159–2163.

[7] J.J.H.B. Sattler, I.D. González-Jiménez, A.M. Mens, M. Arias, T. Visser, B.M. Weckhuysen, Operando UV-Vis spectroscopy of a catalytic solid in a pilot-scale reactor: deactivation of a CrO_x/Al_2O_3 propane dehydrogenation catalyst, Chem. Commun. 49 (2013) 1518.

[8] E. V. Kondratenko, N. Takahashi, N. Nagata, M. Ibe, H. Hirata, H. Takahashi, Operando UV/Vis Analysis of the Synergy Effect between Copper and Gold in Nitric Oxide Reduction over Gold and Copper on Alumina Catalysts, ChemCatChem. 7 (2015) 3956–3962.

[9] L.F. Bobadilla, J.L. Santos, S. Ivanova, J.A. Odriozola, A. Urakawa, Unravelling the Role of Oxygen Vacancies in the Mechanism of the Reverse Water–Gas Shift Reaction by Operando DRIFTS and Ultraviolet–Visible Spectroscopy, ACS Catal. 8 (2018) 7455–7467.

[10] H. Li, M. Rivallan, F. Thibault-Starzyk, A. Travert, F.C. Meunier, Effective bulk and surface temperatures of the catalyst bed of FT-IR cells used for in situ and operando studies, Phys. Chem. Chem. Phys. 15 (2013) 7321–7327.

[11] D. Lorito, H. Li, A. Travert, F. Maugé, F.C. Meunier, Y. Schuurman, C. Mirodatos, Understanding deactivation processes during bio-syngas methanation: DRIFTS and SSITKA experiments and kinetic modeling over Ni/Al_2O_3 catalysts, Catal. Today. 299 (2018) 172–182.

[12] B.M. Weckhuysen, Studying birth, life and death of catalytic solids with operando spectroscopy, Natl. Sci. Rev. 2 (2015) 147–149.

[13] J. Dupré, P. Bazin, O. Marie, M. Daturi, X. Jeandel, F. Meunier, Understanding the

storage function of a commercial NOx-storage-reduction material using operando IR under realistic conditions, Appl. Catal. B Environ. 160–161 (2014) 335–343.

[14] A. Paredes-Nunez, I. Jbir, D. Bianchi, F.C. Meunier, Spectrum baseline artefacts and correction of gas-phase species signal during diffuse reflectance FT-IR analyses of catalysts at variable temperatures, Appl. Catal. A Gen. 495 (2015) 17–22.

[15] A. Rodrigues, J. Tatibouët, E. Fourré, Operando DRIFT Spectroscopy Characterization of Intermediate Species on Catalysts Surface in VOC Removal from Air by Non-thermal Plasma Assisted Catalysis, Plasma Chem. Plasma Process. 36 (2016) 901–915.

[16] J.W. Niemantsverdriet, Spectroscopy in Catalysis, Wiley-VCH Verlag GmbH & Co. KGaA, Weinheim, Germany, 2007.

[17] L. Lemaitre, A. Berliet, S. Maury, M. Rivallan, Surface modifications of cobalt Fischer Tropsch catalyst followed by operando DRIFT and chemometrics, Catal. Today. 283 (2017) 172–175.

[18] M.P. Fuller, P.R. Griffiths, Diffuse reflectance measurements by infrared Fourier transform spectrometry, Anal. Chem. 50 (1978) 1906–1910.

[19] K.W. Van Every, P.R. Griffiths, Characterization of Diffuse Reflectance FT-IR Spectrometry for Heterogeneous Catalyst Studies, Appl. Spectrosc. 45 (1991) 347–359.

[20] F.C. Meunier, Pitfalls and benefits of in situ and operando diffuse reflectance FT-IR spectroscopy (DRIFTS) applied to catalytic reactions, React. Chem. Eng. 1 (2016) 134–141.

[21] F.C. Meunier, The power of quantitative kinetic studies of adsorbate reactivity by operando FTIR spectroscopy carried out at chemical potential steady-state, Catal. Today. 155 (2010) 164–171.

[22] F.C. Meunier, A. Goguet, C. Hardacre, R. Burch, D. Thompsett, Quantitative DRIFTS investigation of possible reaction mechanisms for the water–gas shift reaction on high-activity Pt- and Au-based catalysts, J. Catal. 252 (2007) 18–22.

[23] T. Armaroli, T. Bécue, S. Gautier, Diffuse Reflection Infrared Spectroscopy (Drifts): Application to the in-situ Analysis of Catalysts, Oil Gas Sci. Technol. 59 (2004) 215–237.

[24] J. Sneddon, S. Masuram, J.C. Richert, Gas Chromatography-Mass Spectrometry-Basic Principles, Instrumentation and Selected Applications for Detection of Organic Compounds, Anal. Lett. 40 (2007) 1003–1012.

[25] J. Dewulf, H. Van Langenhove, G. Wittmann, Analysis of volatile organic compounds using gas chromatography, TrAC Trends Anal. Chem. 21 (2002) 637–646.

[26] F.L. Dorman, E.B. Overton, J.J. Whiting, J.W. Cochran, J. Gardea-Torresdey, Gas Chromatography, Anal. Chem. 80 (2008) 4487–4497.

[27] R.L. Grob, E.F. Barry, eds., Modern Practice of Gas Chromatography, John Wiley & Sons, Inc., Hoboken, NJ, USA, 2004.

[28] B.M. Weckhuysen, Snapshots of a working catalyst: possibilities and limitations of in situ spectroscopy in the field of heterogeneous catalysis, Chem. Commun. (2002) 97–110.

[29] B.M. Weckhuysen, Determining the active site in a catalytic process: Operando spectroscopy is more than a buzzword, Phys. Chem. Chem. Phys. 5 (2003) 4351–4360.

[30] B.M. Weckhuysen, Operando spectroscopy: fundamental and technical aspects of spectroscopy of catalysts under working conditions, Phys. Chem. Chem. Phys. 5 (2003) 1.

[31] L. Pinard, P. Bichon, A. Popov, J.L. Lemberton, C. Canaff, F. Maugé, P. Bazin, E.F. S.-Aguiar, P. Magnoux, Identification of the carbonaceous compounds present on a deactivated cobalt based Fischer–Trospch catalyst resistant to "rejuvenation treatment," Appl. Catal. A Gen. 406 (2011) 73–80.

[32] Sulfinert®-Treated Stainless Steel Tubing, (2016). http://www.restek.com/pdfs/302-02-001.pdf (accessed September 6, 2016).

[33] Mass Flow Controllers & Meters, (2016). https://www.brooksinstrument.com/en/products/mass-flow-controllers (accessed October 10, 2016).

[34] GO Regulators, (2016). http://www.goreg.com/products/regulators/back/index.htm (accessed October 10, 2016).

[35] Ceraphant T PTP31, (2016). https://www.nl.endress.com/nl/Field-instruments-overview/pressure/Absolute-gauge-Ceraphant-PTP31 (accessed October 10, 2016).

[36] G.W. Thomson, The Antoine Equation for Vapor-pressure Data., Chem. Rev. 38 (1946) 1–39.

[37] D. Ambrose, N.B. Ghiassee, Vapour pressures and critical temperatures and critical pressures of some alkanoic acids: C_1 to C_{10}, J. Chem. Thermodyn. 19 (1987) 505–519.

[38] A.S. Coolidge, The vapor pressure and heats of fusion and vaporisation of formic acid, J. Am. Chem. Soc. 52 (1930) 1874–1887.

[39] M.L. Nahrwold, P. Archer, P.J. Cohen, Application of the Antoine equation to anesthetic vapor pressure data, Anesth. Analg. 52 (1973) 866–867.

[40] T.O. Eschemann, J.H. Bitter, K.P. de Jong, Effects of loading and synthesis method of titania-supported cobalt catalysts for Fischer–Tropsch synthesis, Catal. Today. 228 (2014) 89–95.

[41] J. Sirita, S. Phanichphant, F.C. Meunier, Quantitative analysis of adsorbate concentrations by diffuse reflectance FT-IR, Anal. Chem. 79 (2007) 3912–3918.

[42] R.L. Mössbauer, Kernresonanzfluoreszenz von Gammastrahlung in Ir191, Zeitschrift Für Phys. 151 (1958) 124–143.

[43] Y. Yoshida, G. Langouche, eds., Mössbauer Spectroscopy, Springer Berlin Heidelberg, Berlin, Heidelberg, 2013.

[44] M.W.J. Crajé, A.M. van der Kraan, J. van de Loosdrecht, P.J. van Berge, The application of Mössbauer emission spectroscopy to industrial cobalt based Fischer–Tropsch catalysts, Catal. Today. 71 (2002) 369–379.

[45] G.J. Long, Industrial Applications of the Mössbauer Effect, Springer US, Boston, MA, 1986.

[46] M.D. Dyar, D.G. Agresti, M.W. Schaefer, C.A. Grant, E.C. Sklute, Mössbauer spectroscopy of Earth and Planetary Materials, Annu. Rev. Earth Planet. Sci. 34 (2006) 83–125.

[47] S. Nasu, General Introduction to Mössbauer Spectroscopy, in: Y. Yoshida, G. Langouche (Eds.), Mössbauer Spectrosc. Tutor. B., Springer Berlin Heidelberg, Berlin, Heidelberg, 2013: pp. 1–22.

[48] F.J. Berry, Industrial Applications of Mössbauer Spectroscopy, Hyperfine Interact. 144 (2002) 381–390.

[49] J.W. Niemantsverdriet, Mössbauer Spectroscopy, in: Spectrosc. Catal., Third Edit, Wiley-VCH Verlag GmbH & Co. KGaA, Weinheim, Germany, 2007: pp. 121–146.

[50] J.-M.M. Millet, Mössbauer Spectroscopy in Heterogeneous Catalysis, in: Adv. Catal. Vol 51, 2007: pp. 309–350.

[51] G.L. Bezemer, T.J. Remans, A.P. Van Bavel, A.I. Dugulan, Direct evidence of water-assisted sintering of cobalt on carbon nanofiber catalysts during simulated Fischer-Tropsch conditions revealed with in-situ Mössbauer spectroscopy, J. Am. Chem. Soc. 132 (2010) 8540–8541.

[52] A.I. Dugulan, M.W.J. Crajé, G.J. Kearley, High-pressure in situ Mössbauer emission spectroscopy study of the sulfidation of calcined Co–Mo/Al_2O_3 hydrodesulfurization catalysts, J. Catal. 222 (2004) 281–284.

[53] J.A. Dumesic, H. Topsøe, Mössbauer Spectroscopy Applications to Heterogeneous Catalysis, in: Adv. Catal., 1977: pp. 121–246.

[54] A.I. Dugulan, J.A.R. van Veen, E.J.M. Hensen, On the structure and hydrotreating performance of carbon-supported CoMo- and NiMo-sulfides, Appl. Catal. B Environ. 142–143 (2013) 178–186.

[55] A.I. Dugulan, E.J.M. Hensen, J.A.R. van Veen, High-pressure sulfidation of a calcined CoMo/Al_2O_3 hydrodesulfurization catalyst, Catal. Today. 130 (2008) 126–134.

[56] A.I. Dugulan, E.J.M. Hensen, J.A.R. van Veen, Effect of pressure on the sulfidation behavior of NiW catalysts: A ^{182}W Mössbauer spectroscopy study, Catal. Today. 150 (2010) 224–230.

[57] P. Gütlich, E. Bill, A.X. Trautwein, Mössbauer Spectroscopy and Transition Metal Chemistry, Springer Berlin Heidelberg, Berlin, Heidelberg, 2011.

[58] P. Gütlich, J. Ensling, Mössbauer Spectroscopy, in: Ullmann's Encycl. Ind. Chem., Wiley-VCH Verlag GmbH & Co. KGaA, Weinheim, Germany, 2001.

[59] R.H. Herber, The Mössbauer Effect and Its Application in Chemistry, in: 1967: pp. 1–20.

[60] S. Nikolov, K. Kantchev, Deconvolution of Lorentzian broadened spectra part I: Direct deconvolution, Nucl. Instruments Methods Phys. Res. Sect. A Accel. Spectrometers, Detect. Assoc. Equip. 256 (1987) 161–167.

[61] Z. Klencsár, Mössbauer spectrum analysis by Evolution Algorithm, Nucl. Instruments Methods Phys. Res. Sect. B Beam Interact. with Mater. Atoms. 129 (1997) 527–533.

[62] M. Blume, J.A. Tjon, Mössbauer Spectra in a Fluctuating Environment, Phys. Rev. 165 (1968) 446–456.

2

Chapter 3

Effect of pressure and temperature on the carboxylates deposition on the catalyst surface during Fischer-Tropsch synthesis

The effect of pressure and temperature on the formation of oxygenated compounds on the surface of the Co/TiO_2 catalyst during Fischer-Tropsch synthesis (FTS) and their possible involvement in the deactivation mechanism were investigated using Diffuse Reflectance Infrared Fourier Transform (DRIFT) spectroscopy. The formation and accumulation of carboxylate compounds on the surface of the catalyst have been observed. High molecular weight carboxylates are dominant at high pressure and low temperature due to the high content of olefins, resulting in the formation of more carboxylates via hydroformylation side reaction.

3.1. Introduction

Fischer-Tropsch synthesis (FTS) is a catalytic process that produces a broad distribution of clean liquid fuels and chemicals from syngas obtained from natural gas, coal and biomass [1,2]. Cobalt-based catalysts are preferred in FTS processes due to their high activity, high selectivity to linear paraffins and low water-gas shift activity. However, the challenge with cobalt-based FTS catalysts is that they deactivate over time [3–8]. To make the FTS process economically effective, a stable performance of the catalyst is required. Therefore, studying the catalyst deactivation is an important topic in the development of better industrial catalysts. The general reasons for catalyst deactivation are poisoning, re-oxidation, deposition of carbonaceous and oxygenated compounds and sintering of active phase [3,4]. The poisoning of cobalt can be avoided by purifying the feed gas properly before the reaction. Oxidation of Co-based catalysts has been studied and ruled out as deactivation mechanism [9,10]. Sintering is the loss of active metal surface area due to the crystalline growth of metal particles and takes place via Ostwald ripening and/or coalescence [3,11,12]. Kistamurty et al. [13] proposed that Ostwald ripening is the most dominating mechanism from transition electron microscopy (TEM) experiments on a Co/SiO_2 catalyst. The deactivation by different carbonaceous species deposition on the catalyst surface has been studied earlier [4–6]. Moodley et al. [6] identified different types of carbon species: atomic carbon, residual wax in the pores of the catalyst and polymeric carbon on a spent $Co/Pt/Al_2O_3$ FTS catalyst, using temperature-programmed hydrogenation mass spectrometry (TPH-MS). From their studies, it was concluded that only polymeric carbon contributes to the long-term deactivation. Peña et al. [14] proposed that strongly adsorbed hydrocarbons and amorphous polymeric carbon seem to be contributing to the catalyst deactivation. Also, Tan et al. [15] found two types of resilient carbon species (surface carbide and poly-aromatic carbon) after wax extraction, when they studied the $Co(20\ wt\%)/\gamma\text{-}Al_2O_3$ FTS catalyst in a fixed bed micro-reactor.

FTS produces not only hydrocarbons but also small quantities of oxygenated compounds such as alcohols, carboxylic acids, ketones and esters [16]. Kollar et al. [17] reported the formation of several oxygenated compounds on the surface of $Co(15\%)+Pt(0.5\%)/\gamma\text{-}Al_2O_3$ catalyst. Paredes-Nunez et al. [18,19] found the presence of two types of formate species (fast reacting and slow reacting formate species) using infrared spectroscopy on a Co/Siralox catalyst. Fast reacting formates located either on the cobalt-alumina interface or on the cobalt oxide phase, were proposed to be the reaction intermediates for the formation of methanol. Whereas, slow reacting formates are inert spectator species located on the support. Jalama et al. [20] investigated the effect of ethanol addition during FTS using a Co/TiO_2 catalyst. They found that the ethanol addition increased the selectivity to light products, increased the olefin to paraffin ratio and decreased the catalyst activity. These effects were reversible when ethanol was removed from the feed. This has been attributed to oxidation of Co to CoO by ethanol and re-reduction to Co when ethanol was removed from the feed to recover its initial activity.

Scalbert et al. [21] found deposition of oxygenated compounds (most likely carboxylic acids and aldehydes) and an increase in their amount with time on a Co/Al_2O_3 FTS catalyst using XRD-DRIFT spectroscopy. They proposed that these strongly adsorbed species are responsible for catalyst deactivation by covering the active sites. Pinard et al. [22] analysed the different

types of carbon species present on the spent $Co/Ru/Al_2O_3$ FTS catalyst. Carbon extracted from the spent catalyst was found to be consisting of atomic carbon, alcohols, carboxylic acids and polymeric carbon. Temperature programmed hydrogenation–infrared (TPH-IR) indicated that complete removal of carboxylate species from the catalyst surface required temperatures above 600 ^oC. They found that only carboxylic acids and polymeric carbon were resistant to a rejuvenation treatment under hydrogen. It was proposed that these high molecular weight (MW) carboxylic acids formed during FTS may also block the cobalt active sites and deactivate the catalyst [22].

Fourier Transform infrared (FTIR) spectroscopy is the most widely used and the most effective spectroscopic technique for characterization of the surface chemistry of heterogeneous catalysts [23]. The chemical nature of the surface species deposited on the catalyst surface, like pure carboxylic acids and their bonding with the catalyst, can be identified using FTIR. Generally, pure carboxylic acids can be identified by their carbonyl C=O stretching vibrational band in the range of 1755-1650 cm^{-1} [24,25]. When carboxylic acids interact with catalyst and form carboxylates (RCOO-), the peak position shifts to lower wavenumber depending on the type of catalyst material [22,26,27]. To study the deposition of carboxylates on the catalyst surface effectively it is necessary to employ an *in-situ* infrared reaction cell, in which infrared spectra could be obtained while the samples are subjected to a wide range of temperatures and pressures. These experiments not only make it possible to study the adsorbed molecules, while FTS reaction is in progress, but also open ways to understand the catalyst deactivation mechanisms and to develop better industrial catalysts.

The effect of pressure and temperature on the performance of the catalyst has been studied extensively [28–32]. However, the formation of oxygenated compounds on the catalyst surface and their role in catalyst deactivation during FTS at different operational conditions is not explored very well. Therefore, the aim of this study is to investigate the effect of pressure and temperature on the formation of oxygenated compounds on the surface of the Co/TiO_2 catalyst during FTS and their possible involvement in the deactivation mechanism, using diffuse reflectance infrared Fourier Transform (DRIFT) spectroscopy.

3.2. Experimental

3.2.1. Catalyst preparation

$Co(10\ wt\%)/TiO_2$ - IWI catalyst provided by Shell Global Solutions International B.V., Amsterdam was prepared by two step impregnation. First, the support material (Degussa P25 with surface area 50 $m^2.g^{-1}$ and pore volume 0.319 $mL.g^{-1}$) was dried and impregnated with 1 pore volume of an aqueous solution of $Co(NO_3)_2$ (17.25 wt% Co). In the second impregnation, the obtained material (pore volume 0.283 $mL.g^{-1}$) was impregnated with 0.95 pore volume of an aqueous solution of $Co(NO_3)_2$ (20.02 wt% Co). After each impregnation step, the obtained material was dried in an oven at 60 ^oC overnight under static air and calcined at 400 ^oC for 2 hours under N_2 flow.

3.2.2. Employment of operando DRIFT reaction setup

To study the effect of pressure and temperature on the carboxylates deposition in FTS, an operando DRIFT reaction setup was employed. The design, optimisation details and the scheme of the reaction setup are described in Chapter 2.

3.2.3. Adsorption of carboxylic acids on TiO_2 support and Co/TiO_2 catalyst

Co/TiO_2 catalyst was reduced at 350 ^oC in 100 mL/min of H_2 standard DRIFT reaction cell and then the reaction cell was cooled down to the room temperature. After this step, a small amount of carboxylic acid was adsorbed on the Co/TiO_2 surface by flowing Ar gas containing carboxylic acids at 0.1 MPa. This was achieved by flowing Ar gas through a saturator containing required pure carboxylic acid (formic, acetic and hexanoic acids). After this step, the Co/TiO_2 catalyst was dried by a continuous flow of Ar gas to remove excess acid in the reaction cell. The same procedure was followed for the adsorption of acids on the TiO_2 support.

3.2.4. Catalytic testing

FTS experiments were performed at different pressures (0.18 MPa and 2 MPa) and at different temperatures (200 ^oC and 220 ^oC) with H_2/CO = 2 v/v and space velocity (SV) = 120 L/g.h. 50 mg of Co/TiO_2 catalyst was loaded into the reaction cell and reduced at 350 ^oC in 100 mL/min of H_2 for 2 hours. The reaction cell was cooled down to the reaction temperature and a background spectrum was measured in a mixture of Ar/H_2. After introducing the reaction gas mixture, the pressure was increased to the desired value. The reaction products were analysed with an on-line Thermo Scientific Trace Ultra GC with split injection mode. Permanent gases were analysed with a Carboxen 1010 column connected to a TCD detector and hydrocarbons were analysed with an Rtx-1 column connected to a FID detector. The olefins to paraffins (O/P) ratio is reported from C_5 to C_9, as they are optimally separated in the FID column.

3.3. Results and discussion

3.3.1. Adsorption of carboxylic acids

To identify the different carboxylates deposited on the catalyst surface during FTS, infrared spectra of Co/TiO_2 catalyst and TiO_2 support with a series of adsorbed carboxylates ($HCOO^-$, CH_3COO^- and $C_5H_{11}COO^-$) were measured and presented in Figure 3.1a and 3.1b. As shown in Figure 3.1a, a broad band at 1590 cm^{-1} and two other bands at 1386 cm^{-1} and 1328 cm^{-1} are corresponding to asymmetric (ν_{as}) and symmetric vibrations (ν_s) of formate species ($HCOO^-$) [18]. The band at 1558 cm^{-1} of adsorbed acetic acid and the band at 1541 cm^{-1} of adsorbed hexanoic acid are corresponding to asymmetric vibrations [22,33]. The band at 1457 cm^{-1} is corresponding to CH_2 bending vibrations of adsorbed acetic and hexanoic acids. The frequency of asymmetric (ν_{as}) vibrations decreased with increasing chain length of carboxylic acids due to the decrease in vibrational energy of the COO^- group with the addition of a $-CH_2-$ group to the carbon chain. In the case of very long chain carboxylates, the effect of $-CH_2-$ addition is negligible because the influence of additional $-CH_2-$ on the COO^- group is very weak [22]. Absorption bands at 1556, 1537 and 1515 cm^{-1} are corresponding to asymmetric (ν_{as}) vibrations of formate, acetate and hexanoate adsorbed on the TiO_2 as shown in Figure 3.1b. As expected,

the frequency of asymmetric (ν_{as}) vibrations decreased with increasing chain length of carboxylic acids. However, the infrared band positions of carboxylates on the TiO_2 support shifted to lower wavenumber compared to infrared band positions of carboxylates on the catalyst. This is due to the difference in interaction energies of carboxylic acids with Co/TiO_2 and TiO_2. Pinard et al. [22] also found a similar trend of decreasing frequency of asymmetric (ν_{as}) vibrations with increasing chain length of carboxylic acids, when studying adsorbed carboxylates on an alumina support. One more point is that the infrared peak of carboxylates on CoO (unreduced catalyst) is ~10 cm^{-1} lower than the frequency of the infrared peak of carboxylate on Co as shown in Figure S3.1.

Wu et al. [27] studied the interaction between oleic acid ($C_{17}H_{33}COOH$) monolayers and Co nanoparticles. They found that the C=O stretching band of the carboxyl group at 1710 cm^{-1} in the infrared spectrum of pure oleic acid, is not present in the spectrum of the oleic acid coated Co nanoparticles. Instead, two new bands at 1556 and 1410 cm^{-1} corresponding to the asymmetric ν_{as}(COO-) and the symmetric ν_s(COO-) stretching appeared. Their results demonstrated that oleic acid was chemisorbed on the surface of Co nanoparticles as a carboxylate and the two oxygen atoms of the carboxylate species are coordinated symmetrically to the Co atoms that lead to the formation of the Co−O covalent bond.

These results clearly show that carboxylates adsorbed on Co/TiO_2 catalyst interact with both Co metal and TiO_2 support. From infrared spectra, it is possible to distinguish formate species adsorbed on Co metal and TiO_2 support. However, it is difficult to make the distinction in the case of the higher carboxylates.

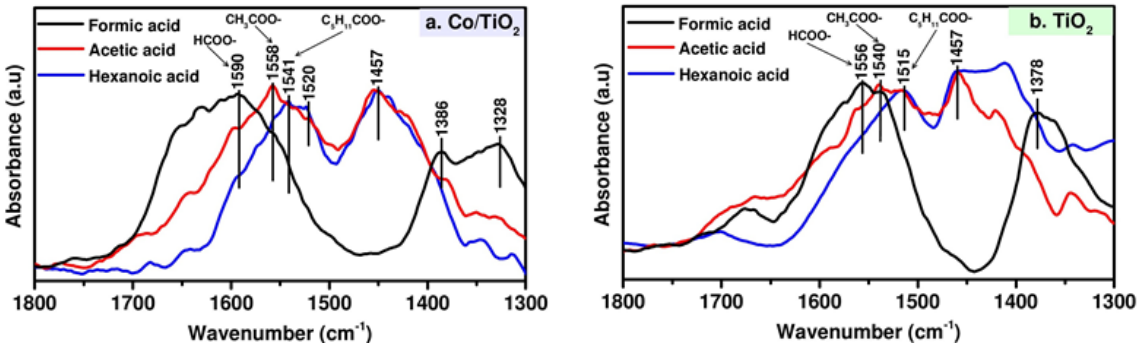

Figure 3.1: DRIFT spectra of model carboxylates (HCOO-, CH_3COO- and $C_5H_{11}COO$-) adsorbed on (**a**) Co/TiO_2 catalyst and **(b)** TiO_2 support.

To get a better view, the infrared spectra of the carboxylates on Co/TiO_2 catalyst and TiO_2 support are presented in the same graph as shown in Figure 3.2. The infrared peak positions of HCOO- on Co/TiO_2 catalyst is at 1590 cm^{-1}; the peak position shifted to lower wavenumber 1556 cm^{-1} when HCOO- is on the TiO_2 support, due to the difference in interaction energy of HCOO- with Co/TiO_2 and TiO_2 (see Figure 3.2a). Similar results are observed for the interaction of acetic acid and hexanoic acid with Co/TiO_2 and TiO_2 as shown in Figure 3.2b and 3.2c.

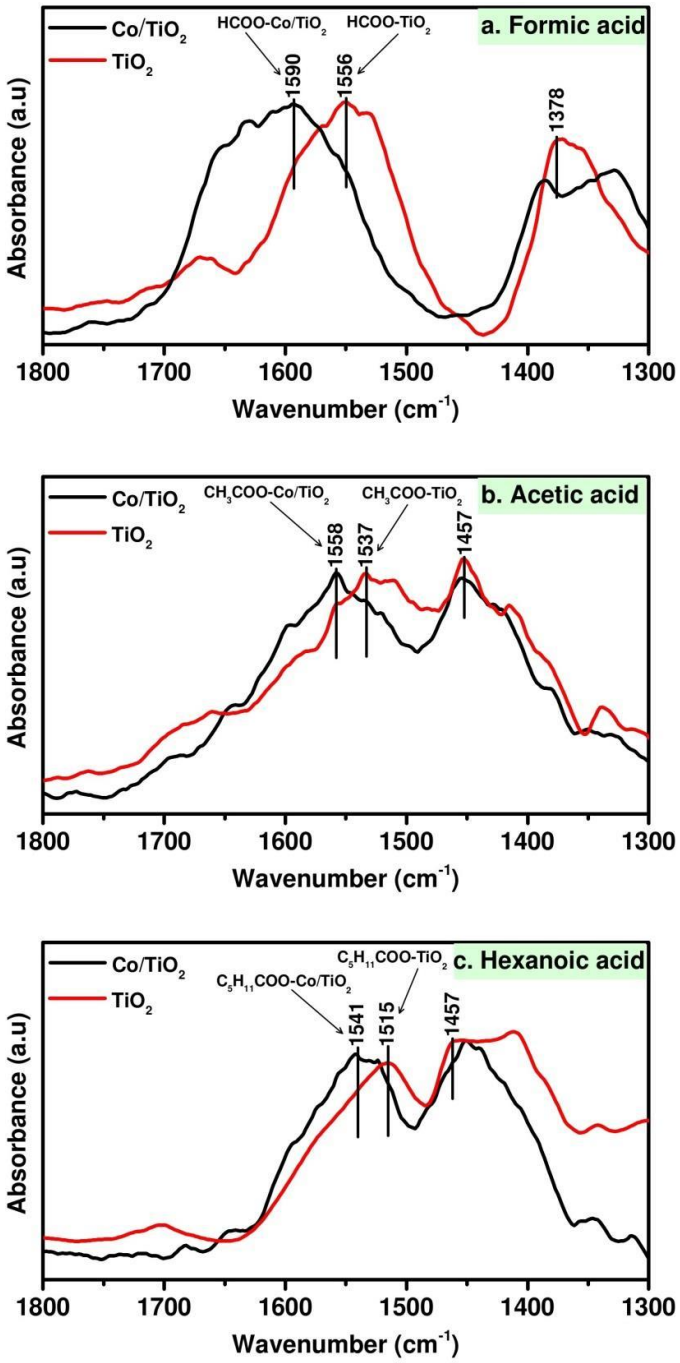

Figure 3.2: DRIFT spectra of model carboxylic acids (**a**) Formic acid, (**b**) Acetic acid and **(c)** Hexanoic acid adsorbed on Co/TiO_2 catalyst and TiO_2 support.

The number of carboxylic acid molecules required to make a full monolayer coverage on Co/TiO_2 catalyst is estimated and shown in Table 3.1. The number of required carboxylic acid molecules to make full coverage decreased from formic acid to hexanoic acid as the cross sectional area of the molecules increases with increasing molecular weight [34]. About 12% of the total carboxylic acid molecules deposit on Co surface and remaining ~88% on TiO_2 surface in Co/TiO_2 catalyst as 10 wt% Co is distributed on the TiO_2 support with an average particle size ~10 nm.

Table 3.1: No. of acid molecules required to make a full monolayer coverage Co/TiO_2 catalyst.

Carboxylic acid	No. of molecules on Co/TiO_2 (Per gram)
HCOOH	$1.694 \cdot 10^{20}$
CH_3COOH	$1.366 \cdot 10^{20}$
$C_5H_{11}COOH$	$0.783 \cdot 10^{20}$

3.3.2. Effect of pressure

As shown in Table 3.2, an increase in pressure from 0.18 MPa to 2 MPa enhances the activity of the catalyst and causes an increase in C_{5+} selectivity and a decrease in C_1-C_4 selectivities. These results are in good agreement with earlier reports of Co-based FTS catalysts. For example, Fierro et al. [28] reported a similar effect of pressure on FTS activity and selectivity with Co/SiO_2 catalyst from 2 to 4 MPa. Mendes et al. [29] also reported an increase in activity and C_{5+} selectivity with increasing pressure from 0.4 to 2 MPa. Also, the chain growth probability (α) increases with increasing pressure and decreasing temperature as shown in Table 3.2, indicating that high pressure and low temperature favour selectivity to higher hydrocarbons. A similar tendency of α with varying pressure and temperature was observed for all other FTS studies [35]. For example, Yan et al. [36] reported an increase in α with increasing pressure, when they studied a Co/SiO_2 catalyst and Johnson et al. [37] reported a decrease in α with increasing temperature, with a Co/Al_2O_3 catalyst.

Table 3.2: Performance of the Co(10 wt%)/TiO_2 (IWI) FTS catalyst at different pressures and temperatures after TOS 4 days.

FTS conditions P=[MPa], T=[°C]	Activity Mol $CO.g_{Co}^{-1}.s^{-1}$	Selectivity (%) on carbon basis				O/P	α
		C_1-C_2	C_3	C_4	C_{5+}		
P=0.18, T=220	$3.5 \pm 0.7 \cdot 10^{-7}$	37.0	21.3	17.3	24.4	1.9	0.46
P=2, T=220	$2.2 \pm 0.2 \cdot 10^{-5}$	8.4	3.4	5.2	83.0	1.4	0.83
P=2, T=200	$4.0 \pm 0.6 \cdot 10^{-6}$	6.8	2.5	6.0	84.7	2.1	0.95

O/P: Olefins C_5 to C_9/Paraffins C_5 to C_9, **α**: Chain growth probability

Not only the chain growth probability (α) but also the ratio of olefins (O) and paraffins (P) is an important parameter in FTS. The O/P ratio not only depends on the carbon number but also strongly depends on the operating conditions such as pressure, temperature and the type of reactor. Anderson–Schulz–Flory (ASF) plots are generally used to analyse the product distribution of FTS [38]. Figures 3.3a and 3.3b show the ASF plots for the FTS reaction at different pressures and temperatures.

Figure 3.3a shows the effect of the reaction pressure on the O/P ratio at 220 °C. The O/P ratio decreased with carbon number (C_5 to C_9). This is most likely related to the readsorption of the

olefins and their secondary hydrogenation. This trend is similar to many reports in the literature [30,31]. Shi and Davis [39] observed a decrease in the O/P ratio with carbon number for their cobalt catalyst. An exponential decrease in the ratio of O/P with chain number was observed for Fe, Co and Ru FTS catalysts [40–42]. This exponential decrease in O/P ratio is attributed to the olefins readsorption mechanism [43]. The probability of olefin readsorption depends on the heat of physisorption of olefins on the catalyst surface and the heat of dissolution and their diffusivity through the wax product. Recently, by using density functional theory (DFT) calculations, Qi et al. [44] proposed that the O/P ratio decreases with carbon chain length and the adsorption energy of olefins is the dominating factor rather than the activation energy of their hydrogenation reactions for carbon number-dependent O/P ratio. The decrease in diffusion coefficients of the products with increasing chain length affects the selectivity to olefins and paraffins [45]. The ratio of O/P depends also on the operating variables such as pressure, temperature, composition of the syngas, nature of the catalyst and type of the reactor [30,31]. The ratio of O/P (total C_5 to C_9) with varying pressure and temperature is shown in Figure 3.4. The ratio of O/P (total C_5 to C_9) is less at 2 MPa compared to 0.18 MPa due to the conversion of olefins into paraffins by re-adsorption and secondary reactions of olefins at high pressure. In the FTS reaction, the growing linear alkyl chains are chemically bound to the catalyst surface. Later this bond can be broken by α-hydrogenation yielding an n-paraffin or by β-hydrogen abstraction yielding an α-olefin. The formed n-paraffins are non-reactive under FTS conditions and not prone to participate in the secondary reactions, while the α-olefins are reactive under FTS conditions and have an opportunity of being hydrogenated or reinserted into chain growth reactions by readsorption on the catalyst surface [41]. One possible secondary reaction is hydroformylation reaction where CO is inserted in α-olefin carbon chain to form oxygenated compounds like alcohols and aldehydes. These alcohols and aldehydes further convert into carboxylic acids by reacting with water [46–48].

The probability of secondary reactions and readsorption properties of α-olefins increases strongly with the carbon number and proportional to the contact time of the olefins with the catalyst surface as proposed by many authors [43,49]. Other experimental conditions like reactor type and operational conditions also influence the residence time of the products on the catalyst. Jacobs et al. [50] tested a Co/Al_2O_3 catalyst in normal fixed bed, fixed bed under supercritical conditions and continuous stirred tank reactor (CSTR). They found that the O/P ratio of hydrocarbon from C_3 to C_{20} was higher for normal fixed bed than fixed bed under supercritical conditions and CSTR. This is due to lower residence times of intermediate olefins in normal fixed bed reactor. Readsorption of olefins in the FTS reaction was also confirmed by olefin co-feeding studies. These studies showed that olefins could undergo secondary hydrogenation, chain initiation and isomerization depending on the reaction conditions and type of the catalyst [51–53].

With increasing carbon number, the vapor pressure of the FTS products decreases [54–60]. Therefore, the residence time of the products in the catalyst bed is longer and this enhances the possibility of readsorption and hydrogenation, causing the decrease of the O/P ratio. Kapteijn et al. [30] proposed that the probability of olefins to re-adsorb on the catalyst increases

exponentially with increasing carbon number, and they are hydrogenated independently of the chain growth process.

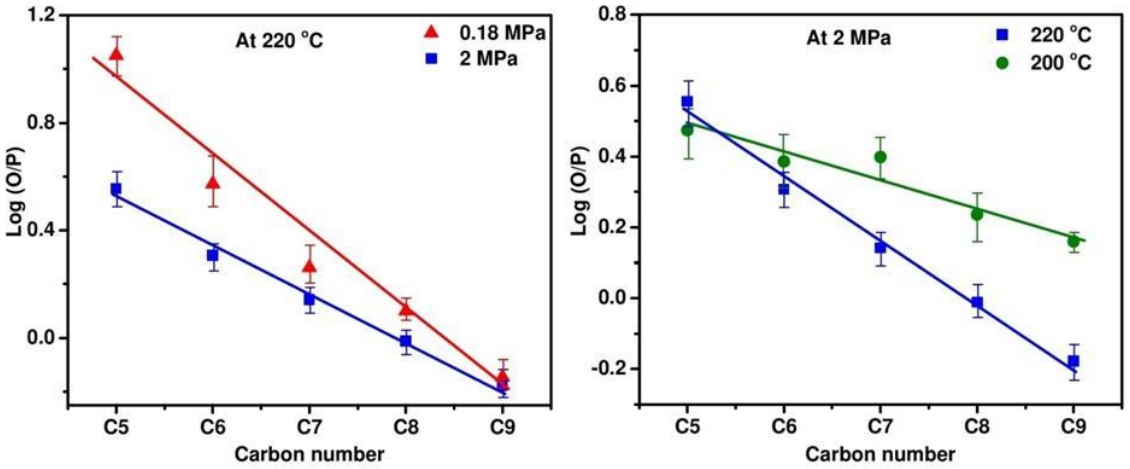

Figure 3.3: O/P ratio against carbon number, **(a)** Effect of the reaction pressure at 220 °C, **(b)** Effect of the reaction temperature at 2 MPa.

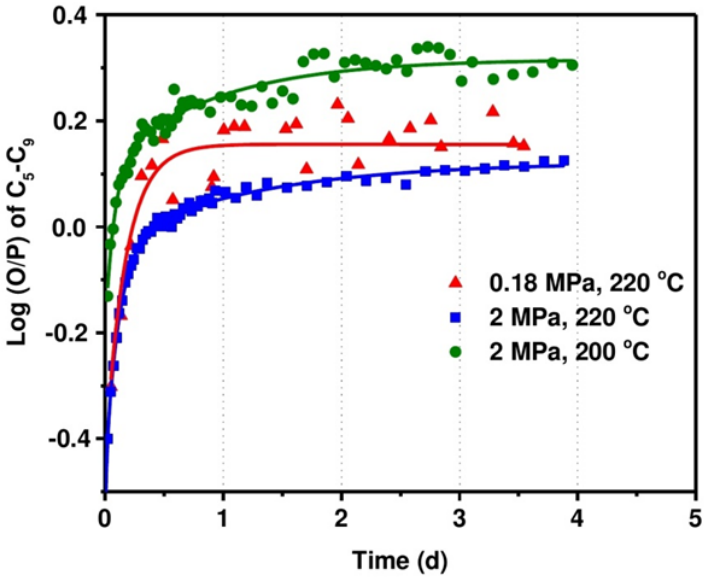

Figure 3.4: O/P ratio as a function of the time on stream.

The infrared spectra of Co/TiO_2 catalyst during FTS at different pressures are shown in Figures 3.5a-b. Different types of carboxylates were deposited on the surface of the catalyst and their amount increased with time. The bands at 1589 cm^{-1} and 1360 cm^{-1} are corresponding to asymmetric ν_{as}(COO-) and symmetric ν_s(COO-) vibrations of formate species on the catalyst surface. The bands at 1560 cm^{-1} and 1540 cm^{-1} at 2 MPa are attributed to asymmetric vibrations of acetate $\nu_{as}(CH_3COO-)$ and hexanoate $\nu_{as}(C_5H_{11}COO-)$ on the catalyst. The peaks 1527 cm^{-1} and 1515 cm^{-1} are corresponding to high molecular weight (MW) carboxylates. The band at 1456 cm^{-1} is due to CH_2 bending vibrations of carboxylic acids and hydrocarbons. At 0.18 MPa, the surface of the catalyst is dominated by low MW carboxylates (formate species) most of the

time and their amount increased with time. At 2 MPa, initially, the catalyst surface is dominated by low MW carboxylates, while later mostly high MW carboxylates are observed. The intensity of these carboxylates increased with time due to their accumulation on the catalyst surface. The formation of carboxylate compounds on the surface of FTS catalyst has been observed previously by Kollar et al. [17] and Paredes-Nunez et al. [18,19] using DRIFT spectroscopy. Formate species are always dominant at 0.18 MPa and for the first 12 hours of the reaction at 2 MPa on the surface of the catalyst. These formate species could be part of the reaction chain initiation as proposed by Davis et al. [61] in Fe-based FTS catalyst. As shown in Figure 3.4a, at 2 MPa, high molecular weight carboxylates became dominant very fast compared to the FTS at 0.18 MPa. The difference in activity between low and high pressure is significant, producing larger amounts of carboxylic acids at 2 MPa. Carboxylates also follow the ASF distribution; so light acids are more prevalent. However, high MW acids are more stable compared to low MW acids on the catalyst surface. The peak at 1650 cm^{-1} assigned to C=C vibrations at 0.18 and 2 MPa is suggesting the formation of olefins on the catalyst surface [62].

The ratio of O/P (C_5-C_9) increased with time on stream (TOS) for all experiments as shown in Figure 3.4. Also from DRIFT measurements, it was observed that the amount of carboxylates increased on the surface of the catalyst with TOS. It is apparent that there is a relation between carboxylates deposition on the catalyst surface and the formation of olefins in the reaction. The same relation between olefins formation and carboxylates deposition was also confirmed with samples containing different amounts of surface carboxylate species [63], results presented in detail in the next chapter. Gu et al. [64] found significant effects on the activity and selectivity of the Co/Al_2O_3 FTS catalyst in the presence of acetic and butyric acids in the feed. A shift in the selectivity from paraffins to olefins in the presence of these carboxylic acids was observed. They proposed that this effect is due to the prevention of secondary hydrogenation of olefins by the intermediate esters formed on the catalyst surface from carboxylic acids. Gnanamani et al. [65] studied the effect of deuterium labelled ethanol co-feeding on an iron catalyst and found the presence of deuterium in both olefins and paraffins and an increase in the olefin to paraffin ratio of C_2, C_3 and C_4 hydrocarbons. They proposed that C_2 species derived from the deuterium labelled ethanol acted as initiators for the FTS process. Jalama et al. [20] also found an increase in olefin to paraffin ratio with ethanol addition during FTS using a Co/TiO_2 catalyst.

Infrared spectra of the Co/TiO_2 catalyst in the C-H stretching region at different pressures are shown in Figure 3.5b. The bands at 2960 cm^{-1} and 2927 cm^{-1} are corresponding to asymmetric vibrations of CH_3 and CH_2 and the band at 2857 cm^{-1} is corresponding to symmetric vibrations of CH_2 species. The intensity of these peaks increases with time due to an accumulation of wax on the catalyst surface. As expected, the intensity of CH_3 and CH_2 bands is higher at 2 MPa than 0.18 MPa because of the faster accumulation of wax due to higher activity with increasing pressure.

The carbon chain length of hydrocarbons produced in the reaction can be estimated by using the ratio of CH_2/CH_3 species as follows [66].

$$\text{Ratio of } CH_2/CH_3 \text{ species} = \frac{\text{Area of } CH_2\text{species}/\varepsilon_1}{\text{Area of } CH_3\text{species}/\varepsilon_2}$$

Where:

1. Area of CH_2 species is the area of the peak at 2925-2930 cm^{-1} corresponding to the asymmetric stretch of CH_2 species
2. Area of CH_3 species is the area of the peak at 2955-2960 cm^{-1} corresponding to the asymmetric stretch of CH_3 species
3. ε_1 is the molar extinction coefficient of the CH_2 species (75 $mole^{-1}.l.cm^{-1}$)
4. ε_2 is the molar extinction coefficient of the CH_3 species (70 $mole^{-1}.l.cm^{-1}$) [66]

Here, in this study, the band areas of CH_2 and CH_3 species is used to identify the hydrocarbon chain length. The ratio of CH_2/CH_3 species increased with pressure from 0.18 MPa to 2 MPa due to increasing the value of α with increasing pressure, leading to the formation of longer chain length hydrocarbons. At 2 MPa, the estimated average carbon chain length of the hydrocarbons deposited on the catalyst surface is 10 on the 4th day of the FTS reaction. Navarro et al. [67] used an *in-situ* scanning tunnelling microscope (STM) to monitor a Co catalyst under reaction conditions. They found that during reaction Co is covered by a parallel array of strips. They proposed that these strips are formed by the self-assembly of linear hydrocarbon product molecules. The estimated carbon chain length of strips was 14 or 15 carbon atoms. The difference in reported carbon chain length may be due to differences in experimental conditions like space velocity and type of the reactor.

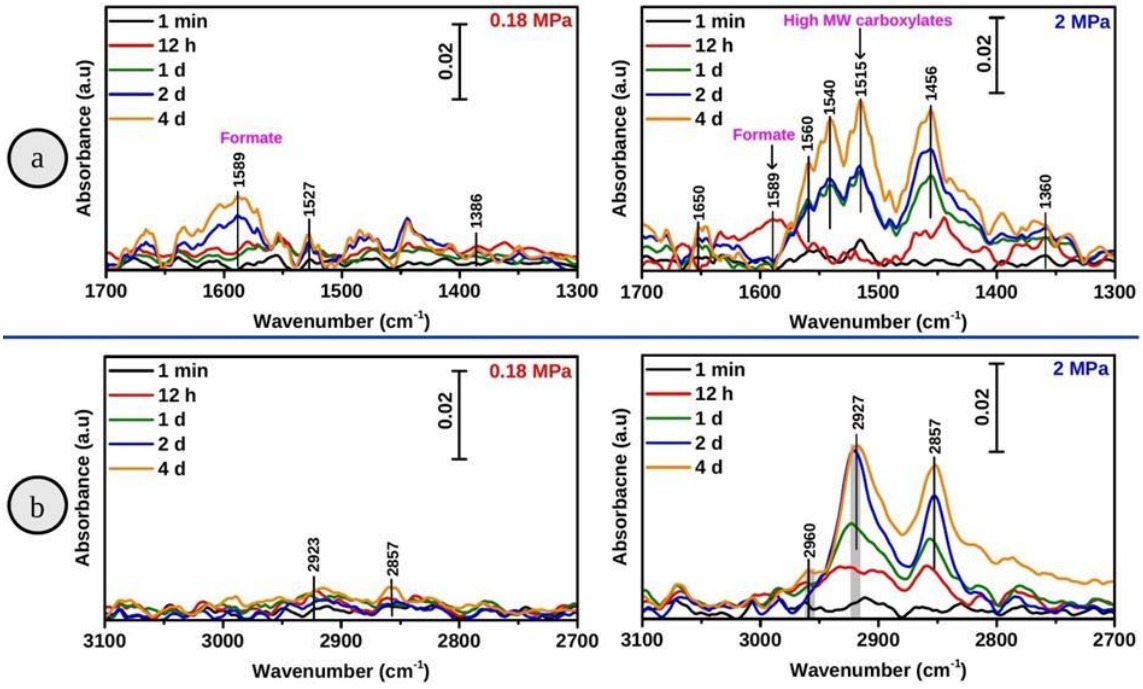

Figure 3.5: DRIFT spectra of the Co/TiO_2 catalyst at 0.18 and 2.0 MPa and at 220 °C, (**a)** Carboxylate region and **(b**) C-H stretching region.

3.3.3. Effect of temperature

As shown in Table 3.2, the temperature shows a remarkable effect on the activity and a small effect on the selectivity of the Co/TiO_2 FTS catalyst. The higher temperature increases the activity of the catalyst, decreases the C_{5+} selectivity and increases the C_1-C_4 selectivities. Kapteijn et al. [30,31] also found an increase in the activity and C_1 selectivity of the monolithic catalysts, when they studied FTS with varying temperatures from 180 ºC to 220 ºC. Pendyala et al. [32] investigated the effect of reaction temperature on the performance of a Pt(0.5%)–$Co(25\%)/Al_2O_3$ catalyst during aqueous phase FTS using a stirred tank reactor in batch mode operation. They reported an increase in activity with increasing temperature and a decrease in selectivity towards oxygenates. They also found that the C_1-C_4 selectivities increased with increasing reaction temperature and the corresponding higher hydrocarbon (C_{5+}) selectivity decreased.

The influence of operating temperature at 2 MPa on the ratio of O/P against carbon number is shown in Figure 3.3b. As expected, the O/P ratio decreased with increasing carbon number and is higher at 200 ºC compared to 220 ºC. This is because the high reaction temperature favours chain termination or desorption reactions towards paraffin formation, as desorption is an endothermic process [32,36].

The DRIFT spectra of the Co/TiO_2 catalyst during FTS at different temperatures are shown in Figures 3.6a-b. At 200 ºC, the high MW carboxylates became dominant from the beginning of the reaction even though the activity of the catalyst is low compared to the activity at 220 ºC. In the case of the 220 ºC experiment, only the low MW carboxylates are present at the beginning of the reaction, but later the surface is also dominated by high MW carboxylates. Mendes et al. [62] also found that the intensity of formate species increased with temperature favouring the formation of low MW carboxylates at high temperatures. The intensity of the band at 1650 cm^{-1} assigned to the C=C vibrations is higher at 200 ºC than at 220 ºC suggesting the preferential formation of more olefins on the catalyst surface at 200 ºC [62].

The O/P ratio (total C_5-C_9) increased with time and is higher at 200 ºC than at 220 ºC as shown in Figure 3.4. In addition, the amount of carboxylates on the catalyst surface increased with time and is higher at 200 ºC. From this observation, again it seems that the formation of carboxylates on the catalyst surface is related to the formation of olefins in the reaction. Pinard et al. [22] analysed the carbon species and wax present on the spent $Co/Ru/Al_2O_3$ catalyst. They found that carboxylic acids on the catalyst surface have shorter chain length than paraffins in the FTS waxes, but the same chain length as that of olefins in the waxes. This again suggests that the carboxylates are formed from olefins via hydroformylation side reaction, as discussed above.

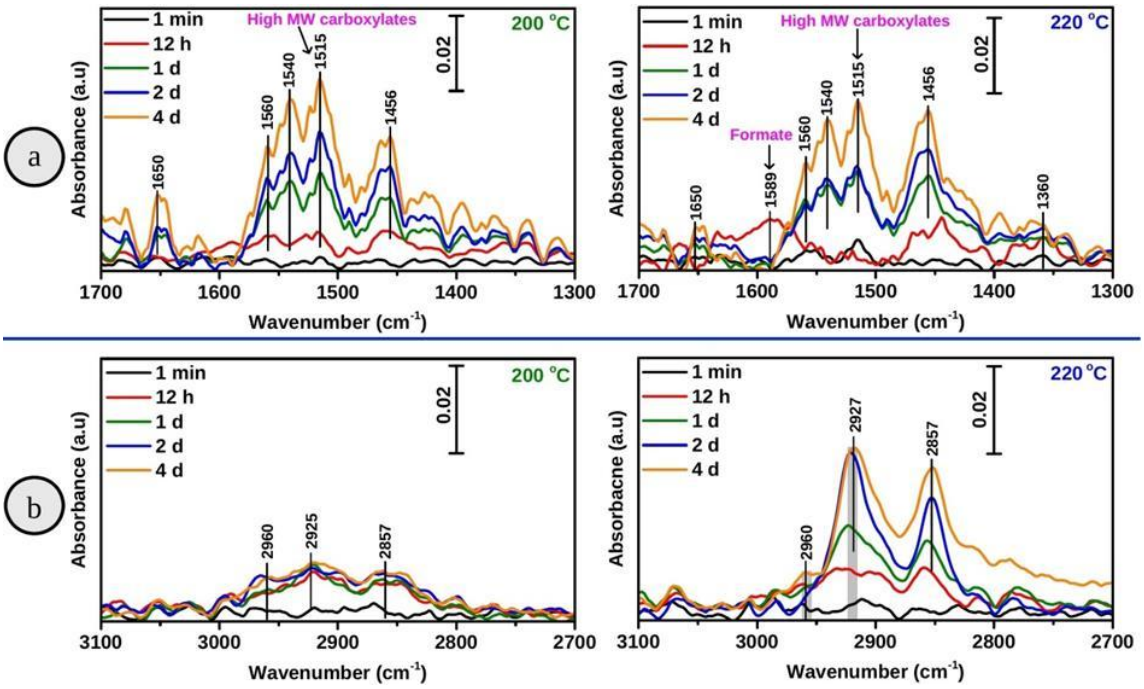

Figure 3.6: DRIFT spectra of the Co/TiO_2 catalyst at 200 °C and 220 °C and at 2 MPa, **(a**) Carboxylate region and **(b)** C-H stretching region.

The activity of the Co/TiO_2 FTS catalyst as a function of time on stream is shown in Figure 3.7. At the beginning of the reaction, the activity decreased drastically at 220 °C and 2 MPa and at 200 °C and 2 MPa and activity decreased modestly at 220 °C and 0.18 MPa. The decrease in activity at the beginning of the reaction is due to diffusion inhibition and pore plugging of the catalyst by high molecular weight non-desorbing wax resulting in diffusion inhibition [4,6,68]. Along with wax deposition, sintering of cobalt is also a major deactivation mechanism. We observed an increase in the average particle size during FTS, with a similar fresh and spent IWI catalyst analysed with TEM [63]. Bezemer et al. [10] also found sintering of cobalt when a Co/CNF catalyst was studied using Mössbauer emission spectroscopy. Sintering of cobalt particles as a deactivation mechanism in FTS has been reported in many studies [8,10–13]. Along with wax, carboxylates are also deposited on the catalyst. It is also proposed that high MW carboxylates deactivate the catalyst by blocking active sites [22]. From this study, it is difficult to distinguish the effect of carboxylates deposition from the effect of wax and sintering on the deactivation mechanism. To distinguish the effect of carboxylates, we studied two catalysts (obtained via different preparation routes), producing different amounts of acids at the same operational conditions [63]. These results are discussed in detail in the next chapter.

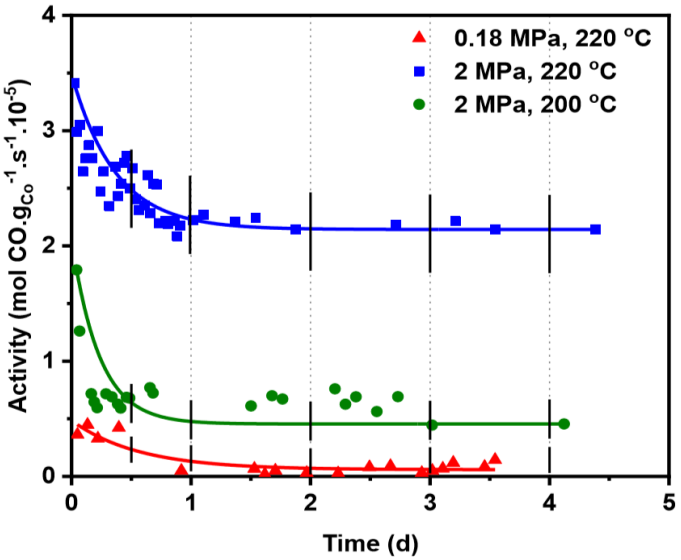

Figure 3.7: Activity of the Co/TiO_2 FTS catalyst as a function of the time on stream. | : Time of DRIFT spectrum measured.

3.4. Conclusions

A Co/TiO_2 catalyst has been studied at different pressures and temperatures using operando DRIFT spectroscopy (under industrial FTS conditions), to understand the possible role of carboxylates in the deactivation mechanism. The activity of the catalyst increased with increasing temperature and pressure, as expected. The formation of carboxylate compounds on the surface of the catalyst has been observed and their amount increased with time. High molecular weight carboxylates are dominant at high pressure and low temperature due to the formation of carboxylates on the catalyst surface from olefins secondary reaction. The effect of high MW carboxylates is not clearly distinguished from the effect of wax and sintering in catalyst deactivation, in this study. Therefore, two catalysts producing different amounts of carboxylates were synthesised and studied in the next chapter.

References

[1] A.Y. Khodakov, W. Chu, P. Fongarland, Advances in the development of novel cobalt Fischer-Tropsch catalysts for synthesis of long-chain hydrocarbons and clean fuels, Chem. Rev. 107 (2007) 1692–1744.

[2] E. Iglesia, Design, synthesis, and use of cobalt-based Fischer-Tropsch synthesis catalysts, Appl. Catal. A Gen. 161 (1997) 59–78.

[3] N.E. Tsakoumis, M. Rønning, Ø. Borg, E. Rytter, A. Holmen, Deactivation of cobalt based Fischer–Tropsch catalysts: A review, Catal. Today. 154 (2010) 162–182.

[4] A.M. Saib, D.J. Moodley, I.M. Ciobîcă, M.M. Hauman, B.H. Sigwebela, C.J. Weststrate, J.W. Niemantsverdriet, J. van de Loosdrecht, Fundamental understanding of deactivation and regeneration of cobalt Fischer–Tropsch synthesis catalysts, Catal. Today. 154 (2010) 271–282.

[5] E. Rytter, A. Holmen, Deactivation and Regeneration of Commercial Type Fischer-Tropsch Co-Catalysts A Mini-Review, Catalysts. 5 (2015) 478–499.

[6] D.J. Moodley, J. van de Loosdrecht, A.M. Saib, M.J. Overett, A.K. Datye, J.W. Niemantsverdriet, Carbon deposition as a deactivation mechanism of cobalt-based Fischer–Tropsch synthesis catalysts under realistic conditions, Appl. Catal. A Gen. 354 (2009) 102–110.

[7] G. Jacobs, P.M. Patterson, Y. Zhang, T. Das, J. Li, B.H. Davis, Fischer–Tropsch synthesis: deactivation of noble metal-promoted Co/Al_2O_3 catalysts, Appl. Catal. A Gen. 233 (2002) 215–226.

[8] T.O. Eschemann, K.P. de Jong, Deactivation Behavior of Co/TiO_2 Catalysts during Fischer–Tropsch Synthesis, ACS Catal. 5 (2015) 3181–3188.

[9] J. van de Loosdrecht, B. Balzhinimaev, J.-A. Dalmon, J.W. Niemantsverdriet, S.V. Tsybulya, A.M. Saib, P.J. van Berge, J.L. Visagie, Cobalt Fischer-Tropsch synthesis: Deactivation by oxidation?, Catal. Today. 123 (2007) 293–302.

[10] G.L. Bezemer, T.J. Remans, A.P. Van Bavel, A.I. Dugulan, Direct evidence of water-assisted sintering of cobalt on carbon nanofiber catalysts during simulated Fischer-Tropsch conditions revealed with in-situ Mössbauer spectroscopy, J. Am. Chem. Soc. 132 (2010) 8540–8541.

[11] C.H. Bartholomew, Mechanisms of catalyst deactivation, Appl. Catal. A Gen. 212 (2001) 17–60.

[12] D. Moodley, M. Claeys, E. van Steen, P. van Helden, D. Kistamurthy, K.-J. Weststrate, H. Niemantsverdriet, A. Saib, W. Erasmus, J. van de Loosdrecht, Sintering of cobalt during FTS: Insights from industrial and model systems, Catal. Today. 342 (2020) 59–70.

[13] D. Kistamurthy, A.M. Saib, D.J. Moodley, J.W. Niemantsverdriet, C.J. Weststrate, Ostwald ripening on a planar Co/SiO_2 catalyst exposed to model Fischer–Tropsch synthesis conditions, J. Catal. 328 (2015) 123–129.

[14] D. Peña, A. Griboval-Constant, V. Lecocq, F. Diehl, A.Y. Khodakov, Influence of operating conditions in a continuously stirred tank reactor on the formation of carbon species on alumina supported cobalt Fischer–Tropsch catalysts, Catal. Today. 215 (2013) 43–51.

[15] K. Fei Tan, J. Xu, J. Chang, A. Borgna, M. Saeys, Carbon deposition on Co catalysts during Fischer–Tropsch synthesis: A computational and experimental study, J. Catal. 274 (2010) 121–129.

[16] F.P. Di Sanzo, Characterization of high boiling Fischer-Tropsch liquids by liquid and gas chromatography, Anal. Chem. 53 (1981) 1911–1914.

[17] M. Kollár, A. De Stefanis, H.E. Solt, M.R. Mihályi, J. Valyon, A.A.G. Tomlinson, The mechanism of the Fischer–Tropsch reaction over supported cobalt catalysts, J. Mol. Catal. A Chem. 333 (2010) 37–45.

[18] D. Lorito, A. Paredes-Nunez, C. Mirodatos, Y. Schuurman, F.C. Meunier, Determination of formate decomposition rates and relation to product formation during CO hydrogenation over supported cobalt, Catal. Today. 259 (2016) 192–196.

[19] A. Paredes-Nunez, D. Lorito, N. Guilhaume, C. Mirodatos, Y. Schuurman, F.C. Meunier, Nature and reactivity of the surface species observed over a supported cobalt catalyst under CO/H_2 mixtures, Catal. Today. 242 (2015) 178–183.

[20] K. Jalama, N.J. Coville, D. Hildebrandt, D. Glasser, L.L. Jewell, Fischer-Tropsch synthesis over Co/TiO_2: Effect of ethanol addition, Fuel. 86 (2007) 73–80.

[21] J. Scalbert, I. Clémençon, P. Lecour, L. Braconnier, F. Diehl, C. Legens, Simultaneous investigation of the structure and surface of a Co/alumina catalyst during Fischer–Tropsch synthesis: discrimination of various phenomena with beneficial or disadvantageous impact on activity, Catal. Sci. Technol. 5 (2015) 4193–4201.

[22] L. Pinard, P. Bichon, A. Popov, J.L. Lemberton, C. Canaff, F. Maugé, P. Bazin, E.F. S.-Aguiar, P. Magnoux, Identification of the carbonaceous compounds present on a deactivated cobalt based Fischer–Trospch catalyst resistant to “rejuvenation treatment,” Appl. Catal. A Gen. 406 (2011) 73–80.

[23] F. Zaera, New advances in the use of infrared absorption spectroscopy for the characterization of heterogeneous catalytic reactions, Chem. Soc. Rev. 43 (2014) 7624–7663.

[24] J.-J. Max, C. Chapados, Infrared Spectroscopy of Aqueous Carboxylic Acids: Comparison between Different Acids and Their Salts, J. Phys. Chem. A. 108 (2004) 3324–3337.

[25] G. Giubertoni, O.O. Sofronov, H.J. Bakker, Observation of Distinct Carboxylic Acid Conformers in Aqueous Solution, J. Phys. Chem. Lett. 10 (2019) 3217–3222.

[26] O. Hadžija, B. Špoljar, Quantitative determination of carboxylate by infrared spectroscopy: application to humic acids, Fresenius. J. Anal. Chem. 351 (1995) 692–693.

[27] N. Wu, L. Fu, M. Su, M. Aslam, K.C. Wong, V.P. Dravid, Interaction of Fatty Acid Monolayers with Cobalt Nanoparticles, Nano Lett. 4 (2004) 383–386.

[28] V.A. De La Peña O’Shea, M.C. Alvarez-Galvan, J.M. Campos-Martin, J.L.G. Fierro, Strong dependence on pressure of the performance of a Co/SiO_2 catalyst in Fischer-Tropsch slurry reactor synthesis, Catal. Letters. 100 (2005) 105–110.

[29] F.M.T. Mendes, F.B. Noronha, C.D.D. Souza, M.A.P. da Silva, A.B. Gaspar, M. Schmal,

The effect of pressure on promoted Ru and Re-Co/Niobia catalysts in the Fischer-Tropsch synthesis, in: Stud. Surf. Sci. Catal., 2004: pp. 361–366.

[30] F. Kapteijn, R.M. de Deugd, J.A. Moulijn, Fischer–Tropsch synthesis using monolithic catalysts, Catal. Today. 105 (2005) 350–356.

[31] R.M. de Deugd, F. Kapteijn, J.A. Moulijn, Using monolithic catalysts for highly selective Fischer–Tropsch synthesis, Catal. Today. 79–80 (2003) 495–501.

[32] V.R.R. Pendyala, W.D. Shafer, G. Jacobs, B.H. Davis, Fischer-Tropsch synthesis: Effect of reaction temperature for aqueous-phase synthesis over a platinum promoted Co/Alumina catalyst, Catal. Letters. 144 (2014) 1088–1095.

[33] A. Mattsson, L. Österlund, Adsorption and Photoinduced Decomposition of Acetone and Acetic Acid on Anatase, Brookite, and Rutile TiO_2 Nanoparticles, J. Phys. Chem. C. 114 (2010) 14121–14132.

[34] A.Y. Meyer, D. Farin, D. Avnir, Cross-sectional areas of alkanoic acids. A comparative study applying fractal theory of adsorption and considerations of molecular shape, J. Am. Chem. Soc. 108 (1986) 7897–7905.

[35] G.P. Van der laan, A.A.C.M. Beenackers, Kinetics and Selectivity of the Fischer–Tropsch Synthesis: A Literature Review, Catal. Rev. 41 (1999) 255–318.

[36] Z. Yan, Z. Wang, D.B. Bukur, D.W. Goodman, Fischer–Tropsch synthesis on a model Co/SiO_2 catalyst, J. Catal. 268 (2009) 196–200.

[37] B. Johnson, C.H. Bartholomew, D.W. Goodman, The role of surface structure and dispersion in CO hydrogenation on cobalt, J. Catal. 128 (1991) 231–247.

[38] H. Schulz, Short history and present trends of Fischer–Tropsch synthesis, Appl. Catal. A Gen. 186 (1999) 3–12.

[39] B. Shi, B.H. Davis, Fischer–Tropsch synthesis: The paraffin to olefin ratio as a function of carbon number, Catal. Today. 106 (2005) 129–131.

[40] E.W. Kuipers, C. Scheper, J.H. Wilson, I.H. Vinkenburg, H. Oosterbeek, Non-ASF Product Distributions Due to Secondary Reactions during Fischer–Tropsch Synthesis, J. Catal. 158 (1996) 288–300.

[41] E. Iglesia, S.C. Reyes, R.J. Madon, Transport-enhanced α-olefin readsorption pathways in Ru-catalyzed hydrocarbon synthesis, J. Catal. 129 (1991) 238–256.

[42] C.-H. Zhang, Y. Yang, B.-T. Teng, T.-Z. Li, H.-Y. Zheng, H.-W. Xiang, Y.-W. Li, Study of an iron-manganese Fischer–Tropsch synthesis catalyst promoted with copper, J. Catal. 237 (2006) 405–415.

[43] E.W. Kuipers, Chain Length Dependence of α-Olefin Readsorption in Fischer-Tropsch Synthesis, J. Catal. 152 (1995) 137–146.

[44] Y. Qi, C. Ledesma, J. Yang, X. Duan, Y.-A. Zhu, A. Holmen, D. Chen, Adsorption energy-driven carbon number-dependent olefin to paraffin ratio in cobalt-catalyzed Fischer-Tropsch synthesis, J. Catal. 349 (2017) 110–117.

[45] T. Bhatelia, C. Li, Y. Sun, P. Hazewinkel, N. Burke, V. Sage, Chain length dependent olefin re-adsorption model for Fischer–Tropsch synthesis over Co-Al_2O_3 catalyst, Fuel Process. Technol. 125 (2014) 277–289.

[46] R.A. van Santen, A.J. Markvoort, I.A.W. Filot, M.M. Ghouri, E.J.M. Hensen, Mechanism and microkinetics of the Fischer–Tropsch reaction, Phys. Chem. Chem. Phys. 15 (2013) 17038–17063.

[47] R.A. van Santen, M. Ghouri, E.M.J. Hensen, Microkinetics of oxygenate formation in the Fischer–Tropsch reaction, Phys. Chem. Chem. Phys. 16 (2014) 10041–10058.

[48] A. de Klerk, Fischer Tropsch Refining, PhD Thesis, University of Pretoria, 2008.

[49] L.M. Tau, H.A. Dabbagh, B.H. Davis, Fischer-Tropsch synthesis: carbon-14 tracer study of alkene incorporation, Energy & Fuels. 4 (1990) 94–99.

[50] G. Jacobs, K. Chaudhari, D. Sparks, Y. Zhang, B. Shi, R. Spicer, T.K. Das, J. Li, B.H. Davis, Fischer–Tropsch synthesis: supercritical conversion using a Co/Al_2O_3 catalyst in a fixed bed reactor, Fuel. 82 (2003) 1251–1260.

[51] R.T. Hanlon, C.N. Satterfield, Reactions of selected 1-olefins and ethanol added during the Fischer-Tropsch synthesis, Energy & Fuels. 2 (1988) 196–204.

[52] H. Schulz, M. Claeys, Reactions of α-olefins of different chain length added during Fischer–Tropsch synthesis on a cobalt catalyst in a slurry reactor, Appl. Catal. A Gen. 186 (1999) 71–90.

[53] G.J. Hutchings, R.G. Copperthwaite, M. van der Riet, Low methane selectivity using Co/MnO catalysts for the Fischer-Tropsch reaction: Effect of increasing pressure and Co-feeding ethene, Top. Catal. 2 (1995) 163–172.

[54] I. V. Derevich, V.S. Ermolaev, V.Z. Mordkovich, Liquid-vapor thermodynamic equilibrium in Fischer-Tropsch synthesis products, Theor. Found. Chem. Eng. 42 (2008) 216–219.

[55] A.P. Raje, B.H. Davis, Effect of Vapor−Liquid Equilibrium on Fischer−Tropsch Hydrocarbon Selectivity for a Deactivating Catalyst in a Slurry Reactor, Energy & Fuels. 10 (1996) 552–560.

[56] S. Rößler, C. Kern, A. Jess, Formation and Vaporization of Hydrocarbons During Cobalt-Catalysed Fischer-Tropsch Synthesis, Chemie Ing. Tech. 90 (2018) 634–642.

[57] J.J. Marano, G.D. Holder, Characterization of Fischer-Tropsch liquids for vapor-liquid equilibria calculations, Fluid Phase Equilib. 138 (1997) 1–21.

[58] C.M. Masuku, W. Ma, D. Hildebrandt, D. Glasser, B.H. Davis, A vapor–liquid equilibrium thermodynamic model for a Fischer–Tropsch reactor, Fluid Phase Equilib. 314 (2012) 38–45.

[59] B.D. Kelly, A. de Klerk, Modeling Vapor–Liquid–Liquid Phase Equilibria in Fischer–Tropsch Syncrude, Ind. Eng. Chem. Res. 54 (2015) 9857–9869.

[60] C.G. Visconti, Vapor–Liquid Equilibria in the Low-Temperature Fischer–Tropsch Synthesis, Ind. Eng. Chem. Res. 53 (2014) 1727–1734.

[61] B.H. Davis, Fischer–Tropsch Synthesis: Reaction mechanisms for iron catalysts, Catal. Today. 141 (2009) 25–33.

[62] F.M.T. Mendes, C.A.C. Perez, F.B. Noronha, C.D.D. Souza, D. V. Cesar, H.J. Freund, M. Schmal, Fischer−Tropsch Synthesis on Anchored $Co/Nb_2O_5/Al_2O_3$ Catalysts: The Nature of the Surface and the Effect on Chain Growth, J. Phys. Chem. B. 110 (2006) 9155–9163.

[63] P. Gonugunta, A.I. Dugulan, G.L. Bezemer, E. Brück, Role of surface carboxylate deposition on the deactivation of cobalt on titania Fischer-Tropsch catalysts, Catal. Today. (2020).

[64] B. Gu, A.Y. Khodakov, V. V. Ordomsky, Selectivity shift from paraffins to α-olefins in low temperature Fischer–Tropsch synthesis in the presence of carboxylic acids, Chem. Commun. 54 (2018) 2345–2348.

[65] M.K. Gnanamani, R.A. Keogh, W.D. Shafer, B. Shi, B.H. Davis, Fischer–Tropsch synthesis: Deuterium labeled ethanol tracer studies on iron catalysts, Appl. Catal. A Gen. 385 (2010) 46–51.

[66] W.M. Hexana, N.J. Coville, Indium as a chemical promoter in Fe-based Fischer-Tropsch synthesis, Appl. Catal. A Gen. 377 (2010) 150–157.

[67] V. Navarro, M.A. van Spronsen, J.W.M. Frenken, In-situ observation of self-assembled hydrocarbon Fischer–Tropsch products on a cobalt catalyst, Nat. Chem. 8 (2016) 929–934.

[68] M.K. Niemelä, A.O.I. Krause, The long-term performance of Co/SiO_2 catalysts in CO hydrogenation, Catal. Letters. 42 (1996) 161–166.

3

Supplementary information

S3.1. Acetic acid adsorption

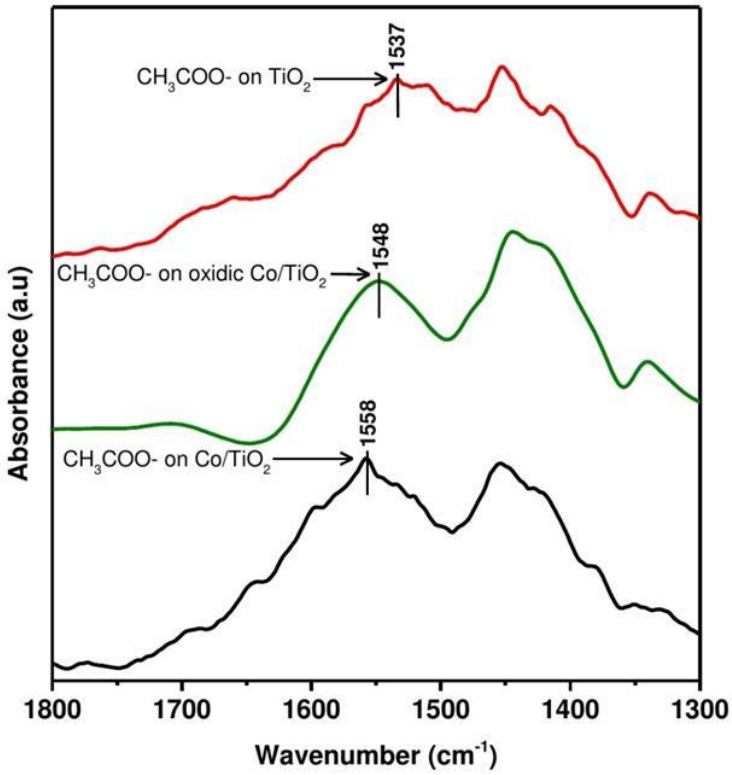

Figure S3.1: DRIFT spectra of CH_3COO- adsorbed on Co/TiO_2 catalyst, oxidic Co/TiO_2 catalyst and TiO_2 support.

The infrared spectra of the acetate adsorbed on Co/TiO_2 catalyst, oxidic Co/TiO_2 catalyst and TiO_2 support are shown in Figure S3.1. The asymmetric stretching (ν_{as}) peak positions of CH_3COO- on Co/TiO_2 catalyst, on oxidic Co/TiO_2 catalyst and TiO_2 support are at 1558 cm^{-1}, 1548 cm^{-1} and 1537 cm^{-1} respectively. The shift in peak position to lower wavenumber for oxidic Co/TiO_2 catalyst and TiO_2 support is due to the difference in interaction energy.

3

Chapter 4

Role of surface carboxylate deposition on the deactivation of cobalt on titania Fischer-Tropsch synthesis catalysts

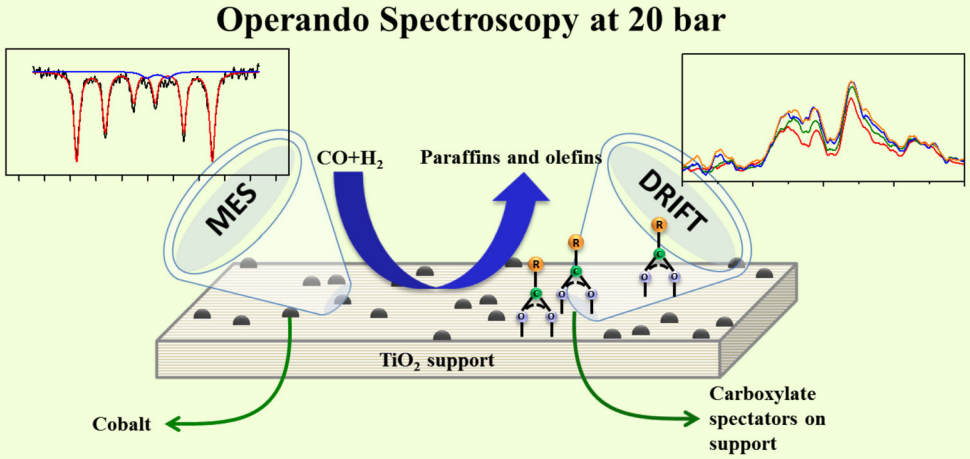

Operando spectroscopic techniques (Diffusive Reflective Infrared Fourier-Transform and Mössbauer emission spectroscopy) were combined to investigate the role of oxygenates deposition on deactivation of cobalt on titania Fischer-Tropsch catalysts at high pressure. Clear formation of carboxylates was seen for catalyst prepared via both impregnation and precipitation, but more and heavier carboxylates were seen on the impregnated catalyst. This effect is related to a higher olefin content in the products obtained with the impregnated sample, resulting to increased formation of oxygenates through the hydroformylation side reaction. The combined gas chromatography/infrared spectroscopy data demonstrated that the surface carboxylate species are not involved in the catalyst deactivation, being most likely spectator species on the titania support.

This chapter is based on the paper: Prasad Gonugunta, A. Iulian Dugulan, G. Leendert Bezemer, Ekkes Brück, Catalysis Today. xx (xxxx) xx-xx. https://doi.org/10.1016/j.cattod.2020.04.037

4.1. Introduction

Fischer-Tropsch synthesis (FTS) is a catalytic process that converts synthesis gas obtained from natural gas, coal and biomass into liquid fuels [1,2]. Shell's Pearl gas to liquid (GTL) is the largest plant in the world producing clean fuels from natural gas by FTS process [3]. Co-based catalysts in FTS process received great interest from industries and academic institutions due to their high activity, high selectivity to linear paraffins and low unwanted water-gas shift activity. However, the major drawbacks of these catalysts are their high cost and deactivation in time [4–9]. Therefore, it is important to increase the lifetime of the catalysts to make the process economically more efficient, requiring a fundamental understanding of the various catalyst deactivation mechanisms. The general Co-based FTS catalysts deactivation mechanisms such as poisoning, re-oxidation, sintering of active phase and deposition of carbon and oxygenated compounds have been reviewed extensively earlier [4–7,10–15]. Formation of different types of carbon compounds on the catalyst surface and their role on deactivation of Co-based FTS catalysts has also been studied earlier [5–7]. Pena et al. [16,17] identified different types of carbon species on a spent Co/Al_2O_3 FTS catalyst using conventional *ex-situ* techniques. They found that strongly absorbed hydrocarbons and polymeric carbon contribute to the catalyst deactivation. Moodley et al. [7] identified three different carbon species, when a spent $Co/Pt/Al_2O_3$ FTS catalyst was studied with temperature-programmed hydrogenation mass spectrometry (TPH-MS) experiments. They were atomic carbon, residual wax in the pores of the catalyst and polymeric carbon. From their studies, it was concluded that only polymeric carbon contributes to long-term deactivation. Scalbert et al. [18] found absorption and an increase in the amount of oxygenated compounds with time on a Co/Al_2O_3 FTS catalyst using XRD-DRIFT spectroscopy. They proposed that these strongly absorbed species are responsible for catalyst deactivation by covering the active sites. As part of the mechanism in cobalt based FTS, the hydroformylation route, where CO is inserted in an (re-)adsorbed alpha-olefin chain, results in formation of alcohols and aldehydes [19,20]. The carboxylic acids also mentioned to be primary FTS products, obtained via equilibrium interconversion reactions from the alcohols and aldehydes [21]. Pinard et al. [22] analysed the carbon species present on a spent $Co/Ru/Al_2O_3$ FTS catalyst using temperature programmed hydrogenation–infrared (TPH-IR) technique. Atomic carbon, alcohols, carboxylic acids and polymeric carbon were found on the spent catalyst surface. Carboxylates are formed when an acid reacts with surface hydroxyl groups under formation of water, so on titania: $RCOOH + TiOH \rightarrow RCOO^{-}Ti^{+} + H_2O$. TPH-IR of spent catalyst indicated that complete removal of carboxylate species required temperatures above 600 ^{o}C. Only carboxylic acids and polymeric carbon were resistant to a rejuvenation treatment under hydrogen. From these studies, Pinard et al. [22] proposed that carboxylates on the catalyst surface deactivate the catalyst, but the exact role of the carboxylates on the catalyst surface is not yet fully understood. The main aim of this research is to investigate the role of carboxylates in the deactivation mechanism of FTS catalysts.

In order to determine if carboxylic acids play a role in the deactivation behaviour of the catalysts, we employed two operando characterisation techniques: diffusive reflective infrared Fourier-Transform (DRIFT) and Mössbauer emission spectroscopy (MES) to monitor the changes in the morphology of the catalysts during FTS operation [18,23–26]. In this study, we

have investigated two catalysts prepared by incipient wetness impregnation (IWI) and homogeneous deposition precipitation (HDP) methods. The uniqueness of this work is that the catalysts were studied by monitoring the surface species with operando DRIFT and the state of the cobalt with operando MES during the FTS reaction.

4.2. Experimental

4.2.1. Catalyst preparation

Two Co/TiO_2 samples Co(9.3 wt%)/TiO_2 - IWI and Co(8.9 wt%)/TiO_2 - HDP were synthesized by incipient wetness impregnation (aq.$Co(NO_3)_2 \cdot 6H_2O$ solution) and homogeneous deposition precipitation (NH_3 evaporation) methods. For Co(9.3 wt%)/TiO_2 - IWI catalyst preparation, the support material (Degussa P25) was dried and impregnated with an aqueous solution of $Co(NO_3)_2 \cdot 6H_2O$ (4 Molar) in two steps. After each impregnation, the obtained material was dried in an oven at 60 ^oC overnight under static air and calcined at 350 ^oC for 2 hours under N_2 flow. For the preparation of Co(8.9 wt%)/TiO_2 catalyst by the HDP method, 24.75 g of $CoCO_3$ and 24.75 g of $(NH_4)_2CO_3$ were dissolved in 255.6 g of 25 wt% of ammonia solution and the mixture was diluted with distilled water to make a total of 500 mL. 5 mL of this stock solution was mixed with 70 mL of 9 wt% ammonia solution to suspend 2 g of P25 TiO_2 powder in a round bottom flask that was stirred and heated at 100 ^oC for 3 hours using a reflux cooler. After cooling down to room temperature, the material was filtered off, washed with water and dried at 60 ^oC overnight. The obtained filter material was crushed, sieved and heat-treated in N_2 flow at 400 ^oC for 4 hours. The catalyst samples used in the current study are similar to the samples used in the work of Eschemann et al. [27] and they were received from Utrecht University.

The two catalyst samples (IWI and HDP) together with an empty TiO_2 support material were post-impregnated with typically 0.3-0.4 µg of radioactive ^{57}Co and dried at 120 ^oC for 6 h in air to enable measurements by Mössbauer Emission Spectroscopy (MES).

4.2.2. Operando Mössbauer emission spectroscopy (MES) study of Co/TiO_2 catalysts

The Mössbauer emission spectroscopy (MES) measurements and FTS measurements were performed under operando conditions, in a high-pressure MES reaction cell as displayed in Figure 2.8 in Chapter 2. The design and details of the MES reaction cell were described previously by Crajé et al. [26]. ^{57}Co-MES technique is used to follow the oxidation state and dispersion of supported cobalt particles [26].

The FTS measurements were carried out at 200 °C, 2 MPa and a H_2/CO feed ratio (FR) of 4 v/v. The catalytic performance was also evaluated at 210 °C, to determine activation energies. The catalytic data is reported after 2 days of operation. The products were analysed with a thermal conductivity detector on a Varian Micro-GC CP4900 (Dual channel) gas chromatograph, equipped with molecular sieve and Porapaq Q columns.

4.2.3. Operando DRIFT study of Co/TiO_2 catalysts

The catalyst samples Co(9.3 wt%)/TiO_2 - IWI and Co(8.9 wt%)/TiO_2 - HDP were also investigated using an operando DRIFT reaction setup (see Figure 2.4 in Chapter 2.), equipped with a Thermo Nicolet Nexus 670 FT-IR spectrometer to monitor the presence of adsorbed surface species on the surface of the FTS catalysts under relevant industrial conditions. Infrared spectra were recorded with 128 scans at a resolution of 4 cm^{-1}. The Co/TiO_2 catalyst was loaded into the DRIFT reaction cell and reduced at 350 ^oC in 100 mL/min of H_2 for 2 hours. Then the reaction cell was cooled down to the reaction temperature (200 ^oC) and a background spectrum was measured in a mixture of Ar/H_2. After this step, CO was introduced into the reactor and the pressure was increased to 2 MPa. Catalyst samples were studied at 200 ^oC and 2 MPa with H_2/CO FR of 4 v/v. After 4 days of reaction, the catalyst was stripped with H_2 at 270 ^oC to remove wax and other products from the catalyst surface and the reaction was restarted at the initial FTS conditions. A ramp rate of 5 ^oC/min was used for all heating and cooling steps. The reaction products and permanent gases were analysed with a Thermo Scientific Ultra Trace GC, equipped with a thermal conductivity detector and a flame ionisation detector.

4.2.4. Transmission electron microscopy (TEM) analysis

The TEM measurements were performed using a FEI Tecnai microscope, with a electron beam voltage of 300 kV. During the TEM procedure, both IWI and HDP catalysts were ground with a mortar, suspended in ethanol and kept in an ultra-sonication bath. A little amount of suspended solutions were dropped on TEM copper grids and dried. In the case of spent samples, first catalysts were cleaned with tetrahydrofuran to remove solid wax in the pores of the catalyst. Surface area averaged cobalt particles sizes are calculated based on the analysis of typically 300 particles.

4.3. Results and discussion

4.3.1. Operando Mössbauer emission spectroscopy (MES) studies

The catalytic performance of IWI and HDP catalysts studied by the operando high-pressure MES reaction cell is presented in Table 4.1. The activity of the HDP catalyst was 2.5 times higher than the IWI catalyst. Eschemann et al. [27] also found that the Co/TiO_2 catalyst prepared by the precipitation method is ~1.5 times more active than the catalyst prepared by the IWI method. They observed well-distributed metal particles on support for the HDP catalyst and clustering of similar-size particles for the IWI catalyst that could tentatively explain the observed difference in catalytic performance. Morales et al. [28] studied a Co/TiO_2 catalysts containing Mn promoter prepared by IWI and HDP methods and they also found that the HDP catalyst was more active than the catalyst prepared by the IWI method, due to the better distribution of Co phase. In addition, an increase in selectivity to C_{5+} and a decrease in selectivity to CH_4 by Mn promoter were found only on HDP catalyst, not on IWI catalyst, which could be due to the better interaction of Co-Mn in HDP catalyst than IWI catalyst.

To understand the difference in activity of the two catalysts, the activation energies (E_a) were calculated and presented in Table 4.1. These values are in the range of the E_a values of Co-

based FTS catalysts from previous studies [29–31]. However, the E_a of IWI catalyst is 1.4 times higher than E_a of HDP catalyst, which could be related to a higher energy barrier due to steric hindrance by strongly adsorbed surface species on the active sites of the IWI catalyst [32].

Table 4.1: Performance of IWI and HDP catalysts at 200 °C and 2 MPa after TOS 2 days.

Catalyst sample	Bulk Co^0 (%)	Activity (mol $CO.g_{Co}^{-1}.s^{-1}$)	Activation energy* E_a (kJ/mol)
^{57}Co:Co(9.3 wt%)/TiO_2 - IWI	95	$1.10\pm0.01\cdot10^{-5}$	122±5
^{57}Co:Co(8.9 wt%)/TiO_2 - HDP	94	$2.84\pm0.02\cdot10^{-5}$	86±5

*E_a was calculated based on two experiments at 200 °C and 210 °C

The MES spectra obtained with ^{57}Co:Co(9.3 wt%)/TiO_2 IWI catalyst are shown in Figure 4.1 and the MES fitted parameters are listed in Table 4.2. The MES spectrum of the fresh catalyst sample (Figure 4.1A) consists of two doublets, with about 89% of the Co atoms present as Co^{3+}. The Mössbauer spectrum of the fresh dried sample (Figure 4.1A) is consistent with the presence of CoO structures, both octahedrally coordinated Fe^{+2} and Fe^{+3} ions being produced by the decay of the Co^{+2} ions [33]. This is because the radioactive decay of ^{57}Co to ^{57}Fe takes place via electron capture, by which a reshuffling of the electrons is generated. The triggered Auger ionisation cascade results in the electrons being trapped in the vicinity of the decayed ^{57}Fe atoms, stabilizing ^{57}Fe charge states different from that of the parent ^{57}Co species. Figure 4.1B shows the state of the catalyst after reduction at 350 °C in H_2. The main sextuplet is assigned to metallic Co obtained via conversion of Co^{+2}/Co^{+3} during reduction. A small doublet corresponding to Co^{+2} is still present in Figure 4.1B. This is related to unconverted CoO that interacts strongly with the support. Figure 4.1C shows the state of the catalyst during FTS after 2 days of reaction, where most Co atoms are present as metallic Co. Even after 2 days of FTS reaction, the main sextuplet assigned to metallic Co did not change, confirming the absence of oxidation.

The MES spectra of ^{57}Co:Co(8.9 wt%)/TiO_2 HDP catalyst are shown in Figure 4.2 and the MES fitted parameters at different treatments are listed in Table 4.3. The MES spectrum of the fresh sample (Figure 4.2A) consists of two doublets with about 3% of Co^{2+} and 97% of Co^{3+}. Figure 4.2B shows the state of the catalyst after reduction at 350 °C in H_2. Figure 4.2C shows the state of the catalyst during FTS after 2 days of reaction, where most Co atoms are present as metallic Co. After 2 days of FTS reaction, the spectra did not change much compared to the reduced state.

Oxidation of cobalt was not found for any of the two catalysts by MES measurements during FTS, confirming the previous observations of the absence of this deactivation mechanism [11–14,34]. From Mössbauer spectra, the percentage of metallic Co after reduction and during the reaction in both catalysts is nearly equal. Therefore, the large difference in the activity of the catalysts cannot be revealed solely on the basis of the MES results.

Table 4.2: The MES fitted parameters of ^{57}Co:Co(9.3 wt%)/TiO_2 IWI catalyst, after different treatments.

Treatment	T (°C)	IS ($mm \cdot s^{-1}$)	QS ($mm \cdot s^{-1}$)	HF (Tesla)	SC (%)	Oxidation state
A. Fresh sample	25	0.22	0.82	-	89	Co^{3+}
		1.10	2.09	-	11	Co^{2+}
B. Reduction	25	- 0.1	-	34.2	97	Co^{0}
(100% H_2, 350 °C)		0.97	2.21	-	3	Co^{2+}
C. FTS reaction, 2 MPa	200	-0.22	-	32.8	95	Co^{0}
(H_2/CO= 4, 200 °C, 2 days)		0.95	1.99	-	5	Co^{2+}

IS: *Isomer shift,* ***QS:*** *Quadrupole splitting,* ***HF:*** *Hyperfine field,* ***SC:*** *Spectral contribution*
Experimental uncertainties: IS: *± 0.05 mm.s^{-1},* ***QS:*** *± 0.05 mm.s^{-1},* ***HF:*** *± 1%,* ***SC:*** *± 3-5%*

Table 4.3: The MES fitted parameters of ^{57}Co:Co(8.9 wt%)/TiO_2 HDP catalyst, after different treatments.

Treatment	T (°C)	IS ($mm \cdot s^{-1}$)	QS ($mm \cdot s^{-1}$)	HF (Tesla)	SC (%)	Oxidation state
A. Fresh sample	25	0.23	0.76	-	97	Co^{3+}
		1.06	2.78	-	3	Co^{2+}
B. Reduction	25	- 0.1	-	34.2	96	Co^{0}
(100% H_2, 350 °C)		1.13	2.42	-	4	Co^{2+}
C. FTS reaction, 2 MPa	200	-0.23	-	32.8	94	Co^{0}
(H_2/CO= 4, 200 °C, 2 days)		0.76	1.62	-	6	Co^{2+}

IS: *Isomer shift,* ***QS:*** *Quadrupole splitting,* ***HF:*** *Hyperfine field,* ***SC:*** *Spectral contribution*
Experimental uncertainties: IS: *± 0.05 mm.s^{-1},* ***QS:*** *± 0.05 mm.s^{-1},* ***HF:*** *± 1%,* ***SC:*** *± 3-5%*

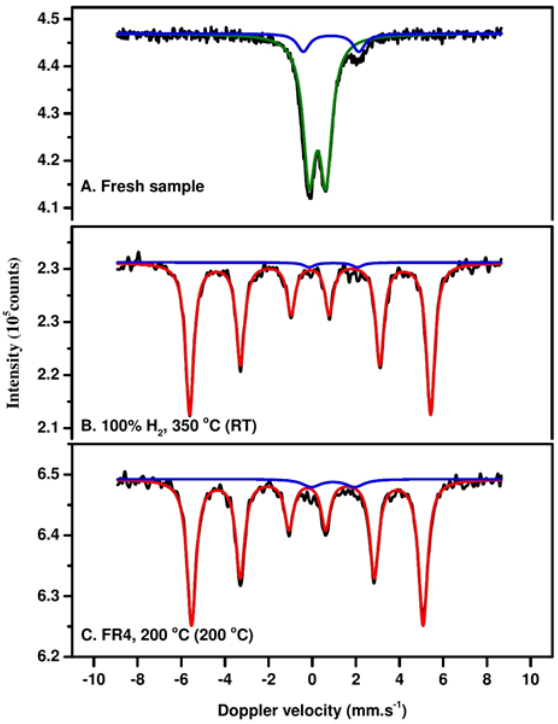

Figure 4.1: MES spectra obtained with ^{57}Co:Co(9.3 wt%)/TiO_2 IWI catalyst, after different treatments.

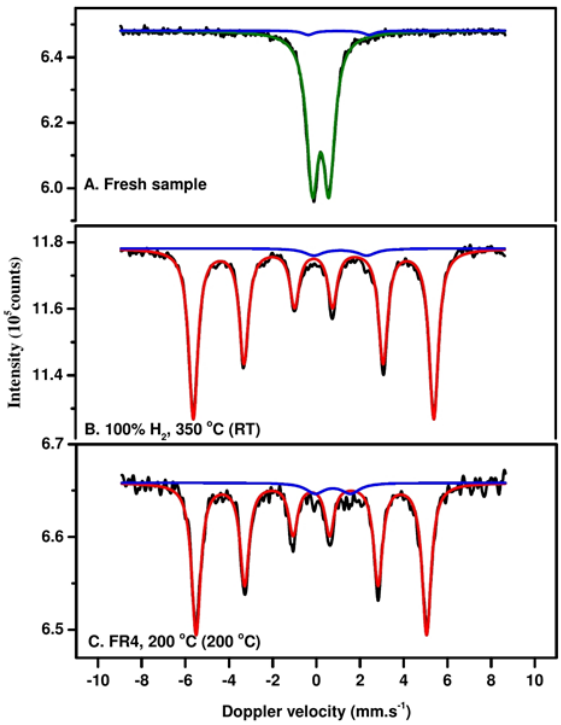

Figure 4.2: MES spectra obtained with ^{57}Co:Co(8.9 wt%)/TiO_2 HDP Catalyst, after different treatments.

4.3.2. Operando DRIFT and TEM studies

The activity and selectivity of IWI and HDP Co/TiO_2 catalysts measured inside the operando DRIFT cell are shown in Table 4.4. The HDP catalyst was found to be 1.6 times more active than the IWI catalyst. In order to understand the difference in activity of the catalysts, both fresh and spent samples were examined with TEM (Figure 4.3) and the particles size distributions are shown in Figure 4.4. The average particle size of both IWI and HDP spent catalysts is higher than in the fresh samples due to sintering during the reaction as expected (see Table 4.5) [12,15]. The average particle size of the spent IWI catalyst is only slightly higher than for the spent HDP catalyst. As observed in Figure 4.4, the HDP preparation method has a significant impact on cobalt distribution on the TiO_2 support, resulting in well-distributed cobalt active structures having higher accessible surface area and improved activity, as previously indicated by Eschemann et al. [27].

Table 4.4: IWI and HDP Co/TiO_2 catalysts at 2 MPa and 200 °C after TOS 4 days.

Catalyst samples	Activity (mol $CO.g_{Co}^{-1}.s^{-1}$)	Selectivity (%) on carbon basis				O/P
		C_1-C_2	C_3	C_4	C_{5+}	
$Co(9.3\ wt\%)/TiO_2$ - IWI	$1.4\pm0.1\cdot10^{-5}$	5.8	2.1	2.1	90.0	0.7
$Co(8.9\ wt\%)/TiO_2$ - HDP	$2.2\pm0.1\cdot10^{-5}$	5.6	1.9	2.0	90.5	0.4

O/P ratio: Olefins C_5 to C_9/Paraffins C_5 to C_9

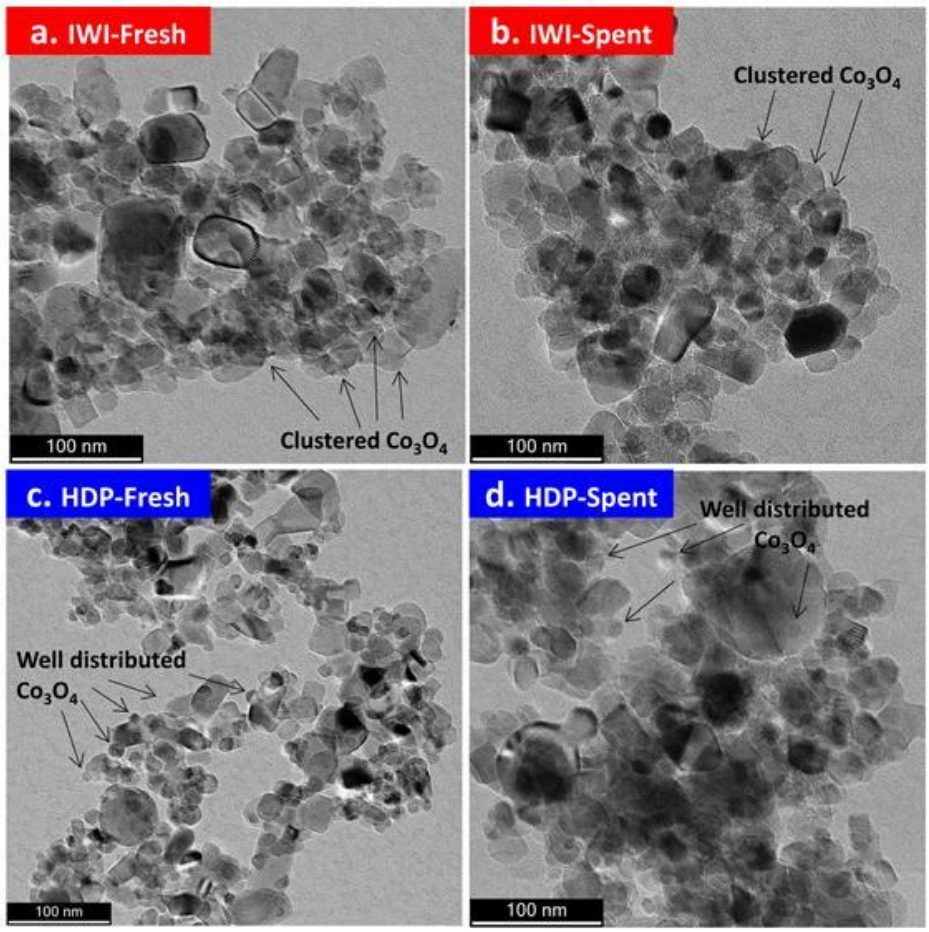

Figure 4.3: TEM micrographs of IWI and HDP catalysts.
Note: Sharp edged particles: TiO_2 & Round shaped particles: Co/Co_3O_4 [35].

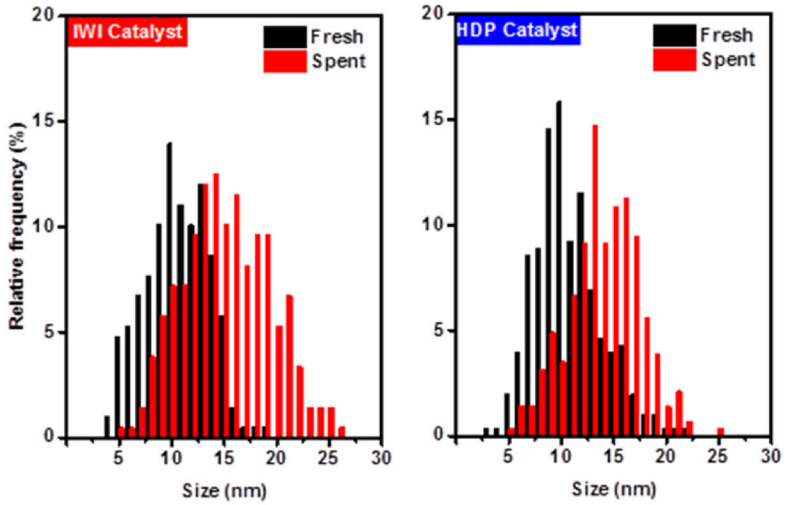

Figure 4.4: TEM Co_3O_4 particle size distribution of IWI and HDP catalysts.

Table 4.5: Average Co_3O_4 particle size of IWI and HDP catalysts.

Catalyst samples	*Average particle size (nm)	
	Fresh	Spent
Co(9.3 wt%)/TiO_2 - IWI	10.4±3.0	15.2±4.1
Co(8.9 wt%)/TiO_2 - HDP	10.7±3.1	14.0±3.4

*Surface area average diameter of ~300 particles.

The infrared spectra of IWI and HDP catalysts during FTS at different reaction times are shown in Figure 4.5. The intensity of infrared bands corresponding to formate, acetate and high molecular weight (MW) carboxylate species increased with time due to their deposition on the surface of the catalyst. The band at 1589 cm^{-1} and two other bands at 1373 cm^{-1} and 1360 cm^{-1} are assigned to asymmetric ν_{as}(COO-) and symmetric ν_s(COO-) vibrations of formate species on the catalyst surface. These formate bands level off after one day of FTS for the IWI catalyst, while the spectra are dominated by signals from higher carboxylates. In the case of HDP catalyst, the low molecular weight formate species are always dominant and reached a maximum intensity after 3 days. The presence of formate species on the surface of Co-based FTS catalysts was also reported earlier using DRIFT spectroscopy [36,37]. Lorito et al. [38,39] found two types of formate species (fast and slow reacting) present on the Co-based catalyst, using DRIFT and monitoring the decomposition rates of formate species at different temperatures. They proposed that formate could potentially be an intermediate in the formation of methanol.

The bands at 1554 cm^{-1} and 1540 cm^{-1} are assigned to asymmetric vibrations of acetate $\nu_{as}(CH_3COO-)$ and hexanoate $\nu_{as}(C_5H_{11}COO-)$ on the catalyst [22]. The peaks 1525 cm^{-1} and 1510 cm^{-1} correspond to high MW carboxylates. The band at 1460 cm^{-1} is due to CH_2 bending vibrations of carboxylic acids and hydrocarbons. In the beginning of the reaction, the IWI catalyst surface is dominated by acetate species, with very small amounts of hexanoate and other high MW carboxylates species. The band at 1444 cm^{-1} corresponds to symmetric

stretching of COO-. The CH_2 band at 1460 cm^{-1} overlaps partially with the COO- band at 1444 cm^{-1}. The ratio between the bands provides an indication of the carboxylate chain length. After 4 days of reaction, the catalyst surface is dominated by high MW carboxylates species. Like all FTS products, also acids follow the ASF chain growth mechanism and hence fewer heavy acids are made compared to the light acids. The observation the ratio of lower to higher acids shift in time, gives the insight in the reversibility of carboxylate deposition on the surface. Moreover, a domination by longer carboxylates is contrary their production ratio and indicates the higher stability of long chain acids on the surface. In the case of HDP catalyst, at the beginning of the reaction, a very small amount of formate, acetate and high MW carboxylates were present on the catalyst surface. Even after 4 days of reaction, the formate peak still dominates the spectra. This clearly indicates that high MW acids were produced at much lower amounts by the HDP catalyst, resulting in far less heavy carboxylates accumulation.

The band at 1640 cm^{-1} is corresponding to the C=C stretching vibrations of olefins on the catalyst surface [18,36]. At the beginning of the reaction, a small peak at 1640 cm^{-1} was observed for the IWI catalyst, while the HDP sample had no band corresponding to C=C stretching vibrations. After 4 days of reaction, there is a very clear band at 1640 cm^{-1} for the IWI catalyst, whereas for HDP catalyst this band is barely visible. This clearly indicates that the IWI catalyst surface contained more olefins than the HDP catalyst surface. Also, the intensity of the band at 1640 cm^{-1} appears to be correlated with the intensity of the carboxylate bands. These results appear to imply a relation between olefins formation and carboxylates compounds present on the catalyst surface. As also the selectivity data indicates an olefin/paraffin ratio almost twice as high for the IWI sample as shown in Table 4.4, we argue that the increased olefin content is related to formation of more carboxylates via a hydroformylation side reaction. The choice of the preparation method resulting in such distinct difference in terms of carboxylates formation is most likely related to the presence of promoters like nitrogen or salts in the HDP sample. The formation of oxygenated intermediates and other products such as alkenes, alcohols and aldehydes can be understood by the CO insertion mechanism of van Santen et al. [19,20]. Compared to iron catalysts, the fraction of oxygenates and acids in the total product is significantly lower. For cobalt on titania catalysts ~3 mol% oxygenates were found, the large majority being linear alcohols [40]. From our own work we estimate that acids consist of 5-10% of the total oxygenates produced.

Most of the reaction products (~97%) in Co-based FTS are paraffins and olefins. As seen in Figure 4.8, the significant decrease in catalyst activity at the beginning of the reaction (first 24 hour) is assigned mainly to the pore filling of the catalyst by waxes [7,41]. Later, the catalyst activity decreased slowly with time due to the irreversible sintering of cobalt particles as observed by TEM analysis (see Figure 4.3). However, the DRIFT data shows continuous deposition of carboxylates on the catalyst surface for another 2-3 days, suggesting that the surface carboxylates are not involved in the deactivation mechanism. The carboxylates deposit continuously on the catalyst surface, as they have a much stronger ionic interaction with the titania surface compared to the weak forces governing the physisorption of wax. The observation that shorter acids can be replaced by heavier acids does however indicate that also the carboxylates bind reversibly.

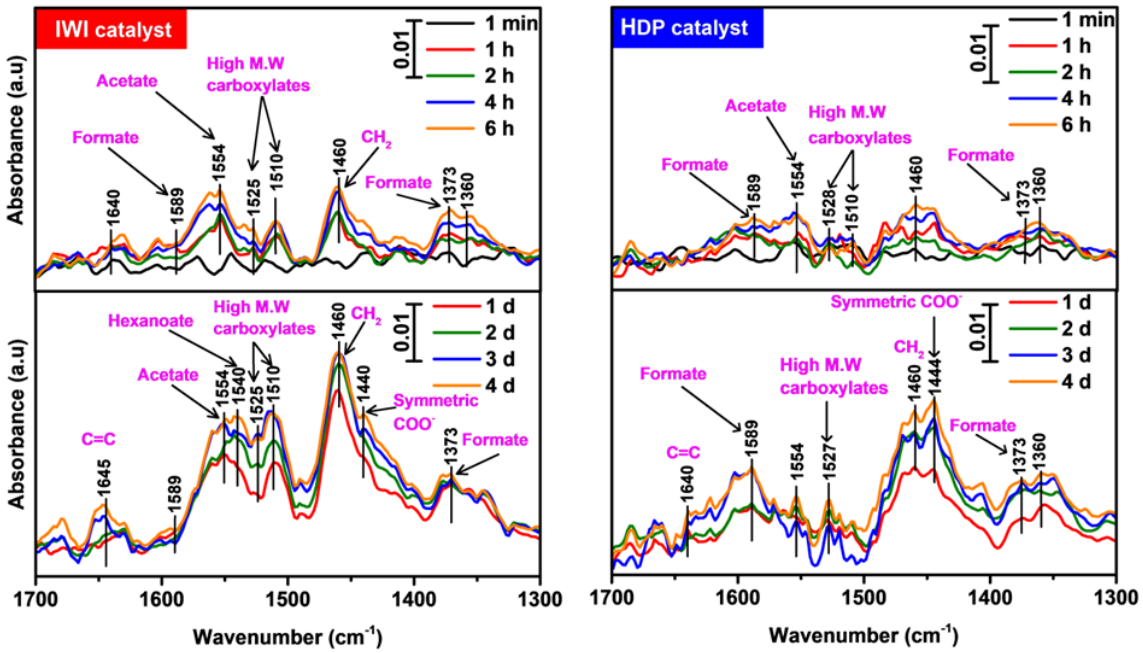

Figure 4.5: DRIFT spectra of IWI and HDP catalysts during FTS reaction.

The C-H region of DRIFT spectra of IWI and HDP catalysts measured during the reaction is shown in Figure 4.6. The bands at 2930, 2925 and 2850 cm^{-1} are corresponding to asymmetric and symmetric stretching vibrations of CH_2 groups of long carbon chain hydrocarbons [22]. As expected, the intensity of these peaks increased with time due to the accumulation of hydrocarbons on the catalyst surface [22]. The intensity of these CH_2 peaks is the same for both IWI and HDP catalysts and became stable after 2 days of FTS. However, there is a clear difference in the band position of CH_2 asymmetric vibrations. The CH_2 band of asymmetric vibrations of the IWI catalyst is at 2925 cm^{-1} whereas for HDP catalyst it is at 2930 cm^{-1}. This difference is due to a decrease in the energy of CH_2 stretching vibrations with increasing carbon chain length. The CH_2 stretching vibrational energy of high MW carboxylates on the IWI catalyst surface is lower than the CH_2 stretching vibrational energy of low MW carboxylates on the HDP catalyst surface. Therefore, the position of the CH_2 asymmetric vibrational band of the IWI catalyst is at slightly lower wavenumber than the position of CH_2 asymmetric vibrational band of HDP catalyst.

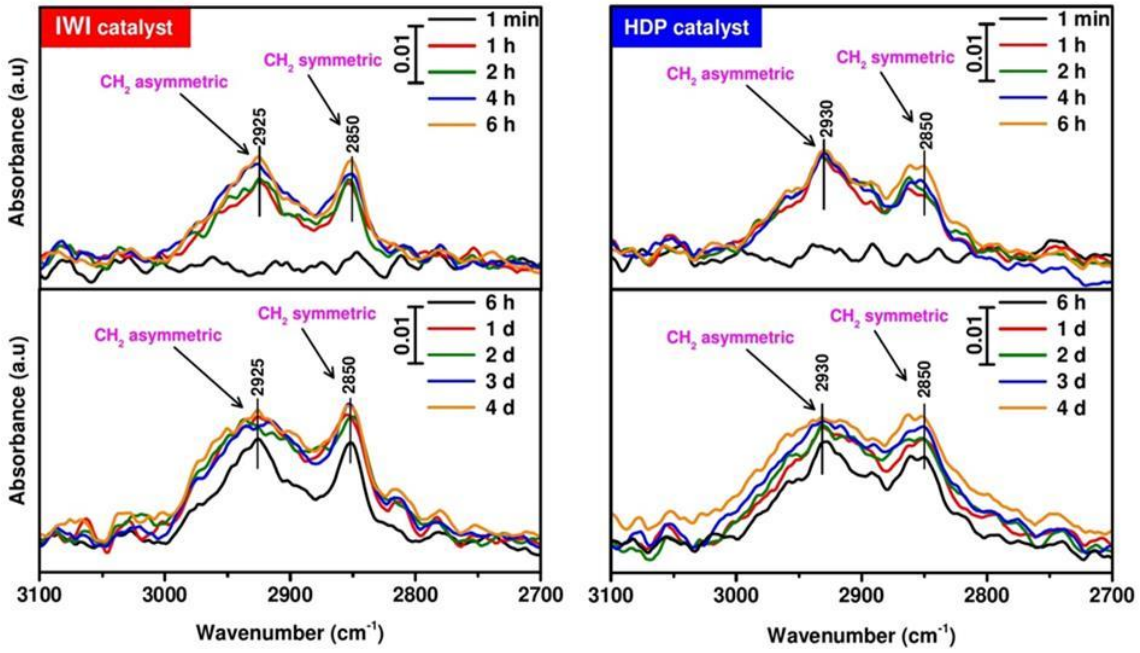

Figure 4.6: DRIFT spectra of IWI and HDP catalysts during FTS reaction.

The carboxylic acids are believed to have a role in the Co-based FTS catalysts deactivation, with Pinard et al. [22] measuring low catalytic performance with a sample containing surface carboxylates resistant to a rejuvenation treatment with hydrogen. Scalbert et al. [18] found absorption and an increase in the amount of oxygenated and unsaturated compounds with time on a Co/Al_2O_3 catalyst using XRD-DRIFT spectroscopy, species believed to be responsible for catalyst deactivation by covering the active sites. Gu et al. [42] found significant effects on the activity of the Co/Al_2O_3 FTS catalyst in the presence of acetic and butyric acids in the feed. The activity decreased by 50% in the presence of acetic acid and stabilised afterwards. The low activity was accredited to the formation of inactive cobalt acetate species, which was confirmed using FTIR and XRD spectroscopy. Addition of butyric acid showed a similar effect on the performance of the catalyst.

To verify the hypothesis that carboxylic acids play a role in the deactivation behaviour of the catalysts, both IWI and HDP samples were stripped under H_2 at 270 ^oC for 16 h to remove the surface species deposited on the catalysts during the initial 4-day reaction, followed by restarting the FTS reaction for an additional 2 days. Figure 4.7 shows the effect of stripping on DRIFT spectra of IWI and HDP catalysts. Acetates, hydrocarbons and part of the high MW carboxylates were removed from the IWI catalyst surface. In the case of HDP catalyst, hydrocarbons were removed significantly, while the carboxylates (formate being dominant) were partially removed. After restarting the reaction, the hydrocarbons and carboxylates on the surface of both catalysts re-appeared.

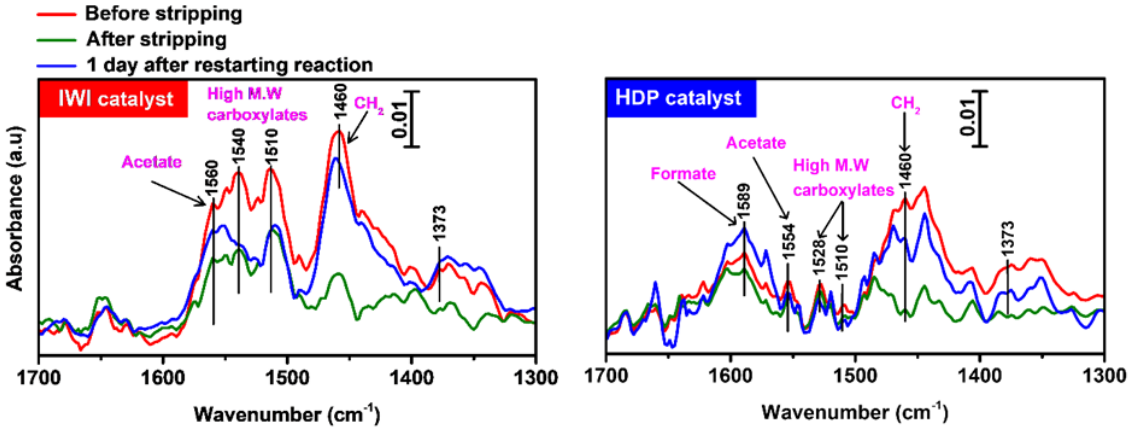

Figure 4.7: Effect of H_2 stripping on DRIFT spectra of IWI and HDP catalysts.

As shown in Figure 4.8, the H_2 stripping procedure results only in a modest activity recovery for both catalysts, suggesting that the surface carboxylates are not involved in a deactivation mechanism, being most likely spectator species on the titania support. The removal of the wax products from the catalyst pores during stripping is expected to have little effect on the activity, as the diffusion limitations are small due to chosen operating conditions with crushed particles and ~4% CO conversion. The similar deactivation pattern observed in Figure 4.8 with IWI and HDP samples, although on HDP far less carboxylates are present, provides another convincing evidence in support of the preferential location of the carboxylates on the support material. Also, the observed 40% drop in activity for both catalysts during FTS reaction would be related to significant presence of an oxidised cobalt phase, if carboxylates were associated with the active site. However, the Mossbauer results (Tables 4.2 and 4.3) showed that this is clearly not the case.

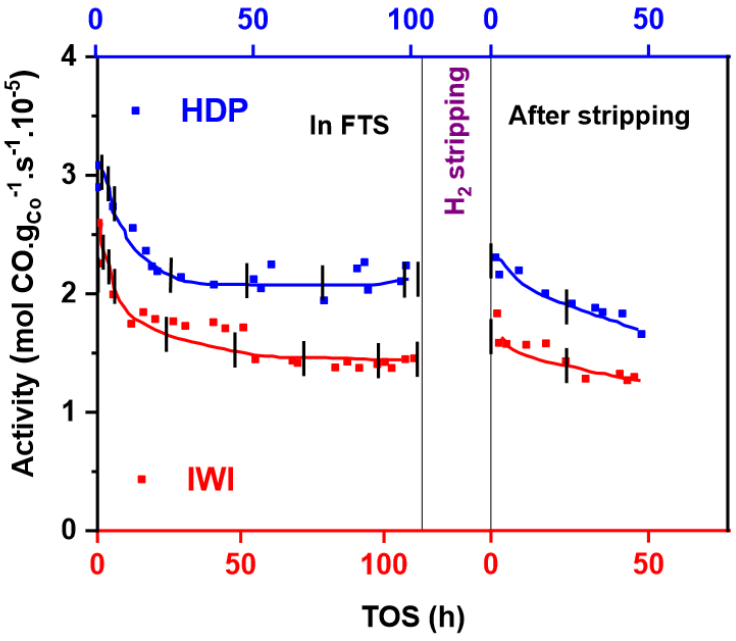

Figure 4.8: Effect of H_2 stripping on the performance of IWI and HDP catalysts.
| : Time of DRIFT spectrum measured.

Pinard et al. [22] showed using TPH that in a 100% H_2 environment the removal of carboxylates from the catalyst surface begins already at 270 ^oC under transient conditions. Therefore, the static 16 h applied stripping method is expected to remove most of the carboxylic acids. Some high MW carboxylates are still observed in the DRIFT spectra measured with the IWI catalyst after stripping (Figure 4.7, left), as carboxylates on cobalt are more easy to remove than on the support, since the removal requires a hydrogenation step. On metallic cobalt the required hydrogen activation is easily accomplished, but on the titania support, without neighbouring cobalt active species, it will take much longer. The presence of the carboxylates preferentially on the support material (before and after the stripping procedure) is backed by Schweicher et al. [37], who showed that the detected oxygenates were not part of the reaction mechanism. Paredes-Nunez et al. [38] demonstrated that the surface formate species present on an alumina-supported cobalt catalyst had two distinct reactivities, both associated to an oxide phase. As the MES results clearly indicate that cobalt oxidation is absent in our samples, we can substantiate the conclusion that most of the carboxylic acids are present on the TiO_2 support, with little influence on the catalytic activity.

4.4. Conclusions

The combination of operando spectroscopy techniques allowed to further elucidate the role of carboxylates during deactivation of cobalt on titania catalysts at industrial pressure. Carboxylate formation was seen on both precipitated and impregnated catalysts, but more and heavier carboxylates were found on the impregnated catalyst. The Mössbauer emission spectroscopy experiments indicated that almost full cobalt reduction is achieved at 350 ^oC and that oxidation was absent during the FTS reaction for both samples, regardless of their preparation method, showing that the large majority of the carboxylates are on the titania surface.

The combined gas chromatography/infrared spectroscopy data demonstrated that the surface carboxylate species are not involved in the catalysts deactivation, being most likely spectator species on the titania support. An interesting observation, which warrants further work, is that the formation of long-chain carboxylates was inhibited in the HDP catalyst, this may be due to the presence of impurities like nitrogen or salts introduced by the preparation procedure.

References

[1] A.Y. Khodakov, W. Chu, P. Fongarland, Advances in the development of novel cobalt Fischer-Tropsch catalysts for synthesis of long-chain hydrocarbons and clean fuels, Chem. Rev. 107 (2007) 1692–1744.

[2] E. Iglesia, Design, synthesis, and use of cobalt-based Fischer-Tropsch synthesis catalysts, Appl. Catal. A Gen. 161 (1997) 59–78.

[3] J. Remans, G. Jenzer, A. Hoek, Gas-to-Liquids, in: Handb. Heterog. Catal., 2nd ed., Wiley-VCH, Weinheim, 2008.

[4] N.E. Tsakoumis, M. Rønning, Ø. Borg, E. Rytter, A. Holmen, Deactivation of cobalt based Fischer–Tropsch catalysts: A review, Catal. Today. 154 (2010) 162–182.

[5] A.M. Saib, D.J. Moodley, I.M. Ciobîcă, M.M. Hauman, B.H. Sigwebela, C.J. Weststrate, J.W. Niemantsverdriet, J. van de Loosdrecht, Fundamental understanding of deactivation and regeneration of cobalt Fischer–Tropsch synthesis catalysts, Catal. Today. 154 (2010) 271–282.

[6] E. Rytter, A. Holmen, Deactivation and Regeneration of Commercial Type Fischer-Tropsch Co-Catalysts A Mini-Review, Catalysts. 5 (2015) 478–499.

[7] D.J. Moodley, J. van de Loosdrecht, A.M. Saib, M.J. Overett, A.K. Datye, J.W. Niemantsverdriet, Carbon deposition as a deactivation mechanism of cobalt-based Fischer–Tropsch synthesis catalysts under realistic conditions, Appl. Catal. A Gen. 354 (2009) 102–110.

[8] G. Jacobs, P.M. Patterson, Y. Zhang, T. Das, J. Li, B.H. Davis, Fischer–Tropsch synthesis: deactivation of noble metal-promoted Co/Al_2O_3 catalysts, Appl. Catal. A Gen. 233 (2002) 215–226.

[9] T.O. Eschemann, K.P. de Jong, Deactivation Behavior of Co/TiO_2 Catalysts during Fischer–Tropsch Synthesis, ACS Catal. 5 (2015) 3181–3188.

[10] C.H. Bartholomew, Mechanisms of catalyst deactivation, Appl. Catal. A Gen. 212 (2001) 17–60.

[11] T.K. Das, W.A. Conner, J. Li, G. Jacobs, M.E. Dry, B.H. Davis, Fischer−Tropsch Synthesis: Kinetics and Effect of Water for a Co/SiO_2 Catalyst, Energy & Fuels. 19 (2005) 1430–1439.

[12] G.L. Bezemer, T.J. Remans, A.P. Van Bavel, A.I. Dugulan, Direct evidence of water-assisted sintering of cobalt on carbon nanofiber catalysts during simulated Fischer-Tropsch conditions revealed with in-situ Mössbauer spectroscopy, J. Am. Chem. Soc. 132 (2010) 8540–8541.

[13] S. Storsæter, Ø. Borg, E.A. Blekkan, A. Holmen, Study of the effect of water on Fischer–Tropsch synthesis over supported cobalt catalysts, J. Catal. 231 (2005) 405–419.

[14] W. Ma, G. Jacobs, D.E. Sparks, R.L. Spicer, B.H. Davis, J.L.S. Klettlinger, C.H. Yen, Fischer–Tropsch synthesis: Kinetics and water effect study over $25\%Co/Al_2O_3$ catalysts, Catal. Today. 228 (2014) 158–166.

[15] D. Kistamurthy, A.M. Saib, D.J. Moodley, J.W. Niemantsverdriet, C.J. Weststrate, Ostwald ripening on a planar Co/SiO_2 catalyst exposed to model Fischer–Tropsch synthesis conditions, J. Catal. 328 (2015) 123–129.

[16] D. Peña, A. Griboval-Constant, C. Lancelot, M. Quijada, N. Visez, O. Stéphan, V. Lecocq, F. Diehl, A.Y. Khodakov, Molecular structure and localization of carbon species in alumina supported cobalt Fischer–Tropsch catalysts in a slurry reactor, Catal. Today. 228 (2014) 65–76.

[17] D. Peña, A. Griboval-Constant, V. Lecocq, F. Diehl, A.Y. Khodakov, Influence of operating conditions in a continuously stirred tank reactor on the formation of carbon species on alumina supported cobalt Fischer–Tropsch catalysts, Catal. Today. 215 (2013) 43–51.

[18] J. Scalbert, I. Clémençon, P. Lecour, L. Braconnier, F. Diehl, C. Legens, Simultaneous investigation of the structure and surface of a Co/alumina catalyst during Fischer–Tropsch synthesis: discrimination of various phenomena with beneficial or disadvantageous impact on activity, Catal. Sci. Technol. 5 (2015) 4193–4201.

[19] R.A. van Santen, A.J. Markvoort, I.A.W. Filot, M.M. Ghouri, E.J.M. Hensen, Mechanism and microkinetics of the Fischer–Tropsch reaction, Phys. Chem. Chem. Phys. 15 (2013) 17038–17063.

[20] R.A. van Santen, M. Ghouri, E.M.J. Hensen, Microkinetics of oxygenate formation in the Fischer–Tropsch reaction, Phys. Chem. Chem. Phys. 16 (2014) 10041–10058.

[21] A. de Klerk, Fischer Tropsch Refining, PhD Thesis, University of Pretoria, 2008.

[22] L. Pinard, P. Bichon, A. Popov, J.L. Lemberton, C. Canaff, F. Maugé, P. Bazin, E.F. S.-Aguiar, P. Magnoux, Identification of the carbonaceous compounds present on a deactivated cobalt based Fischer–Trospch catalyst resistant to “rejuvenation treatment,” Appl. Catal. A Gen. 406 (2011) 73–80.

[23] F.C. Meunier, Coupling kinetic and spectroscopic methods for the investigation of environmentally important reactions, in: Catalysis, Royal Society of Chemistry, Cambridge, 2010: pp. 94–118.

[24] F.C. Meunier, Pitfalls and benefits of in situ and operando diffuse reflectance FT-IR spectroscopy (DRIFTS) applied to catalytic reactions, React. Chem. Eng. 1 (2016) 134–141.

[25] J. Scalbert, I. Clémençon, C. Legens, F. Diehl, D. Decottignies, S. Maury, Development of an Innovative XRD-DRIFTS Prototype Allowing Operando Characterizations during Fischer-Tropsch Synthesis over Cobalt-Based Catalysts under Representative Conditions, Oil Gas Sci. Technol. – Rev. d’IFP Energies Nouv. 70 (2015) 419–428.

[26] M.W.J. Crajé, A.M. van der Kraan, J. van de Loosdrecht, P.J. van Berge, The application of Mössbauer emission spectroscopy to industrial cobalt based Fischer–Tropsch catalysts, Catal. Today. 71 (2002) 369–379.

[27] T.O. Eschemann, J.H. Bitter, K.P. de Jong, Effects of loading and synthesis method of titania-supported cobalt catalysts for Fischer–Tropsch synthesis, Catal. Today. 228 (2014) 89–95.

[28] F. Morales Cano, O.L.J. Gijzeman, F.M.F. de Groot, B.M. Weckhuysen, Manganese promotion in cobalt-based Fischer-Tropsch catalysis, Stud. Surf. Sci. Catal. 147 (2004) 271–276.

[29] I.C. Yates, C.N. Satterfield, Intrinsic kinetics of the Fischer-Tropsch synthesis on a cobalt catalyst, Energy & Fuels. 5 (1991) 168–173.

[30] Z. Yan, Z. Wang, D.B. Bukur, D.W. Goodman, Fischer–Tropsch synthesis on a model Co/SiO_2 catalyst, J. Catal. 268 (2009) 196–200.

[31] C.G. Cooper, T.-H. Nguyen, Y.-J. Lee, K.M. Hardiman, T. Safinski, F.P. Lucien, A.A. Adesina, Alumina-supported cobalt-molybdenum catalyst for slurry phase Fischer-Tropsch synthesis, Catal. Today. 131 (2008) 255–261.

[32] H. Schulz, Z. Nie, M. Claeys, Initial Episodes of Fischer-Tropsch Synthesis with Cobalt Catalysts, in: 1998: pp. 191–196.

[33] C. Wivel, B.S. Clausen, R. Canada, S. Mørup, H. Topsøe, Mössbauer Emission Studies of Calcined $Co-Mo/Al_2O_3$ Catalysts: Catalytic Significance of Co Precursors, J. Catal. 87 (1984) 497–513.

[34] J. van de Loosdrecht, B. Balzhinimaev, J.-A. Dalmon, J.W. Niemantsverdriet, S.V. Tsybulya, A.M. Saib, P.J. van Berge, J.L. Visagie, Cobalt Fischer-Tropsch synthesis: Deactivation by oxidation?, Catal. Today. 123 (2007) 293–302.

[35] T.O. Eschemann, J. Oenema, K.P. de Jong, Effects of noble metal promotion for Co/TiO_2 Fischer-Tropsch catalysts, Catal. Today. 261 (2016) 60–66.

[36] F.M.T. Mendes, C.A.C. Perez, F.B. Noronha, C.D.D. Souza, D. V. Cesar, H.J. Freund, M. Schmal, Fischer−Tropsch Synthesis on Anchored $Co/Nb_2O_5/Al_2O_3$ Catalysts: The Nature of the Surface and the Effect on Chain Growth, J. Phys. Chem. B. 110 (2006) 9155–9163.

[37] J. Schweicher, A. Bundhoo, A. Frennet, N. Kruse, H. Daly, F.C. Meunier, DRIFTS/MS Studies during Chemical Transients and SSITKA of the CO/H_2 Reaction over Co-MgO Catalysts, J. Phys. Chem. C. 114 (2010) 2248–2255.

[38] A. Paredes-Nunez, D. Lorito, N. Guilhaume, C. Mirodatos, Y. Schuurman, F.C. Meunier, Nature and reactivity of the surface species observed over a supported cobalt catalyst under CO/H_2 mixtures, Catal. Today. 242 (2015) 178–183.

[39] D. Lorito, A. Paredes-Nunez, C. Mirodatos, Y. Schuurman, F.C. Meunier, Determination of formate decomposition rates and relation to product formation during CO

hydrogenation over supported cobalt, Catal. Today. 259 (2016) 192–196.

[40] W. Shafer, M. Gnanamani, U. Graham, J. Yang, C. Masuku, G. Jacobs, B. Davis, Fischer–Tropsch: Product Selectivity–The Fingerprint of Synthetic Fuels, Catalysts. 9 (2019) 259.

[41] M.K. Niemelä, A.O.I. Krause, The long-term performance of Co/SiO_2 catalysts in CO hydrogenation, Catal. Letters. 42 (1996) 161–166.

[42] B. Gu, A.Y. Khodakov, V. V. Ordomsky, Selectivity shift from paraffins to α-olefins in low temperature Fischer–Tropsch synthesis in the presence of carboxylic acids, Chem. Commun. 54 (2018) 2345–2348.

Chapter 5

Effect of formic acid addition on the performance of a Co/TiO_2 Fischer-Tropsch synthesis catalyst

Fischer-Tropsch synthesis (FTS) is a catalytic process that converts mixtures of CO and H_2 (synthesis gas) obtained from natural gas, coal and biomass into liquid hydrocarbon fuels and chemicals. Deposition of different carboxylate compounds on the catalyst surface has been identified previously and it was believed that these carboxylates block the active sites of the reaction. Therefore, to understand the role of carboxylates in FTS, co-feeding of formic acid on the catalyst has been investigated with operando DRIFT spectroscopy. A small amount of formic acid was co-fed on a Co/TiO_2 catalyst using a temperature-controlled saturator, resulting in only a negligible change in catalyst performance. When formic acid interacted with the Co/TiO_2 catalyst in the H_2 atmosphere, it decomposed into CO and H_2 on the catalyst surface and produced different hydrocarbons. Some of the formate species on the catalyst surface were transformed into high MW carboxylates which were removed immediately after stopping the co-feeding, by decomposition or hydrogenation, indicating that they were present on the cobalt active sites. These high MW carboxylates formed during co-feeding could be spectator species formed on the terrace sites of the cobalt that are not contributing to catalyst activity.

5.1. Introduction

Fischer-Tropsch synthesis (FTS) is a catalytic process that converts mixtures of CO and H_2 (synthesis gas) obtained from coal, natural gas and biomass into liquid hydrocarbon fuels and fine chemicals [1–4]. FTS reaction mechanism is very complex and involved in many surface elementary reaction steps [5,6]. Various reaction mechanisms, like carbide [7], enolic [7] and CO insertion [8–10] have been proposed to explain the FTS reaction. Whether carbon chain growth occurs via the involvement of intermediate oxygenated or hydrocarbon compounds has gained more attention [11–13]. The most important chain growth mechanism for FTS is the surface carbide mechanism [7,14]. Chen et al. [12] confirmed that CHx species are involved in the chain growth mechanism and this chain growth mechanism is highly reversible. Carbon chain growth by a CO insertion mechanism also has been proposed earlier [8,15,16]. To understand the FTS reaction mechanism, surface species formed on the catalyst were investigated using both *in-situ* and *ex-situ* characterisation techniques. As it is very critical to understand the exact nature of surface species and active sites of the reaction on the catalyst, several studies reported a view of these surface species formed at reaction conditions with *in-situ* infrared spectroscopy [17–20]. Deposition of several oxygenated and carbon compounds on the catalyst surface during FTS was observed already [21–23]. Meunier et al. [24–26] identified two types of formate species: fast reacting and slow reacting formate species on the surface of a Co/Siralox catalyst in CO hydrogenation, based on the decomposition rates. Simultaneously the reaction products were analysed and compared with the formate decomposition rates. They proposed that only fast reacting formate species could be responsible for methanol formation, since formate species are considered as intermediates in methanol synthesis on Cu-based catalysts [27–29].

Previous research proposed that the oxygenated compounds deposited on the catalyst surface could not only participate in the reaction but could also deactivate the catalyst by blocking the active sites of the reaction. Pinard et al. [23] found that carboxylates deposited on the catalyst were resistant to a rejuvenation treatment with hydrogen. From their studies, it was proposed that carboxylates on the catalyst surface deactivate the catalyst. Scalbert et al. [22] found absorption and an increase in the amount of oxygenated and unsaturated compounds with time on a Co/Al_2O_3 FTS catalyst using XRD-DRIFT spectroscopy and proposed that these strongly absorbed species are responsible for catalyst deactivation by covering the active sites. Gu et al. [30] found significant effects on the activity of a Co/Al_2O_3 FTS catalyst in the presence of carboxylic acids in the feed gas. The activity decreased to half when the acetic acid was introduced into the feed and stabilised afterwards. They proposed that the decrease in activity is due to the formation of inactive cobalt acetate species in the presence of acetic acid, which was confirmed by identifying the cobalt acetate species on the spent catalyst using infrared and XRD spectroscopy. We previously observed the deposition of carboxylates species on the surface of catalysts during FTS, using operando DRIFT spectroscopy. It was shown that the carboxylates don't influence the performance of the catalysts and they mostly stay on the support material as spectator species [31]. However, the role of these carboxylic acids FTS mechanism and the chemical nature of the catalyst surface during carboxylic acids co-feeding are not very clear. Therefore to study the catalyst surface during FTS, we adopted

operando DRIFT spectroscopy because it can give valuable information about surface species, reaction products and reaction mechanism [32,33]. The aim of the present study was to investigate the possible role of co-feeding of formate species on the Co/TiO_2 FTS catalyst surface in the deactivation mechanism at industrially relevant conditions.

5.2. Experimental

5.2.1. Catalyst preparation

$Co(10\ wt\%)/TiO_2$ - IWI catalyst provided by Shell Global Solutions International B.V., Amsterdam was prepared by two step impregnation. First, the support material (Degussa P25 with surface area 50 $m^2.g^{-1}$ and pore volume 0.319 $mL.g^{-1}$) was dried and impregnated with 1 pore volume of an aqueous solution of $Co(NO_3)_2$ (17.25 wt% Co). In the second impregnation, the obtained material (pore volume 0.283 $mL.g^{-1}$) was impregnated with 0.95 pore volume of an aqueous solution of $Co(NO_3)_2$ (20.02 wt% Co). After each impregnation step, the obtained material was dried in an oven at 60 ^oC overnight under static air and calcined at 400 ^oC for 2 hours under N_2 flow.

5.2.2. Operando DRIFT spectroscopy

To study the effect of formic acid co-feeding in FTS, an operando DRIFT reaction setup was adopted. The design and optimisation details and the scheme of the reaction setup are described in Chapter 2: Experimental techniques. The surface of the catalyst was monitored with a Thermo Nicolet Nexus 670 FT-IR spectrometer to study the reaction intermediates and products.

For co-feeding experiments, high quality formic acid was obtained from Sigma-Aldrich and used without further modification. To co-feed small concentrations roughly 50-300 parts per million by volume (ppmv) of formic acid into the reaction gas, a temperature-controlled saturator was placed in the CO or H_2 gas lines as shown in Figure 2.4. The temperature of the saturator necessary to flow the required concentration of formic acid was calculated using the Antoine vapor pressure temperature relationship and the calculated vapor pressure values of the formic acid are in agreement with the experimental values of Coolidge [34–37].

5.2.3. Catalytic testing with formic acid co-feeding

Co/TiO_2 catalyst sample was loaded into the operando DRIFT reaction cell and reduced at 350 ^oC in 100 mL/min H_2 for 2 hours. The reaction cell was then cooled down to the reaction temperature (200 ^oC) and a background spectrum was measured in Ar/H_2 mixture. After this step, CO was introduced into the system and pressure was increased to 2 MPa. FTS reaction conditions of 200 ^oC, 2 MPa and H_2/CO= 2 v/v were maintained for 40 hours until a steady state of the reaction was reached. After this step, 65 ppmv of formic acid was co-fed using the saturator by maintaining the corresponding temperature for 48 hours. Again, co-feeding was stopped and the experiment was continued as normal FTS reaction. Then hydrogen stripping was performed at 350 ^oC in 100 mL/min H_2 for 2 hours and the same procedure was repeated with 150 ppmv of formic acid co-feeding. In a third experiment, for a better understanding of

formic acid effect, 150 ppmv of formic acid was co-fed from the beginning of the reaction with a new catalyst sample.

5.2.4. Interaction of formic acid in H_2 with the Co/TiO_2 catalyst

Formic acid was fed into the reaction cell without CO in the inlet gas. First, Co/TiO_2 catalyst sample was loaded into the operando DRIFT reaction cell and reduced at 350 ^oC in 100 mL/min H_2 for 2 hours. Then the reaction cell was cooled down to the reaction temperature and a background spectrum was measured in Ar/H_2. After this step, the pressure was increased to 2 MPa. Varying concentrations of formic acid was co-fed by flowing H_2 gas through the saturator at the corresponding temperature. The reaction products obtained from the formic acid on the catalyst were continuously analysed with the Ultra Trace GC-MS. Simultaneously, infrared spectra of the catalyst were measured to understand the formic acid interaction with the catalyst.

5.3. Results and discussion

5.3.1. Effect of formic acid co-feeding in the middle of the reaction

To better observe the small influence of formic acid on the catalyst performance, the C_1-C_9 hydrocarbon production rates are presented here, as measured by the sensitive FID detector as shown in Figures 5.1 and 5.2. The production rate of hydrocarbons decreased slowly with time in accordance with the literature [38]. The production rate of FTS hydrocarbons by the Co/TiO_2 catalyst with 65 ppmv of formic acid co-feeding is shown in Figure 5.1. The production rate of hydrocarbons decreased slowly with time before co-feeding (up to 40 h). Even during co-feeding (41-88 h) and after co-feeing (89-120 h), the production rate of hydrocarbons decreased slowly as in standard FTS reaction. The influence of 65 ppmv of formic acid addition on catalyst performance was undetectable. Then hydrogen stripping was performed at 350 ^oC in 100 mL/min H_2 for 2 hours and the experiment was repeated with 150 ppmv of formic acid, as shown in Figure 5.2. After 40 hours of FTS, at the beginning of the co-feeding, the rate of formation of hydrocarbons increased slightly and then continued to decrease slowly with time as usual. This could be due to the participation of co-fed formic acid in the FTS reaction and production of an extra amount of hydrocarbons. After stopping co-feeding at 88 h of TOS (48 h of co-feeding), there is a little bit increase in the hydrocarbon production rate and then continued to decrease slowly with time.

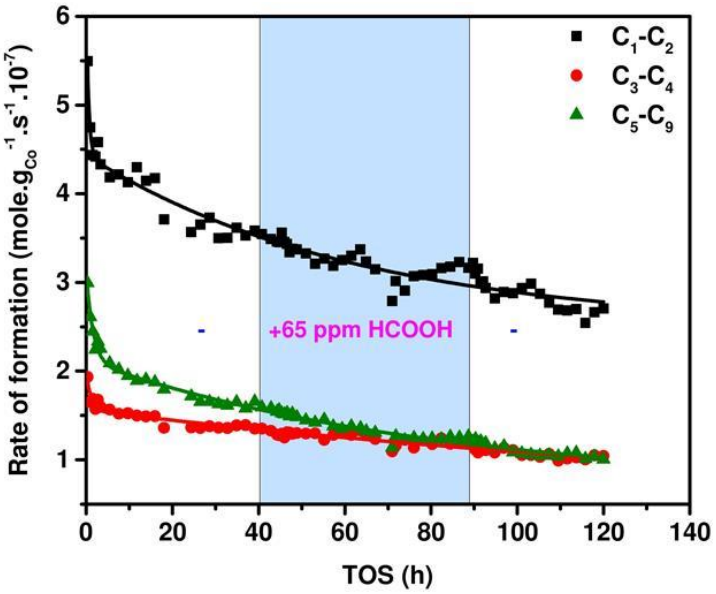

Figure 5.1: Production rate of C_1-C_9 hydrocarbons as a function of the time on stream.

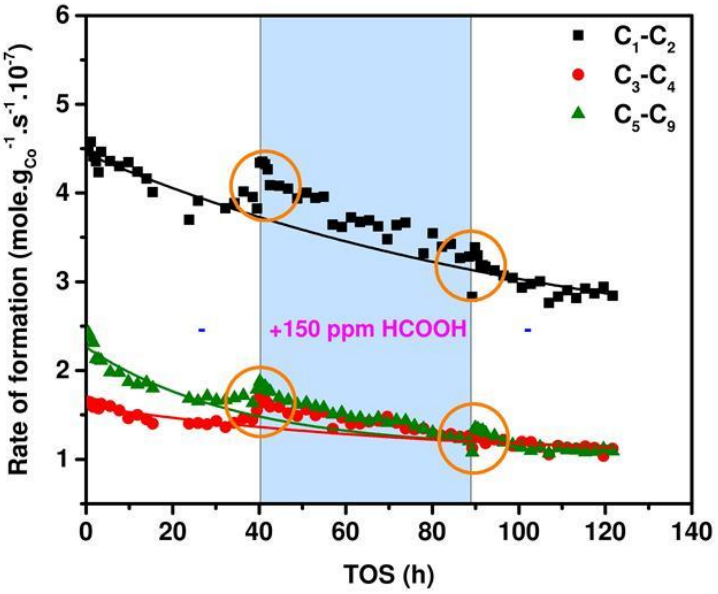

Figure 5.2: Production rate of C_1-C_9 hydrocarbons as a function of the time on stream.

The DRIFT spectra of the Co/TiO_2 catalyst surface in 150 ppmv of formic acid co-feeding are presented in Figure 5.3. The bands at 1560, 1540 and 1515 cm^{-1} correspond to asymmetric vibrations of carboxylates deposited on the catalyst [23]. The band at 1458 cm^{-1} is due to the CH_2 bending vibration of hydrocarbons and carboxylates. When formic acid is co-fed on to the catalyst, new peaks at 1589 and 1368 cm^{-1}, corresponding to asymmetric and symmetric vibrations of formate species, appeared as shown in Figure 5.3b [26,33,39]. It clearly indicates that co-fed formic acid interacted with active cobalt sites. The adsorption measurements of carboxylic acids on Co/TiO_2 catalyst and TiO_2 support confirmed that the peak at 1589 cm^{-1} is due to the adsorption of formate species on active cobalt sites (refer to Chapter 3 - Figure 3.1). After starting co-feeding, ~50% of the catalytic sites were occupied by formate species within 1 h (41 h TOS). The intensity of these formate species increased up

to 60 h of TOS, where ~70% of the catalytic sites were occupied by formate species*. Thereafter, the peaks at 1540 and 1515 cm^{-1} became dominant, indicating that the catalyst surface is replaced by high molecular weight (MW) carboxylates. It is apparent that the formate species transformed into high MW carboxylates, which became dominant on the catalyst surface. Even though formic acid is present in the feed gas, the high MW carboxylates are dominant on the catalyst surface, replacing the formate species on the active cobalt sites and preventing formic acid to reach them further. This is a clear indication that the high MW carboxylates deposit on the active sites of the catalyst. After stopping the formic acid co-feeding at 88 h, the intensity of the high MW carboxylates decreased due to their partial removal from the catalyst surface as shown in Figure 5.3c. The rate of hydrocarbons also increased a little bit after stopping the co-feeding, which could be related to the removal of some high MW carboxylates from the catalyst surface. After 100 h of TOS, the catalyst surface is dominated again by formate species, which can now occupy the active sites vacated by the high MW carboxylates. In the standard FTS reaction, the high MW carboxylates deposited continuously on the catalyst surface (see Figure S5.3 and Chapter 4) and could not be removed so easily from the catalyst as they were spectator species located on the support [31]. The carboxylates formed in the current experiment are easily removed when the formic acid co-feeding is stopped. It indicates that the carboxylates formed exclusively in the presence of formic acid are present on the cobalt active sites, being easily removed by hydrogenation. Even when a clear interaction of carboxylates with Co is observed, the influence of carboxylates on the catalyst performance is very small and they transform and remove very fast on metal. Therefore, these carboxylate species are not spectators on the support. These high MW carboxylates formed during co-feeding could be spectator species sitting on the cobalt terrace sites that are not contributing to the activity as CO dissociation and chain growth happen on step edge B5 sites [40]. Also, olefins to paraffins ratio increased slightly after stopping co-feeding as shown in Figure S5.1, which could be due to the conversion of high MW carboxylates into olefins on the catalyst surface. The relation between olefins presence and carboxylate formation was already discussed in the previous chapters.

* The percentage of catalytic sites occupied by formate species is estimated by comparing the intensities of the formate peak at 1589 cm^{-1}. It is assumed that the formate peak of the spectrum in Figure 5.6 at 200 °C with 300 ppmv co-feeding is due to monolayer full coverage with formate species because the peak at 1758 cm^{-1} corresponding to liquid formic acid appears.

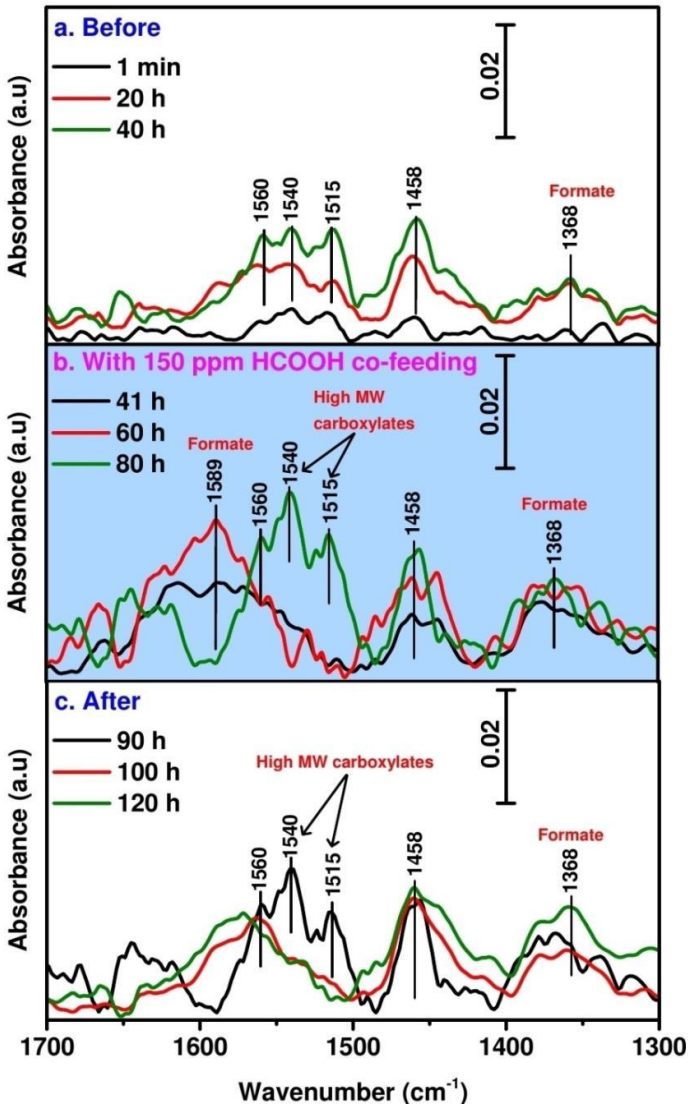

Figure 5.3: DRIFT spectra of the Co/TiO_2 catalyst, **(a)** Before co-feeing **(b)** With 150 ppmv HCOOH co-feeding and **(c)** After co-feeding.

5.3.2. Effect of formic acid co-feeding from the beginning of the reaction

For a better understanding of the formic acid effect, co-feeding was applied from the beginning of the FTS reaction as shown in Figure 5.4. The influence of the formic acid co-feeding on the catalyst performance is negligible. Here also, the rate of production of hydrocarbons decreased slowly with time. After stopping the 150 ppmv co-feeding at 48 h, the rate of production of hydrocarbons increased temporarily as already observed in Figure 5.2. The infrared spectra of the catalyst during co-feeding are shown in Figure 5.5. In formic acid co-feeding, initially, catalyst surface is dominated by formate species at 1589 cm^{-1} as observed already in Figure 5.3b, indicating that formate species are interacting with cobalt active sites. Later, the catalyst surface is dominated by high MW carboxylates as shown in Figure 5.5a. The formate species on the catalyst surface set up the production of high MW

carboxylates, which became dominant in time. After stopping the co-feeding, the intensity of the high MW carboxylates decreased as shown in Figure 5.5b. This is again related to the removal of high MW carboxylates from the catalyst surface by either decomposition or hydrogenation as already observed previously. After 60 h of TOS, the catalyst surface is dominated by formate species similar to the previous experiment shown in Figure 5.3c. Again, it shows that high MW carboxylates formed during formic acid co-feeding are on the surface of the cobalt sites, being easily removed. Here also, olefins to paraffins ratio increased slightly after stopping co-feeding as shown in Figure S5.2 as observed already. One more observation is that after stopping co-feeding, formate species became dominant with a small amount of high MW carboxylates still present on the catalyst surface. Whereas, in normal FTS reaction a large amount of high MW carboxylates remained on the TiO_2 support, as observed in Chapter 4. We propose that the sites involved in carboxylates production during normal FTS are now occupied by high MW carboxylates obtained directly from the co-fed formic acid. Only when the co-feeding is stopped and all decomposition products (low MW carboxylates) are removed from the active sites – the normal FTS operation will resume.

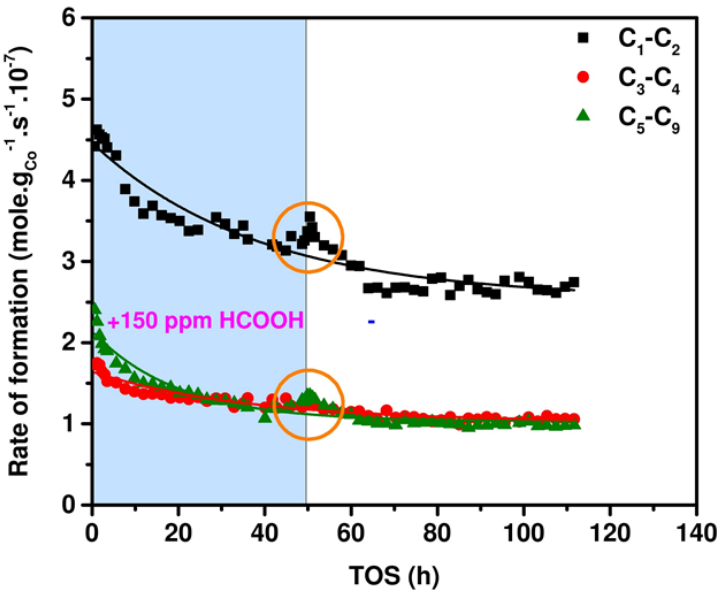

Figure 5.4: Production rate of C_1-C_9 hydrocarbons on the Co/TiO_2 catalyst as a function of the time on stream.

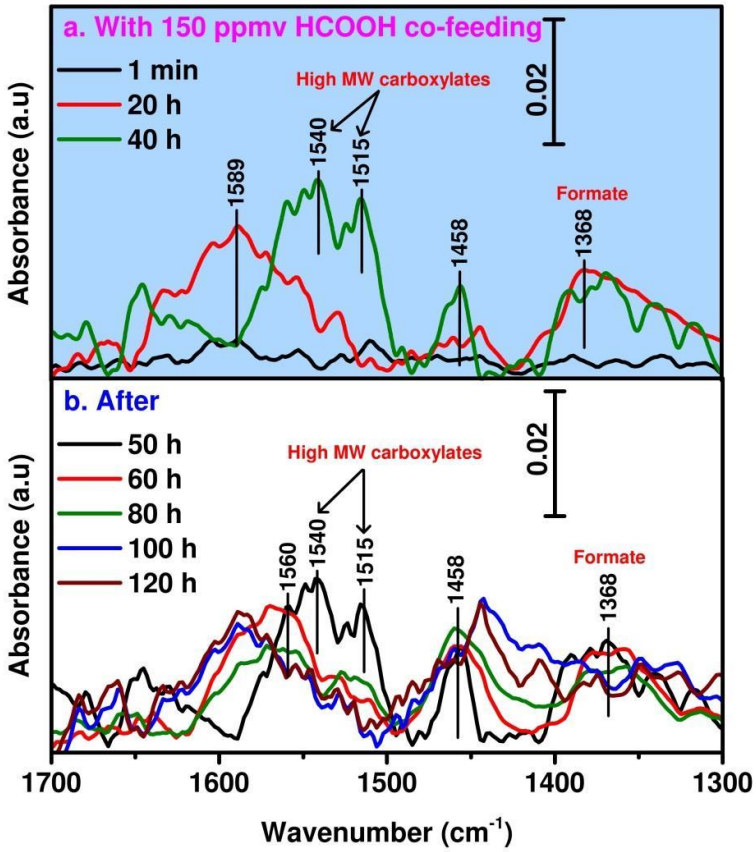

Figure 5.5: DRIFT spectra of the Co/TiO$_2$ catalyst, **(a)** With 150 ppmv HCOOH co-feeding and **(b)** After co-feeding.

5.3.2. Interaction of formic acid and H$_2$ with Co/TiO$_2$

To understand the role of formic acid on the catalyst surface in FTS, formic acid was co-fed without CO in the inlet gas. DRIFT spectra of the Co/TiO$_2$ catalyst surface during co-feeding are shown in Figure 5.6. The peaks at 1589 and 1358 cm^{-1} are corresponding to asymmetric and symmetric vibrations of formate species adsorbed on the active cobalt sites [25,26]. The shoulder at 1560 cm^{-1} is associated with formate species on the TiO$_2$ support. These peaks are due to the rapid adsorption of formic acid on the catalyst to yield surface formate species [41]. The peak at 1758 cm^{-1} is corresponding to physically bonded formic acid molecules on the catalyst surface. Their amount is very small due to weakly adsorption and readily desorption of formic acid on the catalyst surface [39]. When the reaction temperature is increased to 220 ^{o}C, the intensity of the formate peak decreased due to an increase in the decomposition of formate species with increasing temperature. When the amount of co-feeding was increased to 600 ppmv at 220 ^{o}C, the intensity of formate peak increased due to the abundant availability of formic acid.

Figure 5.7 shows the FID chromatogram of the reaction products obtained from formic acid on the Co/TiO$_2$ catalyst. The peaks corresponding to C$_1$-C$_{10}$ hydrocarbons indicated that formic acid first decomposed on the catalyst surface and later converted into hydrocarbons. The decomposition of formic acid on metals and metal oxides has been reported by many

researchers [41–48]. Wescott and Engelder [42,49] studied the catalytic decomposition of formic acid into CO, CO_2, H_2O and H_2 on alumina, titania and nickel. It was found that the dehydrating reaction of formic acid producing CO and H_2O is a predominant reaction on alumina and titania. Kim and Barteau [46] also studied the formic acid decomposition reactions on TiO_2 (anatase) using temperature-programmed desorption. Both formic acid and formate species were observed on the surface of TiO_2 and most of the formic acid decomposed into CO and H_2O. Albert et al. [50] presented a method first transforming formic acid into syngas by decomposition followed by FTS process to produce hydrocarbons on a Co/Al_2O_3 catalyst. They also observed the production of hydrocarbons from formic aid with varying carbon number, similar to our results. The increase in the production rate of hydrocarbons, at the beginning of formic acid co-feeding as shown in Figure 5.2 is mainly due to decomposition of formic acid into CO and H_2 on the catalyst surface and followed by FTS process to produce an extra amount of hydrocarbons. As shown in Figure 5.7, all hydrocarbons (C_1-C_{10}) produced from formic acid are paraffins and the very high amount of C_1-C_2 compared to other hydrocarbons is due to very low CO partial pressure and availability of abundant amount of H_2 in the reaction gas for complete hydrogenation.

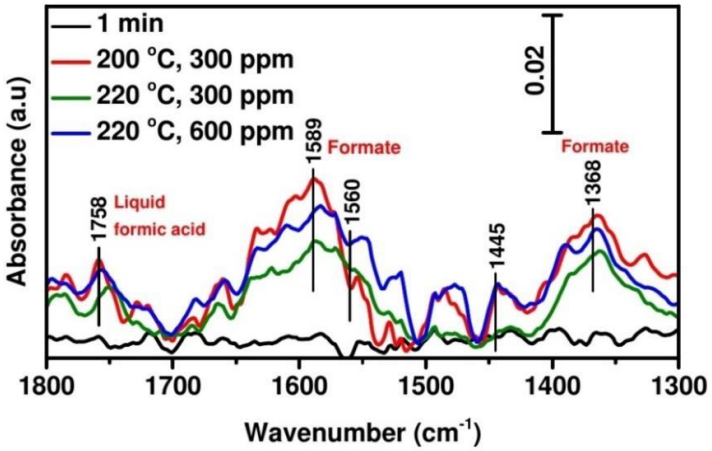

Figure 5.6: DRIFT spectra of the Co/TiO_2 catalyst with HCOOH co-feeding.

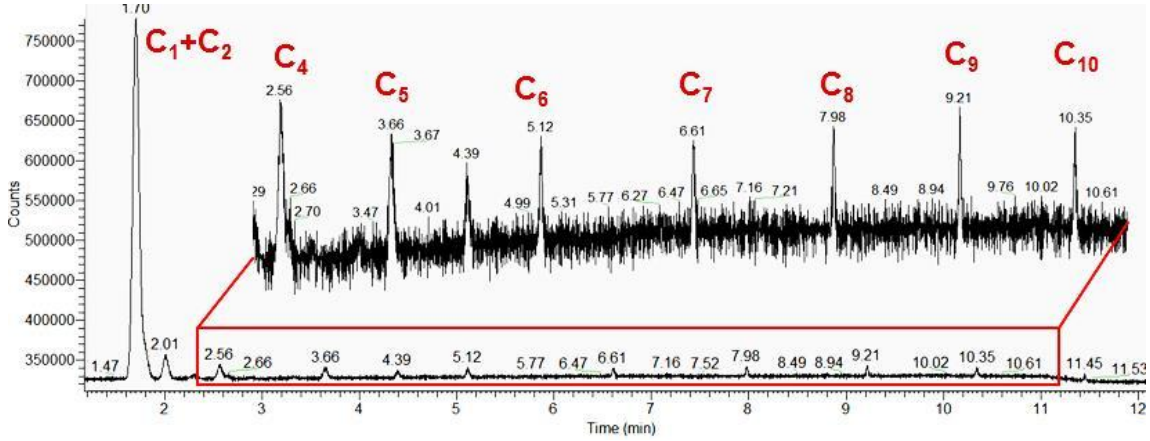

Figure 5.7: FID chromatograph of the reaction products obtained from the formic acid on the Co/TiO_2 catalyst.

5.4. Conclusions

The role of formic acid interaction with the Co/TiO_2 catalyst has been investigated with operando DRIFT spectroscopy. Formic acid co-feeding did not influence the catalyst performance significantly. When formic acid interacted with the Co/TiO_2 sample in H_2 atmosphere, it decomposed on the catalyst surface and produced different hydrocarbons. During formic acid co-feeding, some of the formate species on the catalyst surface were transformed into high MW carboxylates that are removed after stopping co-feeding, by decomposition or hydrogenation, indicating that these carboxylates are present on the cobalt sites. These high MW carboxylates formed during co-feeding could be spectator species formed on the terrace sites of the cobalt that are not contributing to catalyst activity. During co-feeding, the accumulation of high MW carboxylates on the support is limited.

References

[1] E. Iglesia, Design, synthesis, and use of cobalt-based Fischer-Tropsch synthesis catalysts, Appl. Catal. A Gen. 161 (1997) 59–78.

[2] P.J. van Berge, J. van de Loosdrecht, S. Barradas, A.M. van der Kraan, Oxidation of cobalt based Fischer–Tropsch catalysts as a deactivation mechanism, Catal. Today. 58 (2000) 321–334.

[3] M.E. Dry, The Fischer–Tropsch process: 1950–2000, Catal. Today. 71 (2002) 227–241.

[4] G.P. Van der laan, A.A.C.M. Beenackers, Kinetics and Selectivity of the Fischer–Tropsch Synthesis: A Literature Review, Catal. Rev. 41 (1999) 255–318.

[5] C.K. Rofer-DePoorter, A comprehensive mechanism for the Fischer-Tropsch synthesis, Chem. Rev. 81 (1981) 447–474.

[6] M.E. Dry, Practical and theoretical aspects of the catalytic Fischer-Tropsch process, Appl. Catal. A Gen. 138 (1996) 319–344.

[7] R.M. de Deugd, F. Kapteijn, J.A. Moulijn, Using monolithic catalysts for highly selective Fischer–Tropsch synthesis, Catal. Today. 79–80 (2003) 495–501.

[8] R.A. van Santen, A.J. Markvoort, Chain Growth by CO Insertion in the Fischer-Tropsch Reaction, ChemCatChem. 5 (2013) 3384–3397.

[9] R.A. van Santen, A.J. Markvoort, I.A.W. Filot, M.M. Ghouri, E.J.M. Hensen, Mechanism and microkinetics of the Fischer–Tropsch reaction, Phys. Chem. Chem. Phys. 15 (2013) 17038–17063.

[10] R.A. van Santen, M. Ghouri, E.M.J. Hensen, Microkinetics of oxygenate formation in the Fischer–Tropsch reaction, Phys. Chem. Chem. Phys. 16 (2014) 10041–10058.

[11] N. Fischer, E. van Steen, M. Claeys, Structure sensitivity of the Fischer–Tropsch

activity and selectivity on alumina supported cobalt catalysts, J. Catal. 299 (2013) 67–80.

[12] W. Chen, I.A.W. Filot, R. Pestman, E.J.M. Hensen, Mechanism of Cobalt-Catalyzed CO Hydrogenation: 2. Fischer–Tropsch Synthesis, ACS Catal. 7 (2017) 8061–8071.

[13] D.G.H. Ballard, Mechanism of fischer-tropsch synthesis: CH_2 polymerisation versus CO insertion, J. Mol. Catal. 19 (1983) 393–397.

[14] F. Kapteijn, R.M. de Deugd, J.A. Moulijn, Fischer–Tropsch synthesis using monolithic catalysts, Catal. Today. 105 (2005) 350–356.

[15] J. Schweicher, A. Bundhoo, N. Kruse, Hydrocarbon Chain Lengthening in Catalytic CO Hydrogenation: Evidence for a CO-Insertion Mechanism, J. Am. Chem. Soc. 134 (2012) 16135–16138.

[16] I.M. Ciobîcă, G.J. Kramer, Q. Ge, M. Neurock, R.A. van Santen, Mechanisms for Chain Growth in Fischer–Tropsch Synthesis over Ru(0001), J. Catal. 212 (2002) 136–144.

[17] N. Kumar, K. Jothimurugesan, G.G. Stanley, V. Schwartz, J.J. Spivey, In-Situ FT-IR Study on the Effect of Cobalt Precursors on CO Adsorption Behavior, J. Phys. Chem. C. 115 (2011) 990–998.

[18] S. Li, J. Scaranto, M. Mavrikakis, On the Structure Sensitivity of Formic Acid Decomposition on Cu Catalysts, Top. Catal. 59 (2016) 1580–1588.

[19] L. Lemaitre, A. Berliet, S. Maury, M. Rivallan, Surface modifications of cobalt Fischer Tropsch catalyst followed by operando DRIFT and chemometrics, Catal. Today. 283 (2017) 172–175.

[20] G.R. Fredriksen, E.A. Blekkan, D. Schanke, A. Holmen, CO Hydrogenation on Supported Cobalt Catalysts Studied by in situ FTIR-Spectroscopy, Berichte Der Bunsengesellschaft Für Phys. Chemie. 97 (1993) 308–312.

[21] M. Kollár, A. De Stefanis, H.E. Solt, M.R. Mihályi, J. Valyon, A.A.G. Tomlinson, The mechanism of the Fischer–Tropsch reaction over supported cobalt catalysts, J. Mol. Catal. A Chem. 333 (2010) 37–45.

[22] J. Scalbert, I. Clémençon, P. Lecour, L. Braconnier, F. Diehl, C. Legens, Simultaneous investigation of the structure and surface of a Co/alumina catalyst during Fischer–Tropsch synthesis: discrimination of various phenomena with beneficial or disadvantageous impact on activity, Catal. Sci. Technol. 5 (2015) 4193–4201.

[23] L. Pinard, P. Bichon, A. Popov, J.L. Lemberton, C. Canaff, F. Maugé, P. Bazin, E.F. S.-Aguiar, P. Magnoux, Identification of the carbonaceous compounds present on a deactivated cobalt based Fischer–Trospch catalyst resistant to “rejuvenation treatment,” Appl. Catal. A Gen. 406 (2011) 73–80.

[24] F.C. Meunier, Pitfalls and benefits of in situ and operando diffuse reflectance FT-IR spectroscopy (DRIFTS) applied to catalytic reactions, React. Chem. Eng. 1 (2016) 134–141.

[25] A. Paredes-Nunez, D. Lorito, N. Guilhaume, C. Mirodatos, Y. Schuurman, F.C. Meunier, Nature and reactivity of the surface species observed over a supported cobalt catalyst under CO/H_2 mixtures, Catal. Today. 242 (2015) 178–183.

[26] D. Lorito, A. Paredes-Nunez, C. Mirodatos, Y. Schuurman, F.C. Meunier, Determination of formate decomposition rates and relation to product formation during CO hydrogenation over supported cobalt, Catal. Today. 259 (2016) 192–196.

[27] Y. Yang, C.A. Mims, R.S. Disselkamp, C.H.F. Peden, C.T. Campbell, Simultaneous MS-IR Studies of Surface Formate Reactivity Under Methanol Synthesis Conditions on Cu/SiO_2, Top. Catal. 52 (2009) 1440–1447.

[28] F.C. Meunier, Mixing Copper Nanoparticles and ZnO Nanocrystals: A Route towards Understanding the Hydrogenation of CO_2 to Methanol?, Angew. Chemie Int. Ed. 50 (2011) 4053–4054.

[29] F. Le Peltier, P. Chaumette, J. Saussey, M.M. Bettahar, J.C. Lavalley, In situ FT-IR and kinetic study of methanol synthesis from CO_2/H_2 over $ZnAl_2O_4$ and $Cu–ZnAl_2O_4$ catalysts, J. Mol. Catal. A Chem. 132 (1998) 91–100.

[30] B. Gu, A.Y. Khodakov, V. V. Ordomsky, Selectivity shift from paraffins to α-olefins in low temperature Fischer–Tropsch synthesis in the presence of carboxylic acids, Chem. Commun. 54 (2018) 2345–2348.

[31] P. Gonugunta, A.I. Dugulan, G.L. Bezemer, E. Brück, Role of surface carboxylate deposition on the deactivation of cobalt on titania Fischer-Tropsch catalysts, Catal. Today. (2020).

[32] F.C. Meunier, The design and testing of kinetically-appropriate operando spectroscopic cells for investigating heterogeneous catalytic reactions, Chem. Soc. Rev. 39 (2010) 4602–4614.

[33] F.C. Meunier, A. Goguet, C. Hardacre, R. Burch, D. Thompsett, Quantitative DRIFTS investigation of possible reaction mechanisms for the water–gas shift reaction on high-activity Pt- and Au-based catalysts, J. Catal. 252 (2007) 18–22.

[34] G.W. Thomson, The Antoine Equation for Vapor-pressure Data., Chem. Rev. 38 (1946) 1–39.

[35] D. Ambrose, N.B. Ghiassee, Vapour pressures and critical temperatures and critical pressures of some alkanoic acids: C_1 to C_{10}, J. Chem. Thermodyn. 19 (1987) 505–519.

[36] A.S. Coolidge, The vapor pressure and heats of fusion and vaporisation of formic acid, J. Am. Chem. Soc. 52 (1930) 1874–1887.

[37] M.L. Nahrwold, P. Archer, P.J. Cohen, Application of the Antoine equation to anesthetic vapor pressure data, Anesth. Analg. 52 (1973) 866–867.

[38] A.A. Muleja, Y. Yao, D. Glasser, D. Hildebrandt, Variation of the Short-Chain Paraffin and Olefin Formation Rates with Time for a Cobalt Fischer–Tropsch Catalyst, Ind. Eng. Chem. Res. 56 (2017) 469–478.

[39] G. Li, M. Ridd, F. Larkins, An Infrared Study of Formic Acid Adsorption on Co/SiO_2 and SiO_2 Surfaces, Aust. J. Chem. 44 (1991) 623–626.

[40] W. Chen, T.F. Kimpel, Y. Song, F.K. Chiang, B. Zijlstra, R. Pestman, P. Wang, E.J.M. Hensen, Influence of Carbon Deposits on the Cobalt-Catalyzed Fischer–Tropsch Reaction: Evidence of a Two-Site Reaction Model, ACS Catal. 8 (2018) 1580–1590.

[41] D. Ruthven, The catalytic decomposition of aqueous formic acid over suspended palladium catalysts, J. Catal. 21 (1971) 39–47.

[42] B.B. Wescott, C.J. Engelder, The Catalytic Decomposition of Formic Acid, J. Phys. Chem. 30 (1925) 476–479.

[43] D.A. Bulushev, S. Beloshapkin, J.R.H. Ross, Hydrogen from formic acid decomposition over Pd and Au catalysts, Catal. Today. 154 (2010) 7–12.

[44] W.Y. Yu, G.M. Mullen, D.W. Flaherty, C.B. Mullins, Selective Hydrogen Production from Formic Acid Decomposition on Pd–Au Bimetallic Surfaces, J. Am. Chem. Soc. 136 (2014) 11070–11078.

[45] J.M. Trillo, G. Munuera, J.M. Criado, Catalytic Decomposition of Formic Acid on Metal Oxides, Catal. Rev. 7 (1972) 51–86.

[46] K.S. Kim, M.A. Barteau, Pathways for carboxylic acid decomposition on titania, Langmuir. 4 (1988) 945–953.

[47] P. Mars, J.J.F. Scholten, P. Zwietering, The Catalytic Decomposition of Formic Acid, in: Adv. Catal., Academic Press, 1963: pp. 35–113.

[48] G.Q. Lu, A. Crown, A. Wieckowski, Formic Acid Decomposition on Polycrystalline Platinum and Palladized Platinum Electrodes, J. Phys. Chem. B. 103 (1999) 9700–9711.

[49] W.L. Nelson, C.J. Engelder, The Thermal Decomposition of Formic Acid, J. Phys. Chem. 30 (1925) 470–475.

[50] J. Albert, A. Jess, C. Kern, F. Pöhlmann, K. Glowienka, P. Wasserscheid, Formic Acid-Based Fischer–Tropsch Synthesis for Green Fuel Production from Wet Waste Biomass and Renewable Excess Energy, ACS Sustain. Chem. Eng. 4 (2016) 5078–5086.

Supplementary information

S5.1. Formic acid co-feeding in the middle of the reaction

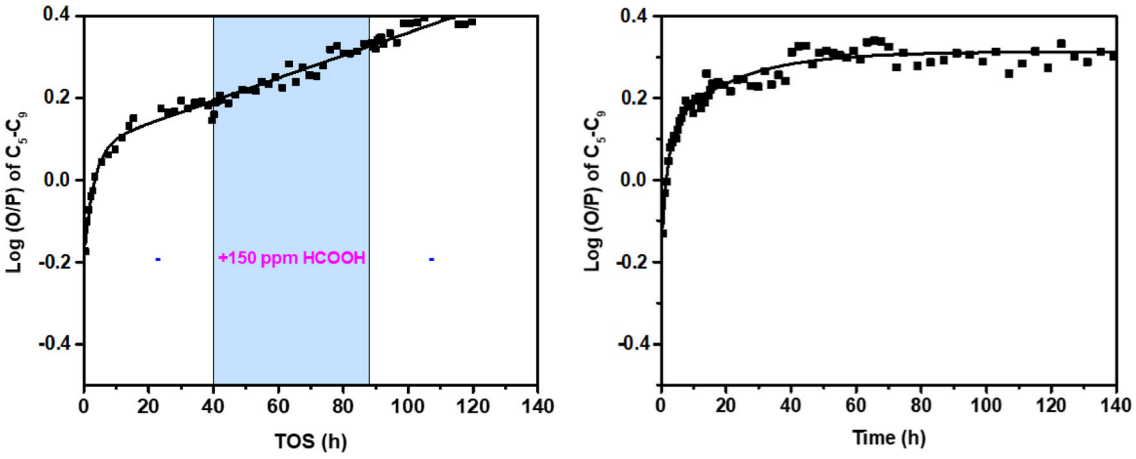

Figure S5.1: Olefins to paraffins ratio with time on stream. With 150 ppmv formic acid co-feeding and without co-feeding at 200 °C and 2 MPa.

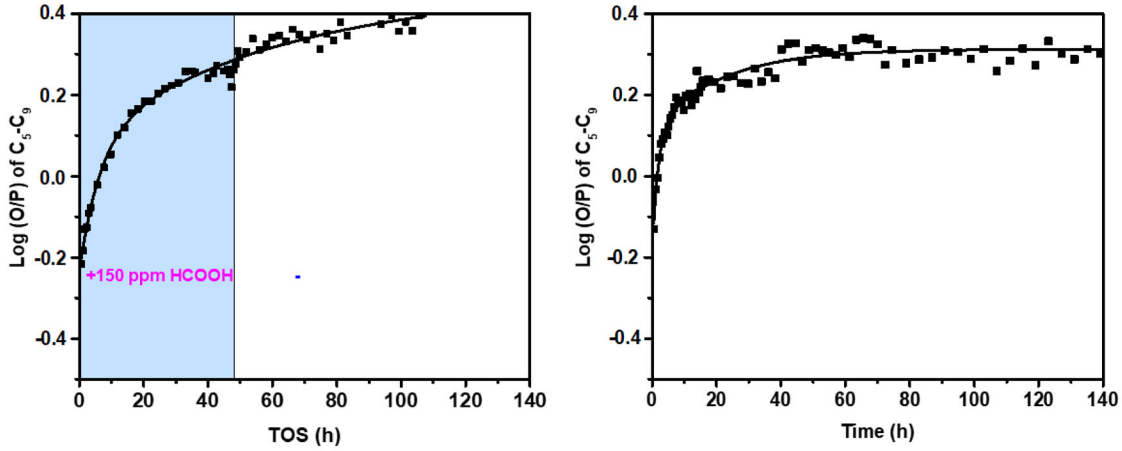

Figure S5.2: Olefins to paraffins ratio with time on stream. With 150 ppmv formic acid co-feeding and without co-feeding at 200 °C and 2 MPa.

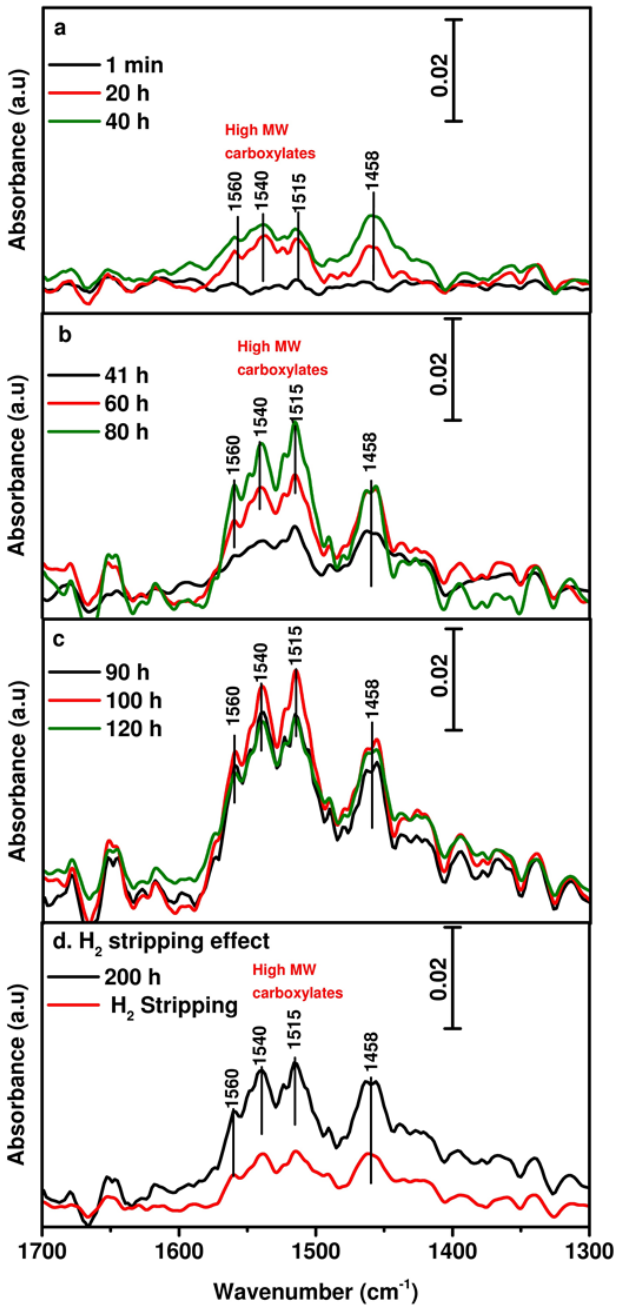

Figure S5.3: DRIFT spectra of the Co/TiO_2 catalyst at 2 MPa, 200 °C, **(a, b & c)** During FTS and **(d)** Effect of H_2 stripping.

The DRIFT spectra of the Co/TiO_2 catalyst during standard FTS at 200 °C and 2 MPa is shown in Figure S5.3. The peaks at 1540 and 1515 cm^{-1} are due to deposition of MW carboxylates on the catalyst surface. The amount of high MW carboxylates increased with time due to their continuous deposition (see Figure S5.3a, b and c). The decrease in peak height at 120 hours is due to the loss of infrared signal by a large amount of wax deposition on the catalyst surface. After H_2 stripping, the intensity of high MW carboxylates decreased due to their removal as shown in Figure S5.3d. In standard FTS, carboxylates deposit on the TiO_2 support as spectator species.

Chapter 6

The role of acetic acid co-feeding on the deactivation of the Co/TiO_2 Fischer-Tropsch synthesis catalyst

Fischer-Tropsch synthesis (FTS) is a catalytic process used for the production of synthetic fuels and other waxy products from synthesis gas obtained from feedstocks such as natural gas, coal and biomass. It was believed that different carboxylate compounds deposited on the catalyst surface block the active sites of the reaction. To investigate the possible influence of carboxylates on the performance of the catalysts, co-feeding of acetic acid during FTS reaction was investigated with operando DRIFT spectroscopy. The co-feeding decreased the activity of the catalyst significantly due to the expected formation of inactive cobalt acetate species. During acetic acid co-feeding, the olefins to paraffins ratio increased slightly due to the prevention of olefins re-adsorption by high MW carboxylates for further hydrogenation into paraffins. The high molecular weight carboxylates formed on the catalyst surface during co-feeding are removed easily by decomposition or hydrogenation and they are not involved in the catalyst deactivation mechanism. These high MW carboxylates formed during acetic acid co-feeding could be spectator species formed on the terrace sites of the cobalt.

6.1. Introduction

Fischer-Tropsch synthesis (FTS) is a catalytic process used for the production of synthetic fuels and other waxy products from synthesis gas obtained from feedstocks such as natural gas, coal and biomass [1,2]. Among all catalysts, Co-based catalysts are the most productive in FTS processes due to their high activity, high selectivity to linear paraffins and low activity in unwanted water-gas shift reaction. However, Co-based FTS catalysts are relatively expensive and deactivate with time [3–8]. Development of catalysts with stable performance is essential to increase the FTS process economic efficiency. Therefore, catalyst deactivation became an important research topic in academia and industry for the development of better industrial catalysts. The general catalyst deactivation mechanisms are extensively studied by many researchers already [3]. The most prominent catalyst deactivation mechanisms are poisoning, oxidation, sintering of active phase and deposition of carbonaceous compounds on the catalyst surface [3,4].

Along with hydrocarbons, a small quantity of oxygenated compounds like carboxylic acids, alcohols, aldehydes, ketones etc., are also produced in FTS [9–11]. These oxygenated compounds may interact strongly with Co active sites, leading to a decrease in the catalyst activity [12]. Deactivation by oxygenated compounds in FTS has been proposed by a few research groups. Jalama et al. [13] found that ethanol addition during FTS at 220 ^{o}C, 0.8 MPa on a Co/TiO_2 catalyst significantly decreased the catalyst activity. They also reported that ethanol addition increased both the selectivity to light products and the olefin to paraffin ratio. These effects were reversible when ethanol was removed from the feed. This is believed to be related to oxidation of Co to CoO by ethanol and re-reduction to Co when ethanol was removed from the feed.

Not only alcohols but also carboxylic acids were proposed to be the cause of catalyst deactivation. Pinard et al. [14] analysed the carbon species present on the $Co/Ru/Al_2O_3$ FTS catalyst. Carbon extracted from the spent catalyst was found to consist of atomic carbon, alcohols, carboxylic acids and polymeric carbon. Temperature programmed hydrogenation–infrared (TPH-IR) spectra indicated that complete removal of carboxylate species from the catalyst surface required temperatures above 600 ^{o}C. Atomic carbon and alcohols were easily hydrogenated from the catalyst below 290 ^{o}C, whereas carboxylic acids and polymeric carbon were resistant to a treatment under hydrogen and required temperatures above 330 ^{o}C. These hydrogen resistant carboxylates could be the cause of deactivation if the active metal sites were blocked by them. Also, Pena et al. [15] detected different oxygenated compounds like carboxylic acids and aldehydes in the organic extract from a spent Co/Al_2O_3 catalyst. Scalbert et al. [16] found adsorption and continuous accumulation of oxygenated compounds on a Co/Al_2O_3 FTS catalyst using X-ray diffraction (XRD) and diffuse reflectance infrared Fourier-Transform (DRIFT) spectroscopy. They also proposed that these strongly adsorbed species are responsible for catalyst deactivation by covering the active sites. Co-feeding of carboxylic acids in FTS has been studied to understand the role of carboxylic acids in catalyst deactivation mechanism. Sarkar et al. [17] found a decrease in the activity of catalysts with acetic acid addition during FTS due to competitive adsorption of acetic acid on the active sites of a Fe-based catalyst in a continuous stirred tank reactor (CSTR) at 270 ^{o}C. Kistamurthy et

al. [18] also investigated the effect of carboxylic acids addition on the deactivation of a Co/Al_2O_3 FTS catalyst. They found that acetic acid interaction with a $Co/Pt/Al_2O_3$ catalyst leads to atomic carbon deposition on the catalyst by decomposition of acetic acid. It is stated that addition of carboxylates does not influence either catalyst deactivation or selectivity significantly [18]. Gu et al. [19] found significant effects on the activity and selectivity of a Co/Al_2O_3 FTS catalyst in the presence of acetic and butyric acids in the feed gas. The activity decreased to half when the acetic acid was introduced into the feed and stabilised afterwards. They proposed that the decrease in activity is due to the formation of inactive cobalt acetate species in the presence of acetic acid, which was confirmed by identifying the cobalt acetate species on the spent catalyst using infrared and XRD spectroscopy. Also, a shift in the selectivity from paraffins to olefins in the presence of acetic acid was observed. This effect is attributed to the intermediate esters formed on the catalyst surface, which prevent secondary hydrogenation of olefins. A similar effect was observed with butyric acid co-feeding.

However, the effect of carboxylic acids addition during FTS is not explored very well. Also, the role of carboxylates deposition on the catalyst surface in the deactivation mechanism is not very clear. Among all carboxylic acids produced in small quantities in FTS, acetic acid is the most abundant acid [9]. Therefore, the present study aims to investigate the effect of acetic acid co-feeding on the performance of a Co/TiO_2 FTS catalyst. An operando DRIFT spectroscopy setup has been employed to study the effect of acetic acid co-feeding in the deactivation mechanism [20,21]. Acetic acid was co-fed into the reaction cell during normal FTS conditions in three ways: in the middle of the reaction, from the beginning of the reaction and without CO in the inlet gas.

6.2. Experimental

6.2.1. Catalyst preparation

$Co(10\ wt\%)/TiO_2$ - IWI catalyst provided by Shell Global Solutions International B.V., Amsterdam was prepared by two step impregnation. First, the support material (Degussa P25 with surface area 50 $m^2.g^{-1}$ and pore volume 0.319 $mL.g^{-1}$) was dried and impregnated with 1 pore volume of an aqueous solution of $Co(NO_3)_2$ (17.25 wt% Co). In the second impregnation, the obtained material (pore volume 0.283 $mL.g^{-1}$) was impregnated with 0.95 pore volume of an aqueous solution of $Co(NO_3)_2$ (20.02 wt% Co). After each impregnation step, the obtained material was dried in an oven at 60 ^oC overnight under static air and calcined at 400 ^oC for 2 hours under N_2 flow.

6.2.2. Operando DRIFT spectroscopy

For acetic acid co-feeding studies, an operando DRIFT spectroscopy setup was used. The employment and optimisation details of the operando spectroscopy setup are described in Chapter 2. During FTS, the surface of the catalyst is monitored with the Thermo Nicolet Nexus 670 FT-IR spectrometer to study the reaction intermediates and surface products.

High quality acetic acid was obtained from Sigma-Aldrich for co-feeding experiments. To co-feed very small concentrations of acetic acid into the reaction cell, a temperature-controlled

saturator was kept in the CO or H_2 gas lines as shown in Figure 2.4. The necessary temperature of the saturator, for the flow of the required concentration of acetic acid, was calculated using the Antoine vapour pressure-temperature relation [22–24]. The concentration of the acetic acid was calibrated by co-feeding acid at varying temperatures and pressures of the saturator and measuring the amount of acetic acid with GC-MS.

6.2.3. Catalytic testing

In a first experiment, the Co/TiO_2 catalyst was loaded into the operando DRIFT reaction cell and reduced at 350 ^oC in 100 mL/min H_2 for 2 hours. Then the reaction cell was cooled down to the reaction temperature (200 ^oC) and a background spectrum was measured in Ar/H_2 mixture. After this step, CO was introduced into the reactor and the pressure was increased to 2 MPa. First FTS reaction was performed at 200 ^oC and 2 MPa 40 hours until a steady state activity is reached. After this step, 100 ppmv of acetic acid was introduced into the feed, this co-feeding has been stopped after 48 h. In a second experiment, acetic acid was co-fed from the beginning of the reaction. Co-feeding was stopped after 48 h of time on stream and continued as normal FTS. In a third experiment, after 6 days of FTS long run, acetic acid was co-fed two times for 4 days with an interval of 4 days.

Thermo Scientific Trace Ultra GC with automatic sampling was used for the analysis of reaction products. Each injected sample was analysed with increasing the temperature of the GC oven from 50 ^oC to 250 ^oC. He was used as a carrier gas and Ar was used as an internal standard gas. Permanent gases were analysed with a Carboxen 1010 column connected to a thermal conductivity detector and hydrocarbons were analysed with an Rtx-1 column connected to a flame ionization detector.

6.2.4. Interaction of acetic acid and H_2 with the Co/TiO_2 catalyst

To understand the role of acetic acid on the catalyst surface in FTS, acetic acid was fed into the reaction cell without CO in the inlet gas. First, the Co/TiO_2 catalyst was loaded into the operando DRIFT reaction cell and reduced at 350 ^oC in 100 mL/min H_2 for 2 hours. Then the reaction cell was cooled down to the reaction temperature (200 ^oC) and a background spectrum was measured in a mixture of Ar/H_2 and the pressure was increased to 2 MPa. After this step, 100 ppmv of acetic acid was co-fed by flowing H_2 gas through the saturator at the corresponding temperature.

6.3. Results

6.3.1. Acetic acid co-feeding in the middle of the reaction

The effect of 100 ppmv of acetic acid co-feeding on the performance of the Co/TiO_2 catalyst is shown in Figure 6.1. When acetic acid was fed into the reactor, the activity of the catalyst decreased significantly and after stopping the co-feeding, the activity of the catalyst recovered again slowly with time (CO conversion level is ~1%). Whereas, C_1-C_4 and C_{5+} selectivities were not influenced much by acetic acid co-feeding as shown in Figure 6.1b. The influence of co-feeding on olefins to paraffins ratio is shown in Figure 6.1c. The O/P ratio increased slightly during acetic acid co-feeding and then decreased after stopping co-feeding.

The DRIFT spectra of the catalyst during FTS in normal conditions and during 100 ppmv of acetic acid co-feeding are shown in Figure 6.2. As seen in Figure 6.2a, the absorption bands at 1540 and 1515 cm^{-1} are corresponding to asymmetric vibrations of the high molecular weight (MW) carboxylate compounds deposited on the catalyst surface during normal FTS conditions. The band at 1458 cm^{-1} is attributed to $-CH_2-$ bending vibrations of wax and carboxylates [14]. The spectra of the catalyst with acetic acid co-feeding are shown in Figure 6.2b. With acetic acid co-feeding, the intensity of high MW carboxylate bands increased slightly. DRIFT spectra of the catalyst in normal FTS reaction after stopping the co-feeding are shown in Figure 6.2c. The intensity of the high MW carboxylate bands decreased and a band corresponding to asymmetric vibrations of formate species at 1589 cm^{-1} became dominant with time [25,26].

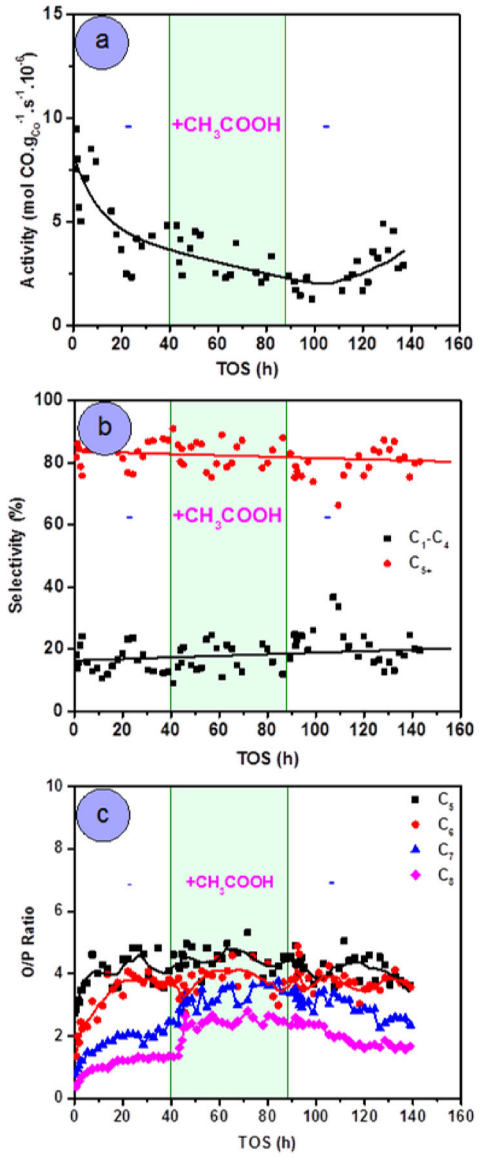

Figure 6.1: (a) Co/TiO_2 catalyst activity, **(b)** C_1-C_4 and C_{5+} selectivities and **(c)** O/P ratio as a function of the time on stream.

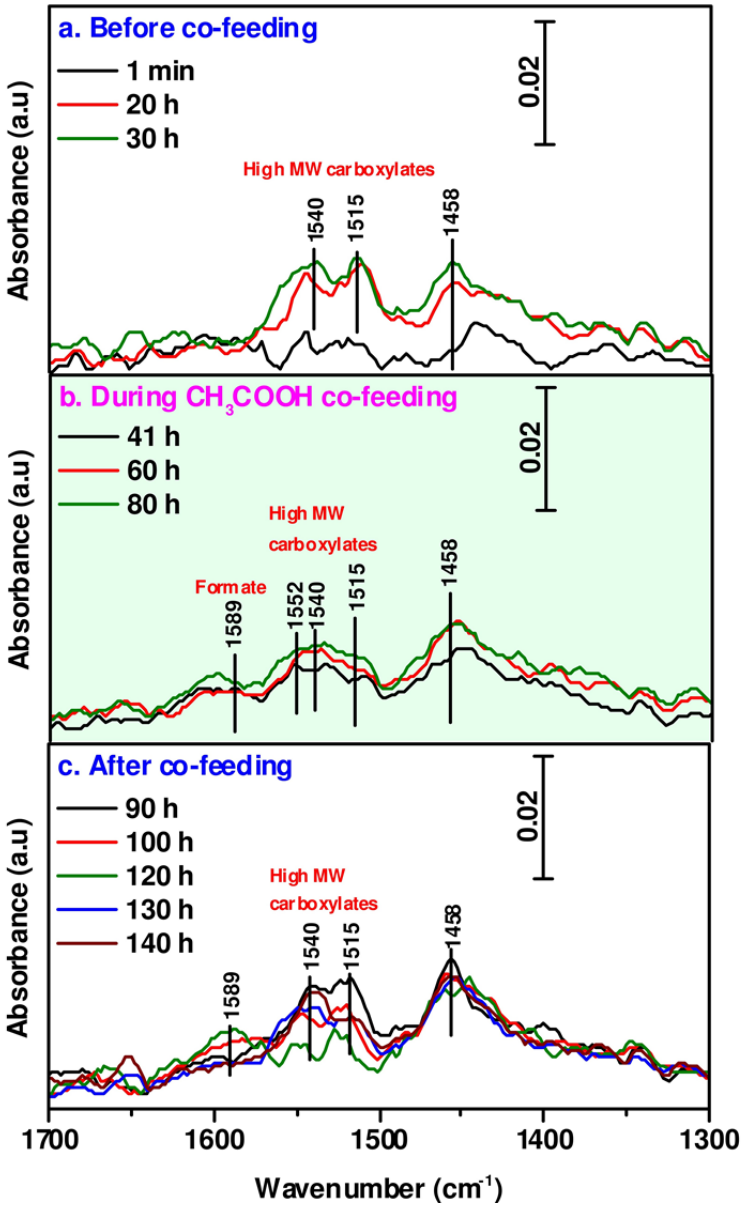

Figure 6.2: DRIFT spectra of the Co/TiO_2 catalyst, **(a)** Before co-feeding, **(b)** During CH_3COOH co-feeding and **(c)** After co-feeding.

6.3.2. Acetic acid co-feeding from the beginning of the reaction

The effect of acetic acid co-feeding in the middle of the reaction on DRIFT spectra is not very clear as reaction products and intermediates are already deposited on the catalyst surface. Therefore, 100 ppmv of acetic acid was co-fed from the beginning of the reaction and its effect on the catalyst performance is shown in Figure 6.3. The co-feeding leads to a significant decrease in activity of the catalyst and after stopping the co-feeding, the activity increased slowly again with time as observed earlier. The C_1-C_4 selectivity is slightly higher in acetic acid co-feeding than the C_1-C_4 selectivity in normal FTS conditions could be due to acetic acid decomposition. Here also, olefins to paraffins ratio increased in acetic acid co-feeding and then decreased after stopping co-feeding as shown in Figures 6.3c.

The DRIFT spectra of the catalyst with acetic acid co-feeding during FTS from the beginning of the reaction are shown in Figure 6.4. In Figure 6.4a, the absorption band at 1560 cm^{-1} is corresponding to asymmetric vibrations of the acetate species adsorbed on the catalyst surface. Two other bands at 1540 and 1515 cm^{-1} are corresponding to asymmetric vibrations of the high molecular weight (MW) carboxylates [14]. The peak at 1458 cm^{-1} is due to bending vibrations of $-CH_2-$ species of waxes and carboxylates. The spectra of the catalyst after stopping acetic acid co-feeding are shown in Figure 6.4b. The intensity of the carboxylate bands decreased significantly and a new band at 1589 cm^{-1} corresponding to the asymmetric vibration of formate species appeared and became dominant after some time. First all high MW carboxylates were removed at 60 h and then a small amount of new high MW carboxylates appeared again at 80 h, from normal FTS reaction.

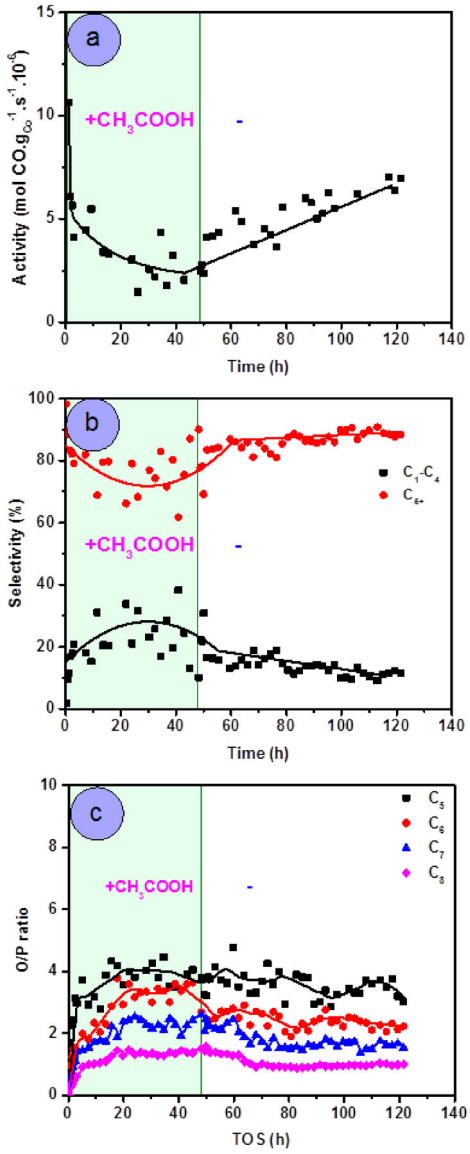

Figure 6.3: (a) Co/TiO_2 catalyst activity, **(b)** C_1-C_4 and C_{5+} selectivities and **(c)** O/P ratio as a function of the time on stream.

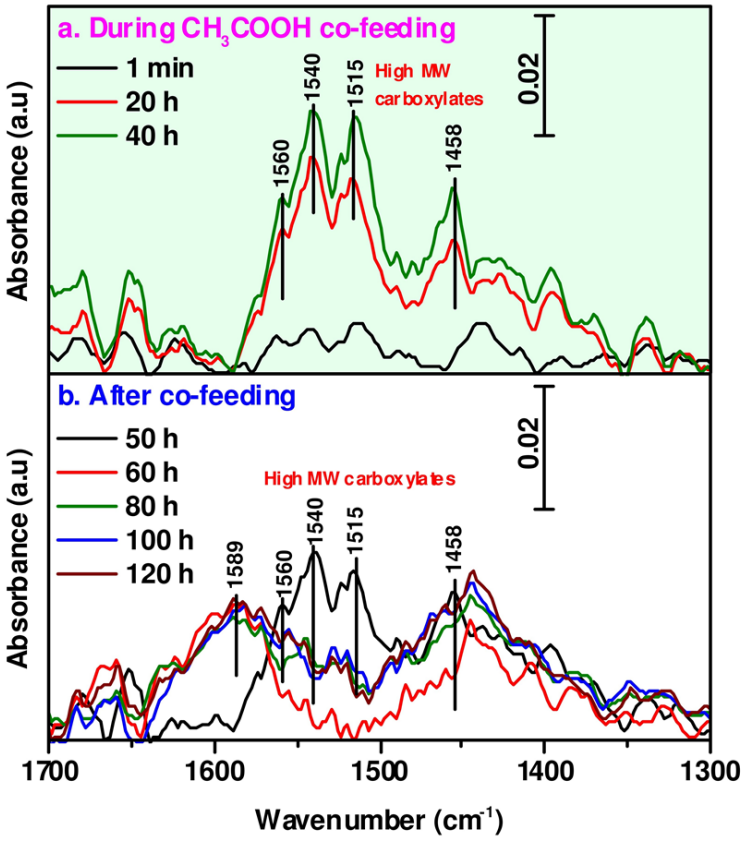

Figure 6.4: DRIFT spectra of the Co/TiO_2 catalyst, **(a)** During CH_3COOH co-feeding and **(b)** After co-feeding.

6.3.3. Comparison of carboxylates deposited on the catalyst during formic and acetic acids co-feeding

DRIFT spectra of the catalyst obtained during formic and acetic acids co-feeding after 48 h of TOS are shown in Figure 6.5. The intensity of the carboxylate bands at 1540 and 1515 cm^{-1} during acetic acid co-feeding is higher than the intensity of the carboxylate bands obtained during formic acid co-feeding.

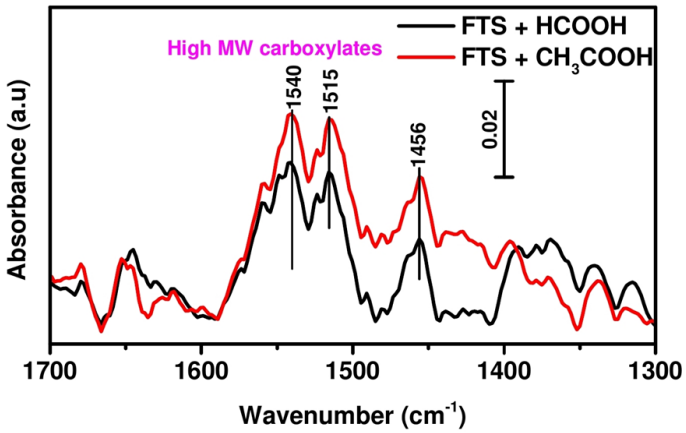

Figure 6.5: DRIFT spectra of the Co/TiO_2 catalyst in HCOOH and CH_3COOH co-feeding.

6.3.4. Interaction of acetic acid with the Co/TiO_2 catalyst

To understand in depth the role of acetic acid co-feeding in FTS, we performed 100 ppmv of acetic acid co-feeding on the catalyst surface without CO gas. The reaction products of acetic acid and H_2 on the catalyst were analysed with GC. Mostly CH_4, C_2H_4 and C_2H_6 were produced in a small quantity on the catalyst. The DRIFT spectra of the Co/TiO_2 catalyst with acetic acid co-feeding are shown in Figure 6.6. The absorption band at 1560 cm^{-1} is due to asymmetric vibrations of acetate species. Two other bands at 1540 and 1515 cm^{-1} are corresponding to asymmetric vibrations of the high MW carboxylates.

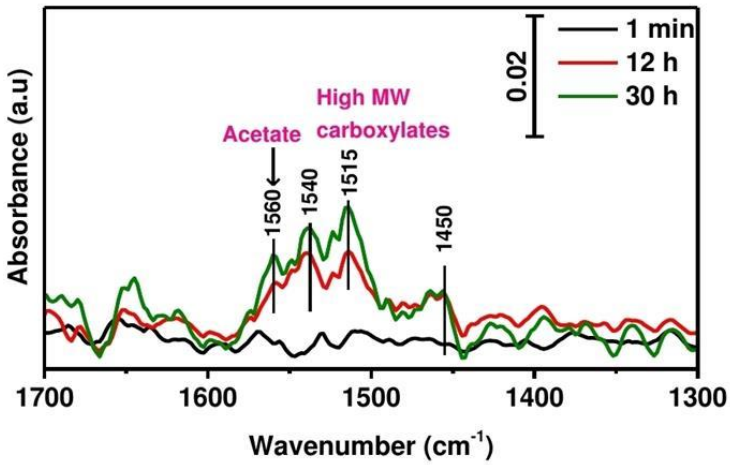

Figure 6.6: DRIFT spectra of the Co/TiO_2 catalyst with CH_3COOH interaction.

6.4. Discussion

Acetic acid co-feeding showed a detrimental effect on the performance of the catalyst (see Figures 6.1, 6.3 and S6.1). When acetic acid was present in the feed gas, the activity of the catalyst decreased significantly and after stopping the co-feeding, the activity of the catalyst recovered slowly with time. Whereas, C_1-C_4 and C_{5+} selectivities were not influenced much by acetic acid co-feeding. Interestingly, in our experiments with acetic acid co-feeding, the olefins to paraffins ratio increased slightly (See Figures 6.1c, 6.2c and S6.1b). This could be due to the blockage of olefins re-adsorption by high MW carboxylates for further hydrogenation into paraffins. The high MW carboxylates formed during co-feeding could be spectator species sitting on the cobalt terrace sites, preventing the olefins re-adsorption. Chen et al. [27] also suggested that two types of sites are involved in the FTS reaction on Co based catalysts. Step edge sites involved in CO dissociation, chain growth and termination and terrace sites involved mainly in the formation of CH_4 and hydrogenation of primary olefins, were proposed.

The DRIFT spectra of the catalyst during FTS in normal conditions and during 100 ppmv of acetic acid co-feeding are shown in Figure 6.2. As seen in Figure 6.2a, the absorption bands at 1540 and 1515 cm^{-1} are corresponding to asymmetric vibrations of the high MW carboxylates deposited on the catalyst surface during normal FTS conditions. The intensity of these carboxylate bands increased with time due to their accumulation on the catalyst surface

during FTS. The deposition of carboxylate compounds on the catalyst surface in FTS has been reported already [14,25,26,28]. The spectra of the catalyst with acetic acid co-feeding are shown in Figure 6.2b. With acetic acid co-feeding, the intensity of carboxylate bands at 1540 cm^{-1} and 1515 cm^{-1} increased slightly. This is due to the conversion of acetic acid into high MW carboxylates on the catalyst surface. The DRIFT spectra of the catalyst in normal FTS reaction after stopping the co-feeding are shown in Figure 6.2c. The intensity of the high MW carboxylate bands decreased due to their removal from the catalyst surface with time either by hydrogenation or by decomposition. Subsequently, the band corresponding to asymmetric vibrations of formate species at 1589 cm^{-1} became dominant with time [25,26]. The small peaks at 1540 and 1515 cm^{-1} are due to normal high MW carboxylates deposited on the support.

An interesting observation is that the high MW carboxylates formed on the surface of the catalyst during acetic acid co-feeding were removed easily after stopping the co-feeding (see Figures 6.2c and 6.4b), similar to formic acid experiments (see Figures 5.3c and 5.5b). Whereas in normal FTS reaction, the high MW carboxylates were removed from the catalyst surface only with H_2 stripping (see Figure S5.3 and Chapter 4). It indicates that the carboxylates formed in the presence of acetic acid are present on the cobalt active sites, being easily removed either by decomposition or hydrogenation, similar to formic acid co-feeding experiments in Chapter 5. Whereas, in normal FTS reaction a large amount of high MW carboxylates deposited on the TiO_2 support as spectators as observed in Chapter 4.

Very clear differences were observed in the DRIFT spectra of the catalyst when acetic acid was co-fed from the beginning of the reaction as shown in Figure 6.4. As expected, the intensity of these carboxylates increased with time due to their accumulation on the catalyst surface (Figure 6.4a). However, the intensity of these carboxylate bands with acetic acid co-feeding from the beginning of the reaction is very high compared with the intensity of carboxylate bands with acetic acid co-feeding in the middle of the reaction (Figure 6.2b). The significant difference can be due to the availability of more sites for acetic acid absorption at the beginning of the reaction to form a large amount of high MW carboxylates. It is estimated that 100 ppmv of acetic acid co-feeding takes about 50 minutes to make a full monolayer coverage on Co/TiO_2 catalyst if all co-fed molecules interacted with the catalyst. In the case of normal FTS, it takes about 8 hours to make full coverage on catalyst with carboxylic acids as the amount of carboxylic acids production is very less in FTS. In the case of acetic acid co-feeding in the middle of the reaction, already the catalyst surface was covered with many FTS products like hydrocarbons and a small amount of carboxylates before co-feeding, blocking the access to catalyst surface. As many CH_x species formed in the FTS reaction are available on the surface of the catalyst, it is possible that the high MW carboxylates were formed from acetates by the involvement of CH_x species in the chain growth mechanism as proposed by Chen et al. [29].

The DRIFT spectra of the catalyst after stopping acetic acid co-feeding are shown in Figure 6.4b. The intensity of the carboxylate bands decreased significantly due to their removal from the catalyst surface. A new band at 1589 cm^{-1} corresponding to the asymmetric vibration of formate species appeared and became dominant after some time. It seems some of the high

MW carboxylates and acetates on the surface were decomposed and converted into formate species because the chain growth mechanism is highly reversible [29]. After some time at 80 h, small bands at 1540 and 1515 cm^{-1} corresponding to normal high MW carboxylates appeared again from normal FTS reaction.

DRIFT spectra of the catalyst obtained during formic and acetic acids (see Figure 6.5) showed that the intensity of the carboxylate bands at 1540 and 1515 cm^{-1} during acetic acid co-feeding is higher than the intensity of the carboxylate bands during formic acid co-feeding. This indicates that acetic acid produced a higher amount of high MW carboxylates than formic acid on the catalyst surface. Acetic acid co-feeding showed a significant effect on the catalyst performance, whereas formic acid co-feeding showed a negligible effect. It looks like that the carboxylates formed during co-feeding are very mobile, easily removed. They are present during both formic and acetic acids co-feeding experiments, but the activity pattern is different. Hence, they are not involved in a deactivation mechanism. Whereas, in normal FTS, the carboxylates will accumulate on support, being spectators, as we showed in chapter 4.

The decrease in catalyst activity (Figures 6.1a and 6.3a) in acetic acid co-feeing can be explained by the formation of inactive species like cobalt acetate due to the presence of more amount of acetic acid in the feed. Gu et al. [19] observed a significant decrease in the activity of the Co/Al_2O_3 FTS catalyst when carboxylic acids (acetic and butyric acids) were introduced in the feed gas. The decrease in activity is due to the formation of inactive cobalt acetate species in the presence of acetic acid, which was confirmed by identifying the cobalt acetate species on the spent catalyst using infrared and XRD spectroscopy.

To understand the role of acetic acid co-feeding in FTS, 100 ppmv of acetic acid was co-fed on the catalyst surface without CO gas. CH_4, C_2H_4, C_2H_6 were produced in a very small quantity on the catalyst. It seems that only a small amount of acetic acid was decomposed on the catalyst surface to form hydrocarbons. As shown in the DRIFT spectra of the Co/TiO_2 catalyst with acetic acid co-feeding (Figure 6.6), the absorption band at 1560 cm^{-1} is assigned to asymmetric vibrations of acetate species and two other bands at 1540 and 1515 cm^{-1} are corresponding to asymmetric vibrations of the high MW carboxylates. It clearly shows that most of the acetic acid was not decomposed, but involved in the formation of high MW carboxylates on the catalyst surface. The high intensity of the peaks at 1540 and 1515 cm^{-1} as shown in Figure 6.4a could be due to a combination of high MW carboxylates formed from acetic acid along with high MW carboxylates formed in standard FTS reaction.

Acetic acid interaction with Co/TiO_2 catalyst decreased the activity because acetic acid did not decompose easily on the catalyst surface. This is in contrast with formic acid interaction with the Co/TiO_2 catalyst in Chapter 5, where formic acid decomposed easily, formed hydrocarbons (C_1-C_{10}) as shown in Figure 5.8 and did not affect the catalyst performance significantly. The co-feeding experiments showed that high MW carboxylates are formed on the cobalt sites from acetic acid and they can be removed easily by decomposition or hydrogenation, not participating in a catalyst deactivation mechanism. These high MW carboxylates formed during co-feeding could be spectator species sitting on the cobalt terrace sites, preventing the olefins re-adsorption.

6.5. Conclusions

The role of acetic acid in FTS has been investigated with operando DRIFT spectroscopy. Acetic acid co-feeding decreased the activity of the catalyst significantly due to the formation of inactive cobalt acetate species. During acetic acid co-feeding, the olefins to paraffins ratio increased slightly due to the prevention of olefins re-adsorption by high MW carboxylates for further hydrogenation into paraffins. The high molecular weight carboxylates formed on the catalyst surface during co-feeding are removed easily by decomposition or hydrogenation and they are not involved in catalyst deactivation mechanism. These high MW carboxylates formed during co-feeding could be spectator species formed on the terrace sites of the cobalt.

References

[1] E. Iglesia, Design, synthesis, and use of cobalt-based Fischer-Tropsch synthesis catalysts, Appl. Catal. A Gen. 161 (1997) 59–78.

[2] P.J. van Berge, J. van de Loosdrecht, S. Barradas, A.M. van der Kraan, Oxidation of cobalt based Fischer–Tropsch catalysts as a deactivation mechanism, Catal. Today. 58 (2000) 321–334.

[3] N.E. Tsakoumis, M. Rønning, Ø. Borg, E. Rytter, A. Holmen, Deactivation of cobalt based Fischer–Tropsch catalysts: A review, Catal. Today. 154 (2010) 162–182.

[4] A.M. Saib, D.J. Moodley, I.M. Ciobîcă, M.M. Hauman, B.H. Sigwebela, C.J. Weststrate, J.W. Niemantsverdriet, J. van de Loosdrecht, Fundamental understanding of deactivation and regeneration of cobalt Fischer–Tropsch synthesis catalysts, Catal. Today. 154 (2010) 271–282.

[5] E. Rytter, A. Holmen, Deactivation and Regeneration of Commercial Type Fischer-Tropsch Co-Catalysts A Mini-Review, Catalysts. 5 (2015) 478–499.

[6] D.J. Moodley, J. van de Loosdrecht, A.M. Saib, M.J. Overett, A.K. Datye, J.W. Niemantsverdriet, Carbon deposition as a deactivation mechanism of cobalt-based Fischer–Tropsch synthesis catalysts under realistic conditions, Appl. Catal. A Gen. 354 (2009) 102–110.

[7] G. Jacobs, P.M. Patterson, Y. Zhang, T. Das, J. Li, B.H. Davis, Fischer–Tropsch synthesis: deactivation of noble metal-promoted Co/Al_2O_3 catalysts, Appl. Catal. A Gen. 233 (2002) 215–226.

[8] T.O. Eschemann, K.P. de Jong, Deactivation Behavior of Co/TiO_2 Catalysts during Fischer–Tropsch Synthesis, ACS Catal. 5 (2015) 3181–3188.

[9] R.R. Anderson, C.M. White, Analysis of Fischer-Tropsch by-product waters by gas chromatography, J. High Resolut. Chromatogr. 17 (1994) 245–250.

[10] R.J.J. Nel, A. de Klerk, Fischer−Tropsch Aqueous Phase Refining by Catalytic Alcohol Dehydration, Ind. Eng. Chem. Res. 46 (2007) 3558–3565.

[11] F.P. Di Sanzo, Characterization of high boiling Fischer-Tropsch liquids by liquid and gas chromatography, Anal. Chem. 53 (1981) 1911–1914.

[12] A. de Klerk, F. Edward, Catalysis in the Refining of Fischer-Tropsch Syncrude, Royal Society of Chemistry, Cambridge, 2010.

[13] K. Jalama, N.J. Coville, D. Hildebrandt, D. Glasser, L.L. Jewell, Fischer-Tropsch synthesis over Co/TiO_2: Effect of ethanol addition, Fuel. 86 (2007) 73–80.

[14] L. Pinard, P. Bichon, A. Popov, J.L. Lemberton, C. Canaff, F. Maugé, P. Bazin, E.F. S.-Aguiar, P. Magnoux, Identification of the carbonaceous compounds present on a deactivated cobalt based Fischer–Trospch catalyst resistant to "rejuvenation treatment," Appl. Catal. A Gen. 406 (2011) 73–80.

[15] D. Peña, A. Griboval-Constant, C. Lancelot, M. Quijada, N. Visez, O. Stéphan, V. Lecocq, F. Diehl, A.Y. Khodakov, Molecular structure and localization of carbon species in alumina supported cobalt Fischer–Tropsch catalysts in a slurry reactor, Catal. Today. 228 (2014) 65–76.

[16] J. Scalbert, I. Clémençon, P. Lecour, L. Braconnier, F. Diehl, C. Legens, Simultaneous investigation of the structure and surface of a Co/alumina catalyst during Fischer–Tropsch synthesis: discrimination of various phenomena with beneficial or disadvantageous impact on activity, Catal. Sci. Technol. 5 (2015) 4193–4201.

[17] A. Sarkar, R.A. Keogh, S. Bao, B.H. Davis, Fischer-Tropsch Synthesis: Reaction Pathways for ^{14}C-Labeled Acetic Acid, Catal. Letters. 120 (2008) 25–33.

[18] D. Kistamurthy, A.M. Saib, D.J. Moodley, H. Preston, I.M. Ciobîcă, W.J. van Rensburg, J.W. Niemantsverdriet, C.J. Weststrate, The role of carboxylic acid in cobalt Fischer-Tropsch synthesis catalyst deactivation, Catal. Today. 275 (2016) 127–134.

[19] B. Gu, A.Y. Khodakov, V. V. Ordomsky, Selectivity shift from paraffins to α-olefins in low temperature Fischer–Tropsch synthesis in the presence of carboxylic acids, Chem. Commun. 54 (2018) 2345–2348.

[20] F.C. Meunier, The power of quantitative kinetic studies of adsorbate reactivity by operando FTIR spectroscopy carried out at chemical potential steady-state, Catal. Today. 155 (2010) 164–171.

[21] F.C. Meunier, A. Goguet, C. Hardacre, R. Burch, D. Thompsett, Quantitative DRIFTS investigation of possible reaction mechanisms for the water–gas shift reaction on high-activity Pt- and Au-based catalysts, J. Catal. 252 (2007) 18–22.

[22] G.W. Thomson, The Antoine Equation for Vapor-pressure Data., Chem. Rev. 38 (1946) 1–39.

[23] D. Ambrose, N.B. Ghiassee, Vapour pressures and critical temperatures and critical pressures of some alkanoic acids: C_1 to C_{10}, J. Chem. Thermodyn. 19 (1987) 505–519.

[24] M.L. Nahrwold, P. Archer, P.J. Cohen, Application of the Antoine equation to anesthetic vapor pressure data, Anesth. Analg. 52 (1973) 866–867.

[25] A. Paredes-Nunez, D. Lorito, N. Guilhaume, C. Mirodatos, Y. Schuurman, F.C. Meunier, Nature and reactivity of the surface species observed over a supported cobalt catalyst under CO/H_2 mixtures, Catal. Today. 242 (2015) 178–183.

[26] D. Lorito, A. Paredes-Nunez, C. Mirodatos, Y. Schuurman, F.C. Meunier, Determination of formate decomposition rates and relation to product formation during CO hydrogenation over supported cobalt, Catal. Today. 259 (2016) 192–196.

[27] W. Chen, T.F. Kimpel, Y. Song, F.K. Chiang, B. Zijlstra, R. Pestman, P. Wang, E.J.M. Hensen, Influence of Carbon Deposits on the Cobalt-Catalyzed Fischer–Tropsch Reaction: Evidence of a Two-Site Reaction Model, ACS Catal. 8 (2018) 1580–1590.

[28] M. Kollár, A. De Stefanis, H.E. Solt, M.R. Mihályi, J. Valyon, A.A.G. Tomlinson, The mechanism of the Fischer–Tropsch reaction over supported cobalt catalysts, J. Mol. Catal. A Chem. 333 (2010) 37–45.

[29] W. Chen, I.A.W. Filot, R. Pestman, E.J.M. Hensen, Mechanism of Cobalt-Catalyzed CO Hydrogenation: 2. Fischer–Tropsch Synthesis, ACS Catal. 7 (2017) 8061–8071.

Supplementary information

S6.1. Acetic acid co-feeding on a long run

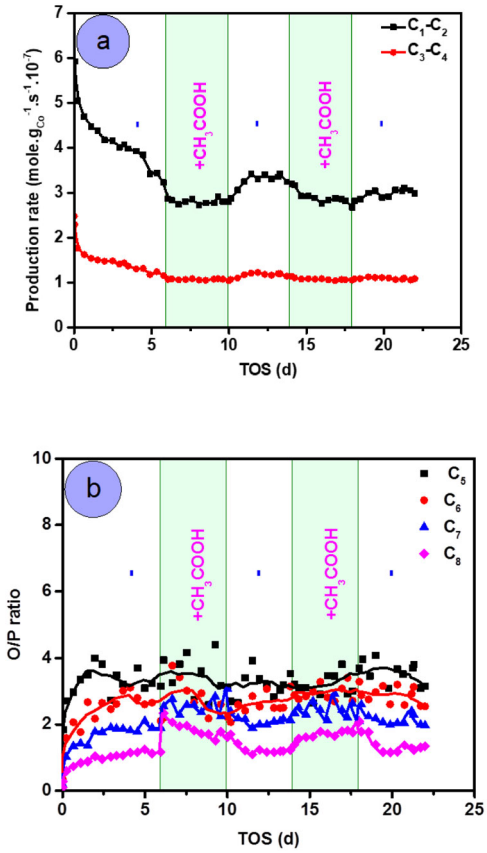

Figure S6.3: (a) Production rates of C_1-C_4 and **(b)** O/P ratio as a function of the time on stream in long run.

To confirm the catalyst deactivation in the presence of acetic acid, after initial 6 days of normal FTS long run, acetic acid co-feeding was performed two times with an interval of 4 days. The effect of acetic acid co-feeding on the production rate of hydrocarbons (C_1-C_4) and olefins to paraffins ratio is shown in Figure S6.3a. As expected, the production rate of hydrocarbons decreased with acetic acid co-feeding. After stopping co-feeding, the production rate recovered slowly with time. However, the recovery of the production rate after a second co-feeding is smaller than the recovery of the production rate after the first co-feeding. During acetic acid co-feeding, the olefins to paraffins ratio increased slightly as shown in Figure S6.3b. DRIFT spectra of the catalyst for these long run experiments are not shown here because infrared signal from the catalyst was lost due to the accumulation of a large amount of wax on the catalyst surface.

6

Summary

Role of surface carboxylate deposition on the deactivation of Fischer-Tropsch synthesis catalysts

PhD thesis by Prasad Gonugunta

Fischer-Tropsch synthesis (FTS) is a catalytic reaction, which involves the production of liquid hydrocarbon fuel from synthesis gas obtained from natural gas, biomass or coal via gasification and steam reforming. From an industrial perspective, both Co and Fe based catalysts have been applied. However, Co-based catalysts are preferred in FTS particularly for gas-to-liquid (GTL) processes as they have high activity, high selectivity to linear hydrocarbons and low activity for the unwanted water-gas shift reaction. However, Co-based catalysts are relatively expensive and deactivate in time. To make the FTS process economically more effective, a stable performance of the catalyst is required. Therefore, studying the catalyst deactivation is an important topic in the development of better industrial catalysts. Oxidation, sintering of active phase and deposition of oxygenated compounds are potential causes for deactivation. The possible role of oxygenates and their effect of catalyst deactivation, however, is less understood. With the aim to investigate the deposition of oxygenated compounds, particularly carboxylates, as hypothetical deactivation mechanism, operando characterisation techniques were adapted to monitor the chemical and physical properties and structure-activity relationship of the catalyst during the reaction. Operando Diffuse Reflectance Infrared Fourier Transform (DRIFT) and Mössbauer emission spectroscopy setups were employed that can be operated at industrially relevant FTS conditions.

In Chapter 3, we study the carboxylates deposition on the surface of the catalyst during the FTS reaction with a Co/TiO_2 catalyst, employing operando DRIFT spectroscopy and varying pressure and temperature. The activity of the catalyst increased with increasing temperature and pressure, as expected. The formation of different carboxylate compounds and hydrocarbons on the surface of the catalyst has been observed and their amount increased with time. High molecular weight (MW) carboxylates were dominant at high pressure and low temperature due to the high content of olefins, resulting in the formation of more carboxylates via hydroformylation side reaction. The effect of high MW carboxylates is not clearly distinguished from the effect of wax and sintering in catalyst deactivation.

To understand the deactivation mechanism by carboxylates in a better way, two catalysts prepared by incipient wetness impregnation (IWI) and homogeneous deposition precipitation

(HDP) methods were analysed in Chapter 4. The samples were studied by monitoring the catalyst surface species with operando infrared and the oxidation state of cobalt with operando Mössbauer emission spectroscopic techniques, during reaction at industrially relevant pressure. The activity of the HDP catalyst was found to be significantly higher than the activity of the IWI catalyst, while the Mössbauer measurements confirmed the absence of cobalt oxidation during FTS reaction for both samples, regardless of their preparation method. Clear carboxylate formation was observed on both IWI and HDP catalysts, but more and heavier carboxylates were found on the IWI catalyst compared to HDP catalyst. This effect is related to the higher olefin content in the products obtained with the impregnated sample, resulting to increased formation of oxygenates through the hydroformylation side reaction. The higher activity of the HDP catalyst is related to well-distributed cobalt active particles having higher accessible surface area compared to clustered cobalt particles in IWI catalyst with lesser accessible surface area, though both catalysts have a similar average particle size. After 4 days of the FTS reaction, both IWI and HDP catalyst were stripped with H_2 at 270 ^oC to remove carboxylates and wax from the catalyst surface and subsequently the FTS reaction was restarted. Acetates, hydrocarbons and part of the high MW carboxylates were removed from the IWI catalyst surface during stripping. In the case of HDP catalyst, hydrocarbons were removed significantly, while the carboxylates (formate being dominant) were partially removed. After restarting the reaction, the hydrocarbons and carboxylates on the surface of both catalysts re-appeared. However, after H_2 stripping, activity recovered modestly for both catalysts, suggesting that the surface carboxylates are not involved in a deactivation mechanism, being most likely spectator species on the titania support. The formation of long-chain carboxylates was inhibited in the HDP catalyst surface, possibly due to the presence of impurities like nitrogen or salts introduced by the preparation procedure.

To understand the role of the surface species, particularly formate species, in the catalyst deactivation, co-feeding of formic acid has been investigated with operando DRIFT spectroscopy in Chapter 5. A small amount of formic acid was co-fed on the Co/TiO_2 catalyst using a temperature-controlled saturator, resulting in only a negligible change in activity. When formic acid interacted alone with the Co/TiO_2 sample (in H_2 atmosphere), it decomposed into CO and H_2 on the catalyst surface and produced different hydrocarbons. During co-feeding, some of the formate species on the catalyst surface were transformed into high MW carboxylates which were removed immediately after stopping the co-feeding, by decomposition or hydrogenation, indicating that they were present on the cobalt active sites. Whereas, in standard FTS reaction, the high MW carboxylates deposited on the surface could not be removed so easily from the catalyst, as they were spectator species located on the support. The high MW carboxylates formed during co-feeding could be spectator species formed on the terrace sites of the cobalt that are not contributing to catalyst activity. During co-feeding, the accumulation of high MW carboxylates on the support is limited.

In Chapter 6, to improve the understanding of the role of carboxylates in deactivation, acetic acid was co-fed on the catalyst during FTS reaction. Acetic acid co-feeding decreased the activity of the catalyst significantly, most likely due to the formation of inactive cobalt acetate species. During acetic acid co-feeding, the olefins to paraffins ratio increased slightly due to

the prevention of olefins re-adsorption by high MW carboxylates for further hydrogenation into paraffins. The high molecular weight carboxylates formed on the catalyst surface during co-feeding are removed easily by decomposition or hydrogenation and they are not involved in catalyst deactivation mechanism. These high MW carboxylates formed during co-feeding could be spectator species formed on the terrace sites of the cobalt.

From these studies, we confirmed that high molecular weight carboxylates present on the catalyst surface during FTS are not involved in the deactivation mechanism in both cases: when carboxylic acids interact with the cobalt terrace sites during co-feeding, being easily removed and when the acids accumulate on the support during standard FTS, as spectators.

Some perspectives for further studies on oxygenated compounds in FTS are given here. The deposition of high MW carboxylates was inhibited in the HDP catalyst, this may be due to the presence of impurities like nitrogen or salts introduced by the preparation procedure. It is recommended to perform experiments to understand the effects of salts or other elements on the oxygenates formation. We performed co-feeding experiments only on IWI catalyst on which usually large amounts of high molecular weight carboxylates are deposited in normal FTS conditions. It is recommended to perform co-feeding experiments also on HDP catalyst on which low amounts of high molecular weight carboxylates are deposited, to get a better insight. It is recommended to conduct studies using also other supports that can reveal more information about carboxylates deposition. We are also recommending to perform Mössbauer experiments during carboxylic acids co-feeding, which will give more information on the interaction of carboxylic acids with active sites. In this work, we performed co-feeding experiments only with carboxylic acids, while co-feeding experiments with other oxygenated compounds like alcohols, aldehydes and ketones could lead to further insight into the deactivation mechanisms of the FTS catalysts.

Samenvatting

De rol van carboxylaatafzetting bij de deactivering van Fischer-Tropsch-synthese katalysatoren

Proefschrift door Prasad Gonugunta

Fischer-Tropsch-synthese (FTS) is een katalytische reactie waarbij vloeibare koolwaterstof brandstof wordt geproduceerd uit synthesegas doorgaans verkregen uit aardgas, biomassa of steenkool via vergassing en/of stoomreforming. Onder industriële condities worden zowel op kobalt als op ijzer gebaseerde katalysatoren toegepast in het FTS proces. Katalysatoren gebaseerd op kobalt hebben echter de voorkeur in FTS, vanwege hun hoge activiteit, hoge selectiviteit voor lineaire koolwaterstoffen en lage activiteit voor de ongewenste water-gas shift (WGS) nevenreactie. Kobalt is echter relatief duur ten opzichte van ijzer en op kobalt gebaseerde katalysatoren deactiveren over tijd. Om het FTS-proces economisch haalbaar te maken, is een stabiele katalysator vereist. Daarom is het bestuderen van de deactivering van de katalysator een belangrijk onderwerp in de ontwikkeling van betere industriële katalysatoren. Mogelijke oorzaken voor deactivering zijn: oxidatie, agglomeratie van de actieve fase en afzetting van zuurstofrijke verbindingen. Over de mogelijke rol van oxygenaten op het deactiveringsmechanisme van de katalysator is echter weinig bekend. Om de afzetting van zuurstofrijke verbindingen, in het bijzonder carboxylaten, als deactiveringsmechanisme te onderzoeken, werden operando-karakteriseringstechnieken toegepast om de chemische en fysische eigenschappen en de structuur-activiteit relatie van de katalysator tijdens de reactie te volgen. Hiervoor is gebruik gemaakt van Operando Diffuse Reflectance Infrared Fourier Transform spectroscopie (operando-DRIFTS) en Mössbauer emissiespectroscopie onder industrieel relevante FTS-omstandigheden.

In Hoofdstuk 3 bestuderen we de afzetting van carboxylaten op het oppervlak van de katalysator tijdens de FTS-reactie. Hiervoor is een Co/TiO_2-katalysator bestudeert met operando-DRIFTS onder variërende druk en temperatuur. De activiteit van de katalysator nam naar verwachting toe met toenemende druk en temperatuur. Verschillende carboxylaatverbindingen en koolwaterstoffen zijn waargenomen op het oppervlak van de katalysator met toenemende hoeveelheid over tijd. Carboxylaten met hoog molecuulgewicht waren dominant bij hoge druk en lage temperatuur vanwege het hoge gehalte aan olefinen, wat resulteerde in de vorming van meer carboxylaten via hydroformylering-nevenreactie. Het effect van carboxylaten met een hoog molecuulgewicht is niet duidelijk te onderscheiden van het effect van de formatie van was en van het effect van agglomeratie bij het deactiveren van de katalysator.

Om het deactiveringsmechanisme van carboxylaten op een betere manier te begrijpen werden twee katalysatoren bereid. Een via incipient wetness impregnation en een via homogene deposition precipitatie, hierna respectievelijk de IWI-katalysator en HDP-katalysator genoemd. Deze katalysatoren zijn geanalyseerd in Hoofdstuk 4. De katalysatoren zijn bestudeerd tijdens reactie onder industrieel relevante druk door de carboxylaten te volgen met operando-DRIFTS en de oxidatietoestand van kobalt met operando Mössbauer emissie spectroscopie. De activiteit van de HDP-katalysator bleek significant hoger te zijn dan de activiteit van de IWI-katalysator. Dit ondanks de afwezigheid van kobaltoxidatie in de Mössbauer metingen tijdens FTS-reactie in beide katalysatoren. Er werd echter duidelijke carboxylaatvorming waargenomen op zowel IWI- als HDP-katalysatoren, waarvan meer op de IWI-katalysator in vergelijking met HDP-katalysator. De carboxylaten op de IWI-katalysator hadden ook een hoger molecuulgewicht in vergelijking met degene op de HDP-katalysator. Dit effect houdt verband met het hogere olefinegehalte in de producten die met de IWI-katalysator zijn verkregen, wat resulteert in een verhoogde vorming van oxygenaten door de hydroformylering-nevenreactie. De hogere activiteit van de HDP-katalysator houdt verband met goed verdeelde actieve kobaltdeeltjes met een hoger toegankelijk oppervlak in vergelijking met de meer geclusterde kobaltdeeltjes op de IWI-katalysator met een minder toegankelijk oppervlak, hoewel beide katalysatoren een vergelijkbare gemiddelde deeltjesgrootte hebben. Na 4 dagen van de FTS-reactie werden zowel de IWI- als de HDP-katalysator met H_2 bij 270 ^oC gestript om carboxylaten en was van het katalysatoroppervlak te verwijderen om vervolgens de FTS-reactie te herstarten. Acetaten, koolwaterstoffen en een deel van de carboxylaten met een hoog molecuulgewicht werden op deze manier van het oppervlak van de IWI-katalysator verwijderd. Op de HDP-katalysator werden de meeste koolwaterstoffen verwijderd, terwijl de carboxylaten (voornamelijk formiaat) gedeeltelijk werden verwijderd. Nadat de herstart van de reactie, verschenen er opnieuw koolwaterstoffen en carboxylaten op het oppervlak van beide katalysatoren. Na H_2 strippen herstelde de activiteit zich echter nauwelijks voor beide katalysatoren. Dit suggereert dat de carboxylaten aan het oppervlak niet betrokken zijn bij het deactiveringsmechanisme, en dat deze zich hoogstwaarschijnlijk op de titaniumdrager bevinden. De vorming van carboxylaten met lange koolwaterstof ketens werd geremd in het HDP-katalysatoroppervlak wat te wijten kan zijn aan de aanwezigheid van onzuiverheden zoals stikstof of zouten die door de bereidingsprocedure zijn geïntroduceerd.

Om de rol van de oppervlaktesoorten, in het bijzonder formiaatsoorten, tijdens de deactivering van de katalysator te begrijpen, is het toedienen van mierenzuur aan de katalysator onderzocht met operando-DRIFTS in hoofdstuk 5. De toevoeging van een kleine hoeveelheid mierenzuur, toegevoegd met behulp van een temperatuur-gestuurde saturator, resulteerde in een verwaarloosbare verandering van de activiteit van de katalysator. Wanneer mierenzuur alleen in wisselwerking stond met de Co/TiO_2-monster (in H_2-atmosfeer), ontleedde het in CO en H_2 op het katalysatoroppervlak en produceerde het verschillende koolwaterstoffen. Tijdens het gelijktijdig toedienen werden sommige van de formiaatsoorten op het katalysatoroppervlak getransformeerd in carboxylaten met een hoog molecuulgewicht die na het stoppen van de toevoeging van het mierenzuur direct door ontleding of hydrogenering werden verwijderd, wat aangeeft dat ze aanwezig waren op de actieve plaatsen van de kobalt

katalysator. Dit terwijl bij standaard FTS-reactie de op het oppervlak afgezette carboxylaten met een hoog molecuulgewicht moeilijk van de katalysator konden worden verwijderd, omdat het toeschouwers waren die zich op de titaniumoxide drager bevonden. De carboxylaten met een hoog molecuulgewicht kunnen toeschouwers zijn die zijn gevormd op de terrassen van het kobalt en die niet bijdragen aan de katalysatoractiviteit. Tijdens toevoeging van mierenzuur was de ophoping van carboxylaten met een hoog molecuulgewicht op de drager beperkt.

In Hoofdstuk 6 is het effect van azijnzuur toevoeging tijdens de FTS-reactie op de katalysator onderzocht om meer inzicht te krijgen in de rol van carboxylaten tijdens deactivering. Toevoeging van azijnzuur verminderde de activiteit van de katalysator aanzienlijk, waarschijnlijk als gevolg van de vorming van inactieve kobaltacetaatsoorten. Tijdens het FTS-proces in de aanwezigheid van azijnzuur namen de verhouding olefinen tot paraffinen licht toe als gevolg van het voorkomen van her-adsorptie van olefinen door carboxylaten met een hoog molecuulgewicht voor verdere hydrogenering tot paraffinen. De carboxylaten met hoog molecuulgewicht die op het katalysatoroppervlak gevormd worden, worden gemakkelijk verwijderd door ontleding of hydrogenering en ze zijn niet betrokken bij het mechanisme voor deactivering van de katalysator. Deze carboxylaten met een hoog molecuulgewicht zouden toeschouwers kunnen zijn die gevormd werden op de terrassen van de kobaltkatalysator.

Uit deze onderzoeken hebben we bevestigd dat de carboxylaten met een hoog molecuulgewicht, die tijdens FTS op het katalysatoroppervlak aanwezig zijn, in beide gevallen niet betrokken zijn bij het deactiveringsmechanisme. De carbonzuren staan in wisselwerking met de kobaltterrasplaatsen tijdens de co-voeding van azijnzuur en worden gemakkelijk verwijderd wanneer de carbonzuren zich verzamelen zich op de titaniumoxide drager tijdens FTS.

Enkele perspectieven voor verder onderzoek naar zuurstofrijke verbindingen in FTS worden hier gegeven. De afzetting van carboxylaten met een hoog molecuulgewicht werd geremd in de HDP-katalysator, dit kan te wijten zijn aan de aanwezigheid van onzuiverheden zoals stikstof of zouten die tijdens de bereidingsprocedure zijn achtergebleven. Het wordt aanbevolen om experimenten uit te voeren om de effecten van zouten of andere elementen op de vorming van oxygenaten te begrijpen. We hebben alleen experimenten uitgevoerd op een IWI-katalysator waarop gewoonlijk grote hoeveelheden carboxylaten met een hoog molecuulgewicht worden afgezet onder normale FTS-omstandigheden. Het wordt aanbevolen om ook experimenten uit te voeren op HDP-katalysator waarop kleine hoeveelheden carboxylaten met een hoog molecuulgewicht worden afgezet om een beter inzicht te krijgen. Het wordt aanbevolen om onderzoek uit te voeren met behulp van andere dragers die meer informatie kunnen opleveren over de afzetting van carboxylaten. Het wordt aanbevolen om Mössbauer-experimenten uit te voeren tijdens het gelijktijdig voeden van carbonzuren, wat meer informatie zal geven over de interactie van carbonzuren met actieve sites. In dit werk voeren we alleen experimenten uit met carbonzuren, experimenten met gelijktijdig voeden met andere zuurstofrijke verbindingen zoals alcoholen, aldehyden en ketonen zou tot verder inzicht in de de-activatie mechanismen van de FTS-katalysator kunnen leiden.

Acknowledgements

After years of hard work and dedication, finally, the time to complete my PhD life has arrived. I received a great deal of support and assistance throughout the PhD journey from my supervisors, fellow researcher, technicians, friends and family members. I would like to use this opportunity to express my sincere thanks to the people who contributed to the completion of this thesis.

First, I am deeply grateful to my promotor, Prof. Ekkes Brück for allowing me to pursue PhD. He provided valuable suggestions, encouraged and supported me throughout this journey. I appreciate his humble nature and caring approach towards students. Furthermore, I would like to express my deep and sincere gratitude to my copromotor, Dr. Iulian Dugulan for his continuous encouragement. His tenacious and supportive nature helped me complete this project successfully despite there being numerous technical challenges. He is a perfectionist, very critical about presenting the results and very kind. I was very fortunate to work with him to gain indepth analytical and scientific writing skills.

I would also like to convey special thanks to Dr. Leendert Bezemer for his valuable suggestions in conducting experiments and writing the thesis. His support in publishing the paper in Catalysis Today was invaluable. I would like to thank Dr. Johan den Breejen for providing catalyst sample for my experiments and his valuable suggestions in the initial phase of the project. He supported and encouraged me to give a talk in N3C 2015 conference. I would also like to thank Dr. Michel Ligthart for his guidance and support in the later stage of the project. He encouraged me to present posters in N3C 2016, NanoCity 2015 and NanoCity 2016 conferences. I would also like to extend my gratitude to my other collaborators in Shell, Dr. Alexander van Bavel and Dr. Heiko Oosterbeek for their fruitful discussions.

Shell Global Solutions International B.V. and NanoNextNL are greatfully acknowledged for their financial support.

I am also thankful to my thesis assessment committee members, Prof. Emiel Hensen, Prof. Wiebren de Jong, Prof. Atsushi Urakawa and Dr. Monique A. van der Veen for critical evaluation, providing feedback and approving on time.

I would like to thank Thomas Eschemann and Prof. Krijn de Jong from Utrecht University for providing catalyst samples. I would like to thank my labmates Maxim Ariens and Luke van Koppen for their help in TEM measurements and analysis.

I would like to thank Michel Steenvoorden for his technical support and friendly discussion about life throughout my PhD journey. I am thankful for his help in repairing high pressure reaction cell, development of operando DRIFT setup, co-feeding experiments and ordering chemicals and other necessary components. I would like to thank Kees Goubitz for helping in XRD measurements and analysis of catalyst samples. Also, I extend my gratitude towards Dr. Jouke Heringa for his technical maintenance on the computer and software. The people in the

DEMO workshop particularly Rene and Rien have been very helpful in providing technical support for the DRIFT operando setup for which I am grateful. I would also like to thank the gas team for supplying gas bottles on time for my experiments. I would like to extend my thanks to Reactor Institute security team for allowing me into the building even during night hours to check the status of my experiments.

I am also grateful to the secretaries Nicole, Ilse and Trudy for their help in administrative support without any delay, hesitation and being very nice. I was very fortunate to work with helpful and joyful members of the FAME, NPM2 and SEE colleagues for their scientific discussions, collaboration and their friendliness over the years we have worked together. My special thanks to Dr. Niels van Dijk and Dr. Stephan Eijt for their feedback in work discussions.

I would like to thank my colleagues in NanoNextNl consortium for their friendly discussions and feedback during review meetings and conferences. I am particularly thankful to Prof. Freek Kapteijn for his critical comments on my work.

I would like to thank my previous supervisors Prof. Satyanarayana Nallani, Prof. Manju Misra and Prof. Amar Mohanty for their encouragement and support.

My special thanks to Shiv, Deepak, Sreekar and Surendra for their care and immense support during the tough phase of my life, I will never forget your help.

My sincere thanks to friends Dr. Murali Mohan Reddy, Raji, Swami, Vamsi, Reddy, Malli, Jayaram, Pardhu, Ravi, Srinu, Krishna, Pranav, Naveen, Vinayak, Aniketh, Aravind, Ankit, Selva, Sandeep, Harsha, Sudheer, Hari, Madhava, Konda and Manoj.

I would like to thank శ్రీ లక్ష్మీ నరసింహ స్వామి and రామాచార్య for their blessings.

Finally, I must express my very profound gratitude to all my family members: Amma (Mother), Nanna (Father), Ammamma (Grandmother), Tata (Grandfather) and brother for their constant support. Without the support of my mother and grandmother, I would not have completed my higher studies, their determination and love made me to reach this level.

Prasad Gonugunta

ప్రసాద్ గోనుగుంట

Publications and Presentations

Publications:

1. P. Gonugunta, A.I. Dugulan, G.L. Bezemer, E.H. Brück, *Effect of carboxylic acids addition on the performance of a Co-based Fischer-Tropsch synthesis catalyst* (In preparation).

2. P. Gonugunta, A.I. Dugulan, G.L. Bezemer, E.H. Brück, *Role of surface carboxylate deposition on the deactivation of cobalt on titania Fischer-Tropsch catalysts,* Catalysis Today.

Conference Presentations:

1. P. Gonugunta, A.I. Dugulan, E.H. Brück, *Influence of T and P on the formation of oxygenated compounds on the Co surface of a FTS catalyst,* NanoCity 2016 conference, Amsterdam, The Netherlands.

2. P. Gonugunta, A.I. Dugulan, E.H. Brück, *On the presence of oxygenated compounds formed during Fischer-Tropsch synthesis over a Co-based catalyst*, NCCCXVII, The Netherlands' Catalysis and Chemistry Conference 2016, The Netherlands.

3. P. Gonugunta, A.I. Dugulan, E.H. Brück, *To study the formation of oxygenated compounds during FTS,* NanoCity 2015 conference, October 2015, Amersfoort, The Netherlands.

4. P. Gonugunta, A.I. Dugulan, E.H. Brück, *Formation of oxygenated compounds during Fischer-Tropsch synthesis and their role in catalyst deactivation,* NCCCXVI, The Netherlands' Catalysis and Chemistry Conference 2015, The Netherlands.

5. P. Gonugunta, A.I. Dugulan, E.H. Brück, *A combined DRIFT, Mössbauer and GC instrument for in-situ and operando characterization of Fischer-Tropsch catalysts,* NanoCity 2014, Utrecht, The Netherlands.

Other publications

1. N.K. Singh, S.K. Singh, D. Dash, **P. Gonugunta**, M. Misra, P. Maiti, *CNT induced β-Phase in polylactide: Unique crystallization, biodegradation, and biocompatibility*, The Journal of Physical Chemistry C, 2013, 117, 10163-10174.

2. **P. Gonugunta**, S. Vivekanandhan, A.K. Mohanty, M. Misra, *A study on synthesis and characterization of biobased carbon nanoparticles from lignin,* World Journal of Nanoscience and Engineering, 2012, 2, 148-153.

3. N.K. Singh, B.P. Das Purkayastha, J.K. Roy, R.M. Banik, **P. Gonugunta**, M. Misra, P. Maiti, *Tuned biodegradation using poly(hydroxybutyrate-co-valerate) nanobiohybrids: Emerging biomaterials for tissue engineering and drug delivery*, Journal of Materials Chemistry, 2011, 21, 15919-15927.

Patent:

1. A.K. Mohanty, M. Misra, S. Vivekanandhan, **P. Gonugunta**, T. Wang, A. Rodriguez, M. Tiessen, A. Bali *Novel methods for creation of sub-micron biocarbon materials from biomass and their fields of application,* WO 2018/085918, 17-05-2018 & US 2019/0276315 A1, 12-09-2019

Curriculum Vitae

Prasad Gonugunta
Born on 10th May 1986
Ilavara, Andhra Pradesh, India

2012 September – till now
PhD in Fundamental Aspects of Materials and Energy (FAME)
Radiation Science and Technology (RST), Delft University of Technology, The Netherlands

2019 January – 2020 July
Research Scientist
Coval Energy B.V., The Netherlands

2010 May – 2012 May
MASc (Biological Engineering)
Bio-products Discovery and Development Centre (BDDC) and School of Engineering, University of Guelph, Canada

2007 July – 2009 June
MSc (Physics)
Department of Physics, Pondicherry University, India

2004 June – 2007 April
BSc (Mathematics, Physics and Chemistry)
Silver Jubilee Government College, Sri Krishnadevaraya University, India


TU Delft
Delft
University of
Technology


nanonextnl
innovating with micro and nanotechnology